STUDY ON THE NUCLEAR CHARACTERISTICS OF A LIGHT-WATER-MODERATED AND HEAVY-WATER-REFLECTED CORE LOADED WITH MEDIUM-ENRICHED-URANIUM FUEL

SEIJI SHIROYA

Study on the Nuclear Characteristics of a Light-Water-Moderated and Heavy-Water-Reflected Core Loaded with Medium-Enriched-Uranium Fuel

Seiji Shiroya

Research Reactor Institute, Kyoto University
Kumatori-cho, Sennan-gun, Osaka 590-04, Japan

ABSTRACT

In order to examine the feasibility on the use of medium-enriched-uranium [MEU] fuel for a high flux reactor, the nuclear characteristics of a light-water-moderated and heavy-water-reflected annular core loaded with MEU fuel were investigated through the critical experiments using the Kyoto University Critical Assembly [KUCA]. Items of the critical experiments were measurements of (1) the critical mass, (2) the control rod worth, (3) the reactivity effect of boron loaded side-plates, (4) the neutron flux distribution, (5) the kinetic parameter, (6) the void effect on reactivity, and (7) the temperature effect on reactivity. The effect of reducing fuel enrichment on the nuclear characteristics were also investigated through the comparison between the cores loaded with MEU and highly-enriched-uranium [HEU] fuels.

It is concluded from the present study that MEU fuel is feasible for a high flux reactor in place of HEU fuel without any significant reduction in reactor performance. The main features of the nuclear characteristics in

the MEU core are determined by the fact that MEU fuel contains more ^{235}U and more ^{238}U than HEU fuel, and the $H/^{235}U$ ratio in the MEU core is smaller than that in the HEU core. The main features of the MEU core are as follows:

(1) The minimum critical mass of ^{235}U in the MEU core is around 20 % larger than that in the HEU core.

(2) The control rod worth in the MEU core is around 10 % lower than that in the HEU core.

(3) The reactivity effect of boron loaded side-plates in the MEU core is sufficient for suppressing the excess reactivity in an initial loading core of a high flux reactor.

(4) The level of the thermal neutron flux in the fueled region of the MEU core is around 10 % lower than that of the HEU core, however, they become much closer in the reflector region.

(5) The value of β/ℓ in the MEU core is approximately equivalent to that in the HEU core.

(6) The void effect on reactivity in the fueled region of the MEU core is slightly more negative than that of the HEU core.

(7) The temperature effect on reactivity in the MEU core is approximately equivalent to that in the HEU core, although the Doppler effect in the MEU core is slightly negative and that in the HEU core is nearly zero.

A self-consistent system of the neutronics calculations for the analyses of the KUCA critical experiments is basically established through the present study including some assessments on the capability of computer codes. This self-consistent system of the neutronics calculations provides a possibility to investigate the nuclear characteristics of the MEU and HEU cores in more detail with a certified accuracy.

CONTENTS

I. INTRODUCTION

Research reactors have been mostly used as a very effective thermal neutron source. In this view point, it is essential for a research reactor to provide the thermal neutron flux as high as possible. The higher is the level of the thermal neutron flux per reactor power, the better the reactor performance becomes. Usually, the highest peak of the thermal neutron flux is attained not in a fuel region but in a reflector region. In order to obtain the higher peak of the thermal neutron flux in the reflector region, a so-called under-moderated core of a small size is desirable, although this is a condition of contradiction. The smaller is the core size, the higher the neutron flux in the fuel region grows up with the increase in power density and the more the fast neutron leakage from the fuel region becomes, which serves as a source term of thermal neutrons in the reflector region. In the under-moderated core, the fast neutron flux in the fuel region becomes relatively higher, whereas the minimum critical mass becomes larger and then the core size becomes larger. The above contradiction is dissolved to some extent by the increase of ^{235}U loading into the core. Therefore, highly-enriched-uranium [HEU] fuel with a high U density is currently used in research reactors,[1] although a low power density and a low temperature of primary coolant are desirable from a thermal-hydraulic point of view. From both view points of the thermal-hydraulics and the neutron economy, plate type fuels with aluminum cladding are currently adopted in research reactors.[1]

Several high flux reactors have been constructed to provide the high thermal neutron flux for the research purposes.[1-3] In such reactors, high density fuels such as UAl_x-Al and U_3O_8-Al dispersion aluminide fuels are currently used, whereas U-Al alloy fuel is conventionally used in most

research reactors.[1-3] Recent development in the techniques of the fue fabrication is quite remarkable.[4-6] At the beginning of the present study 1978, the maximum U densities of U-Al alloy, UAl_x-Al and U_3O_8-Al dispersio aluminides were approximately 0.7, 1.7 and 1.2 g/cc in commercial base respectively.[4] It makes possible to fabricate fuel having much more l density than current fuel. This development in the fuel fabricatio technique provides a possibility to use reduced-enrichment-uranium [REU fuels, including medium-enriched-uranium [MEU] and low-enriched-uraniu [LEU] fuels, instead of current HEU fuel in a research reactor including high flux reactor with a minor reduction in the reactor performance withou changing any core dimensions.

From the above view points, the present study is concerned with th use of REU fuel comparable to current HEU fuel in a high flux reactor an is focused mainly on the nuclear characteristics of a core loaded with ME fuel. The undesirable effects of increasing ^{238}U content in REU fuel ma well be cancelled by the increases in ^{235}U and total U densities. Th expected demerits for the use of REU fuel are as follows;[4] (1) the neutro flux may fall down in proportion to the increase in ^{238}U content, (2) th peak value of the power density may grow up at a boundary of the fue region with the increase in ^{235}U content, that may be undesirable from a

---

Note : Definitions of HEU, MEU, LEU, and REU

	^{235}U Enrichment	
	IAEA[4,6]	Present Study
HEU	≥ 70 wt%	93 wt%
MEU	45 wt%	45 wt%
LEU	< 20 wt%	20 wt%

REU includes MEU and LEU.

thermal-hydraulic point of view, and (3) the initial cost of the fuel fabrication may go up with the increase in U density of REU fuel. On the contrary, the expected merits are as follows;[4] (1) the Doppler effect[7] may grow larger and become more effective to suppress an accidental power excursion with the increase in ^{238}U content, and (2) the fuel life may become longer because of the accumulation of Pu during burnup, although a main fissile material is ^{235}U throughout the fuel life. It is worthwhile to investigate quantitatively these merits and demerits.

Several studies on the use of REU fuel in a research reactor have been performed. However, there has been no study on the use of MEU fuel and all studies have been concerned with LEU fuel. For example, the TRIGA type reactor originally utilized LEU fuel of 20 wt% ^{235}U enrichment,[8] and all TRIGA type reactors in Japan are using LEU fuel.[9] The graphite-moderated Semi-Homogeneous Critical Experimental Assembly [SHE] at Japan Atomic Energy Institute [JAERI] is using LEU fuel.[9,10] The first critical state in the Japan Research Reactor-2 [JRR-2] at JAERI, which uses heavy-water as a moderator and a reflector, was attained with use of LEU fuel in 1960,[11] and LEU fuel was converted to HEU fuel in 1962. Especially, after the US Government declared to stop a supply of HEU fuel in relation to the nonproliferation policy issued in 1977, the special efforts have been internationally focused on the research concerning the reduced enrichment for research and test reactors [RERTR].[12-14] Under the instruction of the International Atomic Energy Agency [IAEA], the RERTR program is systematically being performed in many countries to investigate the feasibility on the use of REU fuel in research and test reactors.[4,6,15-19] This program includes (1) a development of high density REU fuel, (2) a burnup test of REU fuel, (3) a neutronics calculation for an REU core, (4) a full core mock-up experiment using REU fuel, and (5) a thermal-hydraulic study on ar

REU core. In order to investigate the nuclear characteristics of an REU core in detail, the experimental study should be unavoidable. The full core mock-up experiments are being carried out in the Ford Nuclear Reactor [FNR] of Michigan University using LEU fuel of 20 wt% ^{235}U enrichment[20~27] and in the critical facility of the Japan Materials Testing Reactor [JMTRC] at JAERI using MEU fuel of 45 wt% ^{235}U enrichment[28,29]. Both experiments are performed for the core conversions of existing research and test reactors from HEU to REU fuels. The experiment in the JMTRC was started two years later after a first critical state of an MEU core had been attained in the present study.

In the present study, a light-water-moderated and heavy-water-reflected annular core with a flux trap region[30] at the core center is chosen as an object of study. The reason is that this type core has recently been proposed and become popular for high flux reactors.[31~42] High flux reactors now in operation use either light-water or heavy-water as a moderator.[1~3] A light-water-moderated high flux reactor uses beryllium as a reflector, because a capability of neutron reflection in light-water is rather poor, whereas a heavy-water-moderated high flux reactor uses heavy-water as a reflector. Generally, sharper and narrower flux peak of thermal neutrons is obtained in light-water than in heavy-water, and a value of this peak in light-water is 2 ∿ 3 times larger than that in heavy-water. Therefore, a light-water-moderated high flux reactor has a flux trap region usually at the core center where a peak of thermal neutron flux is attained. This type reactor is suitable for the neutron irradiation experiments. On the other hand, considering a certain wide region in a reflector, the total number of usable thermal neutrons in a light-water reflector is smaller than that in a heavy-water reflector. The neutron flux peak is located at a reflector region in a heavy-water-moderated high flux reactor.

This type reactor is suitable for the neutron beam experiments. In the objective core of study, the merits of the above two type high flux reactors are taken into consideration.

The neutronics calculations were performed to examine the feasibility on the use of REU fuel in a light-water-moderated and heavy-water-reflected type high flux reactor.[43-45] The fuel enrichment examined in the survey calculations were selected to 93, 45, and 20 wt%.[43] At first, the criticality calculation on the basis of diffusion theory was performed for 93 wt% HEU fuel utilizing U-Al alloy of 22 wt% U content. Next, with preserving all the core dimensions used in the HEU case, the criticality calculations were performed for 45 wt% MEU and 20 wt% LEU fuels until the same reactivities as the HEU fuel were obtained by increasing total U content in UAl_x-Al dispersion aluminide. The results of survey calculations show that 45 wt% MEU fuel with 42 wt% U content is feasible in this type high flux reactor and further development in the fuel fabrication technique is necessary to use 20 wt% LEU fuel. Then, the critical experiments was planned to investigate experimentally the feasibility on the use of the above MEU fuel in the proposed high flux reactor.[12,46,47]

The main purposes of the present study are to investigate experimentally the nuclear characteristics of a light-water-moderated and heavy-water-reflected annular core loaded with MEU fuel, and to establish a self-consistent system for the neutronics calculations in the KUCA through the analyses of the experimental data using the computer codes. The objectives of the present study can be summarized as follows:

(1) To examine the nuclear characteristics of a light-water-moderated and heavy-water-reflected core loaded with MEU fuel comparable to current HEU fuel through the critical experiments using the KUCA and provide the benchmark data for the use of MEU fuel.

(2) To investigate experimentally the effects of reducing fuel enrichment on the core characteristics through the comparison between the cores loaded with HEU and MEU fuels.

(3) To establish a self-consistent system of the neutronics calculations for the analyses of the KUCA experiments which employed a rather complex core configuration and assess the accuracies of the calculated results in comparison with the experimental data.

(4) To provide the possibility for the further detailed survey on the use of REU fuel with use of the self-consistent system for the neutronics calculations in the KUCA established through the present study.

For these purposes, MEU fuel was fabricated using a currently developed technique and the critical experiments were carried out using a light-water-moderated and heavy-water-reflected annular core constructed in the KUCA.[48-58] Items of the KUCA critical experiments using MEU fuel were as follows; measurements of (1) the critical mass, (2) the control rod worth, (3) the reactivity effect of boron loaded side-plates, (4) the neutron flux distribution, (5) the kinetic parameter, (6) the void effect on reactivity, and (7) the temperature effect on reactivity. Most experimental data of the MEU core were compared with those of the HEU core. Some of the experimental data were analyzed by the neutronics calculations based on diffusion theory in order to establish a self-consistent system.[56,59-66] The computer codes utilized in the present study were (1) the generation code of neutron group constants, EPRI-CELL,[67] (2) the multi-dimensional neutron diffusion code based on the finite-difference method, DIF3D,[68] (3) the two-dimensional neutron diffusion code based on the finite-element method, 2D-FEM-KUR,[69,70] and (4) the standard reactor analysis code system in JAERI, SRAC.[71,72]

The present thesis provides the results of studies on the nuclear characteristics of a light-water-moderated and heavy-water-reflected annular core loaded with MEU fuel. The survey study on the use of REU fuel comparable to current HEU fuel for a research reactor and the determination procedures of MEU fuel specifications are described in Chapter II. The results of the series of critical experiments using MEU fuel in the KUCA are described in Chapter III in comparison with those of HEU fuel. The analytical studies on the criticality and the boron reactivity effect are described in Chapter IV. The analytical study on the void reactivity effect is described in Chapter V. The analytical study on the temperature reactivity effect is described in Chapter VI. The conclusions obtained through the present series of studies are summarized in Chapter VII.

II. MEDIUM-ENRICHED-URANIUM FUEL

II-1. Introduction

It is worthwhile to study on the compatibility of REU fuel with HEU fuel in a research reactor from a reactor physics point of view, since REU fuel is considered to have the superiority over HEU fuel in the Doppler effect and the fuel life.[4]

At first, the basic physics on the use of REU fuel is investigated by simple theoretical considerations. On the basis of this consideration, the feasibility of REU fuel comparable to HEU fuel in a high flux reactor is examined by the neutronics calculations based on diffusion theory. A high flux reactor is chosen as the object of study, since most researchers want to use thermal neutrons for their experiments as much as possible. A type of high flux reactor is selected to be a light-water-moderated and heavy-water-reflected annular core which have recently been proposed and become popular for a high flux reactor.[31~42] Under an assumption of the unchangableness in the main core dimensions, the survey calculations were performed to examine the feasibility of REU fuel in the above type high flux reactors.[43~45] The results of survey calculations showed that 45 wt% MEU fuel with 42 wt% U content is feasible to this type high flux reactor, even under the condition of having the same excess reactivity as an HEU core. Then, this MEU fuel was fabricated using the currently developed fabrication technique for the critical experiments in the KUCA.[48,50]

II-2. Basic Physics on the Use of Reduced-Enrichment-Uranium Fuel

In this section, the basic physics on the use of REU fuel is investigated by simple theoretical considerations, under an assumption of the unchangeableness in the main core dimensions.

Let's try to explain the effects caused by reduced ^{235}U enrichment of fuel using a well-known equation (4-factor formula) for the multiplication factor in an infinite system, k_∞; that is,[7]

$$k_\infty = \eta f p \varepsilon \ , \qquad \text{(II-1)}$$

where, η: average number of fission neutrons emitted per thermal neutron absorbed by fuel,

f: thermal utilization,

p: resonance escape probability,

ε: fast fission factor.

For the simplicity, a simplified heterogeneous cell which consisted of fuel and moderator is assumed in the following discussion. Note that, in the following equations, the subscript F means fuel and the subscript M moderator. A value of η is calculated by,[7]

$$\eta = \nu \Sigma_f \ / \ \Sigma_{aF} \ , \qquad \text{(II-2)}$$

where, ν : number of neutrons emitted per thermal fission,

Σ_f: macroscopic fission cross section for thermal neutrons,

Σ_a: macroscopic absorption cross section for thermal neutrons.

A value of f is calculated by,[7]

$$f = \Sigma_{aF} V_F \ / \ [\Sigma_{aF} V_F + \Sigma_{aM} (\Phi_{thM} / \Phi_{thF}) V_M] \ , \qquad \text{(II-3)}$$

where, V : volume,

Φ_{th}: average thermal neutron flux.

A value of p is approximately calculated by,[7]

$$p = \exp[- N_F V_F I_R / (\xi_F \Sigma_{pF} V_F + \xi_M \Sigma_{sM} V_M)] , \qquad \text{(II-4)}$$

where, N : atomic number density,

I_R: resonance integral,

ξ : average increase in lethargy per collision,

Σ_p: macroscopic potential scattering cross section,

Σ_s: macroscopic scattering cross section.

A value of ε is calculated by.[7]

$$\varepsilon = \int_{all} \nu(E)\Sigma_f(E)\Phi(E)dE \; / \; \int_{th} \nu(E)\Sigma_f(E)\Phi(E)dE , \qquad \text{(II-5)}$$

where, $\nu(E)$: number of neutrons emitted per fission due to neutrons of energy E,

$\Sigma_f(E)$: macroscopic fission cross section for neutrons of energy E,

$\Phi(E)$: neutron flux of energy E.

The integral in the numerator of Eq. (II-5) is carried out over the whole energy range, whereas that of the denominator only over the thermal energy range. For the actual use of ε, Eq. (II-5) is slightly corrected so as to be consistent with the calculation of p.

When the total U density of REU fuel is assumed to be the same as that of HEU fuel, the effective multiplication factor k_{eff} would decrease rapidly with reducing the ^{235}U enrichment. From Eqs. (II-2) through (II-5), it is evident that all values of η, f and ε decrease with reducing the ^{235}U enrichment, whereas only p increases. These behaviors in f, p, and ε values can be easily guessed by considering that the $H/^{235}U$ ratio increases with reducing the ^{235}U enrichment.[7] Therefore, k_{eff} decreases in accordance with the decrease in k_∞. In order to assure the above argument,

a cell calculation was performed using SRAC[71] and the result is shown in Fig. II-1. In this cell calculation, a slab geometry option is utilized. The thicknesses of the fuel meat, Al cladding, and light-water moderator are assumed as 0.5, 0.45, and 2.4 mm, respectively, and the total U density is preserved as 0.636 g/cc, which are equal to those in HEU core constructed in the KUCA.

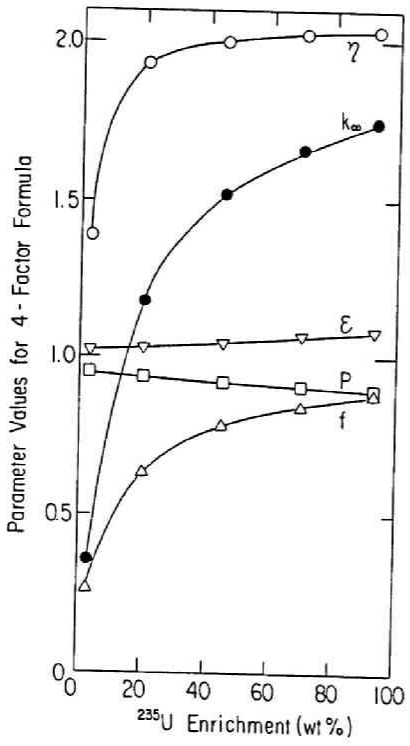

Fig. II-1
Parameter Values of Eq. (II-1) versus ^{235}U Enrichment

When the total U density of REU fuel is increased, k_{eff} increases. The reason is that η approximately maintains its value (in actual, η slightly increases with the decrease in $H/^{235}U$ ratio) regardless of the increase in total U density, and both ε and f increase with the increase in total U density, whereas only p decreases. Therefore, it is considered to be possible that an REU core has the same k_{eff} as an HEU core by the increase in total U density of REU fuel. In order to attain the same k_{eff} as an HEU core, the ^{235}U content in REU fuel should be higher than that of HEU fuel.

The excess reactivity ρ_{ex} is essential for the operation of a research reactor. A value of ρ_{ex} should be sufficiently enough to cover the negative reactivity effects caused by the buildup of fission products including xenon and samarium, the ^{235}U burnup, etc. during the steady operation of a certain period.[7] Therefore, in the survey on the use of REU fuel described in this chapter, another assumption is made that ρ_{ex} of an REU core is kept equal to that of an HEU core. This assumption is convenient to investigate the fuel life, since the difference between REU and HEU fuels can be directly observed. This assumption inevitably indicates that the ^{235}U density of REU fuel is higher than that of HEU fuel.

The most different feature of the burnup in REU and HEU cores is the Pu accumulation which occurs mainly in an REU core, although a main fissile material is ^{235}U even in an REU core. The fuel life in an REU core is longer than that of an HEU core, because the accumulation of fissile Pu causes a positive reactivity effect. This indicates that a lower value of k_{eff} is necessary for the reactor operation of an REU core to obtain the same fuel life as an HEU core.

The average fission density in the cell is approximately expressed by,

$$\text{fission density} \cong \Sigma_f \Phi_{th} , \qquad \text{(II-6)}$$

using the average thermal neutron flux in the cell Φ_{th}. At a specified reactor power, a value of $\Sigma_f \Phi_{th}$ is approximately constant regardless of the ^{235}U enrichment of fuel loaded in a core, since the fission density is proportional to the power density. Under the condition that an REU core has the same excess reactivity as an HEU core, this indicates that Φ_{th} in an REU core is smaller than that in an HEU core and Φ_{th} is approximately inversely proportional to the ^{235}U concentration in a core. In addition, it is indicated that the control rod worth in an REU core is smaller than

that in an HEU core, because Φ_{th} in an REU core is smaller than that in an HEU core and a usual control rod is designed to absorb mostly thermal neutrons.

However, a ratio of the average fast neutron flux in the cell Φ_f to Φ_{th} of an REU core is larger than that of an HEU core, because the $H/^{235}U$ ratio in an REU core is lower than that in an HEU core. This is also indicated from the fact that a value of p in an REU core is smaller than that in an HEU core and a value of ε in an REU core is larger than that in an HEU core. A level of Φ_f in the fuel region has a special meaning in a high flux reactor, because Φ_f is a source term of thermal neutrons in the reflector region including the flux trap region. Therefore, it is possible to recover the decrease in Φ_{th} to some extents in the reflector region of an REU core. This also indicates that a peak value of the power density at the boundary of the fuel and reflector (including flux trap) regions in an REU core is higher than that in an HEU core.

The void reactivity effect in the cell of an REU core is considered to be slightly more negative than that of an HEU core. From Eq. (II-3), the generation of voids in a moderator region causes the increase of f value, since Σ_{aM} decreases with the decrease in moderator density. The increase of f in an REU core having the same k_{eff} as an HEU core is slightly smaller than that in an HEU core, since Σ_{aF} of an REU core is larger than that of an HEU core. On the other hand, from Eq. (II-4), the generation of voids causes the decrease of p value, since Σ_{sM} decreases with the decrease in moderator density and I_R increases due to the spectral hardening effect. The decrease of p in an REU core is slightly larger than that in an HEU core, since I_R of an REU core is larger than that in an HEU core. Although ε increases due to the increase in the first collision probability with

^{238}U nuclei and the increase of ε in an REU core is slightly larger than that in an HEU core, the variance of ε usually causes a minor effect to k_{eff} compared with that of f or p. Therefore, it is expected that the void reactivity effect in an REU core is slightly more negative than that in an HEU core.

The temperature effect on reactivity in the cell of an REU core is considered to be slightly more negative than that of an HEU core. The temperature effect can be divided into 3 effects;[7,73] namely, (1) the thermal expansion effect, (2) the Doppler effect, and (3) the thermal neutron spectral shift effect. The thermal expansion effect causes an approximately identical effect to the void reactivity effect, since the decrease in moderator density causes a major effect. The Doppler effect gives a negative reactivity effect by the decrease of p in accordance with the increase in I_R of Eq. (II-4). The Doppler effect in an HEU core is approximately zero, since HEU fuel contains only few portion of ^{238}U. The thermal neutron spectral shift effect decreases η value, because Σ_f/Σ_a of ^{235}U decreases with the increase in neutron temperature. The decrease of η in an REU core is slightly larger than that in an HEU core, since the non-1/v factor for Σ_a of ^{238}U increases monotonically with the increase of neutron temperature, whereas that of ^{235}U decreases monotonically. The variances of ε and f are considered to be very small. In view of the above, it is expected that the temperature effect on reactivity in an REU core is more negative than that in an HEU core.

II-3. Light-Water-Moderated and Heavy-Water-Reflected High Flux Reactor

Several high flux reactors are now in operation using HEU fuel.[1-3] They can be classified into two types according to the material used as a moderator; namely, light-water and heavy-water. The High Flux Reactor [HFR][2] at Petten in Netherlands, the High Flux Isotope Reactor [HFIR][3] of Oak Ridge National Laboratory [ORNL] in the USA and the SM-2 Reactor[1] at Dimitrovgrad in the USSR are light-water-moderated and beryllium-reflected cores. The HFIR and SM-2 have central flux traps[30] where the maximum thermal neutron flux can be obtained. The High Flux Beam Reactor [HFBR][3] of Brookhaven National Laboratory [BNL] in the USA and the Grenoble High-Flux Reactor [GHFR][1] at Grenoble in France are heavy-water-moderated and heavy-water-reflected cores. The HFIR and GHFR use involute type fuels and have annular cylinder cores, whereas the HFR, HFBR, and SM-2 use MTR type fuels and have basically rectangular parallelepiped cores. Reactor powers of the HFR, HFBR, SM-2, HFIR, and GHFR are 20, 40, 75, 100, and 100 MW(th), respectively. Maximum thermal neutron fluxes achieved in the HFR, HFBR, SM-2, HFIR, and GHFR are 2.5×10^{14}, 7×10^{14}, 3.3×10^{15}, 5×10^{15}, and 1.5×10^{15} n/cm^2sec, respectively.[1-3]

In view of the above, a light-water-moderated high flux reactor with a central flux trap has a superiority over a heavy-water-moderated high flux reactor for obtaining a high peak of the thermal neutron flux. A current light-water-moderated high flux reactor uses beryllium as a reflector, since light-water has a poor capability for the neutron reflection. Whereas a current heavy-water-moderated high flux reactor uses heavy-water as a reflector, since heavy-water has a good capability for the neutron reflection as well as beryllium. However, the use of beryllium reflector restricts the flexibility to extract neutrons for the beam experiments.

Therefore, with taking into account the merits of the above two type high flux reactors, a light-water-moderated and heavy-water-reflected core has recently become popular.[33~40] The ORPHEE reactor of Léon Brillouin Laboratory in France is being operated since 1980 and a maximum thermal neutron flux of 3×10^{14} n/cm^{2}sec is attained at a reactor power of 14 MW(th).[33~35] The upgrading program of the Japan Research Reactor-3 [JRR-3] of JAERI is currently being executed to construct the JRR-3(M) reactor which is scheduled to start a regular operation in 1988.[36~40] Each reactor uses MTR type fuel and has basically a rectangular parallelepiped light-water-moderated core which is contained in a cylindrical core vessel surrounded by a large annular heavy-water reflector. A light-water-moderated and heavy-water-reflected annular core with a central flux trap has recently been proposed for a high flux reactor.[31,32,41,42] A cross-sectional view of this type core is shown in Fig. II-2 as an example.

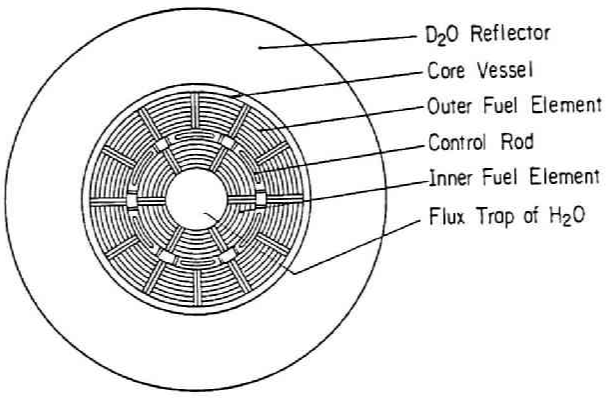

Fig. II-2 Cross-Sectional View of a Light-Water-Moderated and Heavy-Water-Reflected Annular Core with a Central Flux Trap

This core has a central flux trap region of light-water for a heavy irradiation facility and uses heavy-water as a reflector for the convenience of the several beam experiments. Light-water serves as a coolant and a moderator, because high flow rate of coolant is necessary in a high

flux reactor to remove intense heat generated in the fueled region of high power density. The reason is that light-water can be handled more easily than heavy-water which causes a heavy tritium contamination due to $D(n,\gamma)T$ reactions, when heavy-water is used as a coolant and a moderator. In this core, basically MTR-type fuel is used and the fuel region is separated into two parts by a space for control rods.

II-4. Determination of the Uranium-235 Enrichment of Reduced-Enrichment-Fuel Comparable to High-Enriched-Uranium Fuel

The survey on the core conversion from the use of HEU to REU fuels should be carried out through the neutronics calculations. In the Phase A of the joint study program between Argonne National Laboratory [ANL] and Kyoto University Research Reactor Institute [KURRI], the survey calculations were performed to check the feasibility of REU fuel in the proposed Kyoto University High Flux Reactor [KUHFR].[43,44] The proposed KUHFR has basically a light-water-moderated and heavy-water-reflected annular core, though the KUHFR is a coupled-core.[32] Therefore, the results of the Phase A of the ANL-KURRI joint study is quoted here in this section.

In this study, ANL and KURRI independently performed the neutronics calculations with preserving the main core dimensions in the initial design of the proposed KUHFR. Computer codes used in ANL were the EPRI-CELL[67] and PDQ-7[74] codes, whereas they were the GGC-4,[75] THERMOS,[76] and KR302DPT[77] codes in KURRI. The EPRI-CELL, GGC-4 and THERMOS codes were used to generate the few-group constants for the subsequent diffusion calculations. The PDQ-7 and KR302DPT codes were based on diffusion theory and utilized

the finite-difference method. The two-dimensional core calculations were performed using the PDQ-7 and KR302DPT codes.

In order to determine the enrichment applicable to the proposed KUHFR, the neutronics calculations were performed for two types of REU fuels; namely, 45 wt% MEU and 20 wt% LEU fuels. The calculated results by ANL and KURRI are tabulated in Table II-1 in comparison with a reference case of 93 wt% HEU fuel which has 22 wt% uranium in the fuel meat. Note here that HEU fuel contains U-Al alloy in the fuel meat and reduced enrichment fuels contain UAl_x-Al dispersion aluminide. For the reduced enrichment cases, the uranium contents were increased to maintain the same ^{235}U density as in the HEU case.

Table II-1 Comparison of k_{eff} Values for Different Enrichments in the KUHFR[43]

Uranium-235 Enrichment	Uranium Content in the Fuel Meat	Calculated k_{eff} Value ANL	KURRI
93 wt%	22.0 wt% 0.72 g/cc	1.1947	1.2081
45 wt%	38.8 wt% 1.50 g/cc	1.1732	1.1775
20 wt%	63.4 wt% 3.37 g/cc	1.1493	1.1419

Table II-1 shows that the agreements between two series of calculated results by ANL and KURRI are good. The k_{eff} value goes down with the reduction in ^{235}U enrichment, namely with the increase in ^{238}U content of REU fuel. The maximum uranium content currently qualified was 42 wt% for UAl_x-Al dispersion aluminide.[4] Therefore, there was a possibility to use MEU fuel in the proposed KUHFR without changing any core dimension. On the other hand, it was impossible to use LEU fuel in the current stage. Further development of the fuel fabrication techniques should be necessary to use LEU fuel in the proposed KUHFR.

Generally, the excess reactivity of the initial loading core is essential for the steady operation of a certain period in a research reactor. For the steady operation, even an REU core should have a sufficient excess reactivity, although the life of REU fuel is considered to be longer than that of HEU fuel due to the accumulation of Pu. In this survey, as a first step, the U content of MEU fuel was determined so as to attain the same k_{eff} value as the HEU reference core. Then, in this MEU core, the effect of reduced ^{235}U enrichment on the thermal neutron flux was investigated as shown in Table II-2.

Table II-2 Effect of Reduced ^{235}U Enrichment on the Thermal Neutron Flux in the KUHFR at 30 MW Operation[43]

Uranium-235 Enrichment	Uranium Content in the Fuel Meat		Calculated k_{eff}	Thermal Neutron Flux D_2O Gap	Thermal Neutron Flux H_2O Trap
93 wt%	22.0 wt%	0.72 g/cc	1.1947	1.938E14	3.214E14
45 wt%	42.0 wt%	1.67 g/cc	1.1992	1.844E14	3.109E14

Table II-2 shows that the k_{eff} value of 45 wt% MEU fuel with 42 wt% U content is approximately equivalent to that of the reference HEU core. The total mass of ^{235}U in the MEU core is approximately 6.5 % larger than that of the HEU core.[44] The reductions in the thermal neutron flux at the center of the heavy-water gap between two coupled cores and at the center of each central flux trap of light-water are less than 5 % for the both positions. This result indicate that 45 wt% MEU fuel with 42 wt% U content is feasible for a high flux reactor without any significant reduction in the reactor performance.

II-5. Fabrication of Medium-Enriched-Uranium Fuel

On the basis of the results described in the previous section, 45 wt% MEU fuel with 42 wt% U content were fabricated using the currently developed techniques for the KUCA critical experiments.[34,36]

The total number of fabricated fuel plates were 294 with 32 different widths and curvatures. Specifications of MEU fuel plates are tabulated in Table II-3. An illustration of a fuel plate is shown in Fig. II-3. For reference, specifications of HEU fuel plates which were previously fabricated for the KUCA experiments are tabulated in Table II-4. Note that a design pitch between MEU fuel plates is 3.80 mm, whereas that of HEU fuel is 3.84 mm.

Table II-3 Specifications of MEU Fuel Plates

Plate No.	Inner fuel plate					Outer fuel plate				
	Width of fuel (mm)	Width of meat (mm)	Curvature (mm)	U (g)	^{235}U (g)	Width of fuel (mm)	Width of meat (mm)	Curvature (mm)	U (g)	^{235}U (g)
1	48.70	39.50	54.4	20.00	8.99	61.16	51.96	133.3	25.96	11.67
2	52.68	43.48	58.2	21.64	9.72	63.15	53.95	137.1	26.94	12.11
3	56.66	47.46	62.0	23.67	10.64	65.14	55.94	140.9	28.51	12.81
4	60.64	51.44	65.8	25.67	11.54	67.13	57.93	144.7	28.99	13.00
5	64.62	55.42	69.6	27.57	12.39	69.12	59.92	148.5	30.12	13.54
6	68.60	59.40	73.4	29.57	13.29	71.11	61.91	152.3	31.04	13.91
7	72.58	63.38	77.2	31.87	14.21	73.10	63.90	156.1	31.92	14.36
8	76.56	67.36	81.0	34.26	15.41	75.09	65.89	159.9	32.85	14.76
9	80.54	71.34	84.8	36.18	16.24	77.08	67.88	163.7	33.89	15.23
10	84.51	75.31	88.6	38.27	17.16	79.07	69.87	167.5	35.55	15.99
11	88.49	79.29	92.4	40.34	18.10	81.06	71.86	171.3	36.49	16.41
12	92.47	83.27	96.2	43.09	19.26	83.05	73.85	175.1	37.10	16.61
13	96.45	87.25	100.0	44.49	19.98	85.04	75.84	178.9	38.25	17.10
14	100.43	91.23	103.8	46.74	20.89	87.03	77.83	182.7	39.68	17.76
15	104.41	95.21	107.6	48.30	21.64	89.02	79.82	186.5	40.69	18.27
16	—	—	—	—	—	91.01	81.81	190.3	41.45	18.63
17	—	—	—	—	—	93.00	83.80	194.1	42.69	19.11

Fabricator: Compagnie pour l'Etude et la Realisation de Combustibles Atomiques (CERCA) in France.
Fuel meat: 600 mm long and 0.5 mm thick UAl_x-Al dispersion aluminide
^{235}U enrichment: 44.88%, U content: 41.70%
Fuel plate: 650 mm long and 1.4 mm thick Al plate
Designed fuel pitch: 3.80 mm

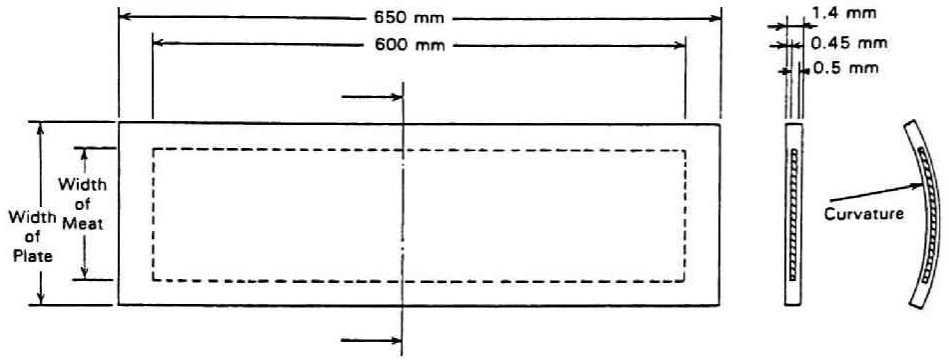

Fig. II-3 Illustration of a Fuel Plate

Table II-4 Specifications of HEU Fuel Plates

Plate No.	Inner fuel plate					Outer fuel plate				
	Width of fuel (mm)	Width of meat (mm)	Curvature (mm)	U (g)	^{235}U (g)	Width of fuel (mm)	Width of meat (mm)	Curvature (mm)	U (g)	^{235}U (g)
1	51.71	42.95	56.17	8.09	7.54	62.60	53.84	133.83	10.22	9.52
2	55.74	46.98	60.01	8.83	8.22	64.61	55.85	137.67	10.54	9.82
3	59.76	51.00	63.85	9.69	9.03	66.62	57.86	141.51	10.97	10.22
4	63.78	55.02	67.69	10.49	9.77	68.63	59.87	145.35	11.32	10.55
5	67.80	59.04	71.53	11.22	10.45	70.64	61.88	149.19	11.83	11.02
6	71.82	63.06	75.37	12.06	11.23	72.65	63.89	153.03	12.13	11.30
7	75.84	67.08	79.21	12.84	11.96	74.66	65.90	156.87	12.57	11.71
8	79.86	71.10	83.05	13.60	12.67	76.67	67.91	160.71	12.98	12.09
9	83.88	75.12	86.89	14.37	13.38	78.69	69.93	164.55	13.54	12.61
10	87.91	79.15	90.73	15.07	14.04	80.70	71.94	168.39	14.03	13.07
11	91.93	83.17	94.57	15.68	14.60	82.71	73.95	172.23	14.17	13.20
12	95.95	87.19	98.41	16.46	15.33	84.72	75.96	176.07	14.73	13.72
13	99.97	91.21	102.25	17.41	16.22	86.73	77.97	179.91	14.90	13.88
14	103.99	95.23	106.09	18.32	17.06	88.74	79.98	183.75	15.28	14.23
15	108.01	99.25	109.93	18.96	17.66	90.75	81.99	187.59	15.54	14.47
16	—	—	—	—	—	92.76	84.00	191.43	15.90	14.81
17	—	—	—	—	—	94.77	86.01	195.27	16.42	15.29

Fabricator: Nuclear Fuel Industries (NFI) in Japan
Fuel meat: 600 mm long and 0.5 mm thick U-Al alloy
^{235}U enrichment: 93.14%, U content: 22.11%
Fuel plate: 650 mm long and 1.4 mm thick Al plate
Designed fuel pitch: 3.84 mm

One by one, each fuel plate can be inserted between two aluminum side-plates to form a fuel element (refer to Fig. III-2). Illustrations of side-plates are shown in Fig. II-4. Special side-plates containing natural boron for MEU fuel plates were also fabricated.

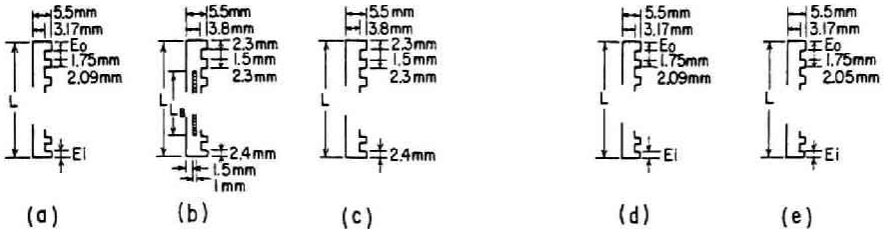

For MEU Fuel Plates

For HEU Fuel Plates

(a) Side-plate with 3.84 mm Pitch (without boron)
Inner fuel element : L=59.34 mm, Ei=1.75mm, Eo=2.08mm
Outer fuel element : L=67.41mm, Ei=2.10mm, Eo=2.12mm

(b) Side-plate with 3.80 mm Pitch (with boron)
Inner fuel element : L=59.40mm, L_B=48mm, ^{10}B=104 mg
Outer fuel element : L=67.00mm, L_B=55mm, ^{10}B=117 mg

(c) Side-plate with 3.80mm Pitch (without boron)
Inner fuel element : L=59.40 mm
Outer fuel element : L=67.00 mm

(d) Side-plate with 3.84 mm Pitch (without boron)
Inner fuel element : L=59.34 mm, Ei=1.75mm, Eo=2.08 mm
Outer fuel element : L=67.41 mm, Ei=2.10mm, Eo=2.12 mm

(e) Side-plate with 3.80 mm Pitch (without boron)
Inner fuel element : L=59.34 mm, Ei=2.42mm, Eo=1.97 mm
Outer fuel element : L=67.41 mm, Ei=2.42mm, Eo=2.44mm

Fig. II-4 Illustration of Side-Plates for MEU and HEU Fuels

III. CRITICAL EXPERIMENTS USING MEDIUM-ENRICHED-URANIUM FUEL

III-1. Introduction

The main objectives of the KUCA critical experiments using MEU fuel were as follows:

(1) To examine the nuclear characteristics of a light-water-moderated and heavy-water-reflected core loaded with MEU fuel comparable to HEU fuel through the critical experiments in the KUCA.

(2) To investigate experimentally the effects of reducing fuel enrichment on the core characteristics through the comparison between the cores loaded with HEU and MEU fuels.

(3) To provide the benchmark data for the use of MEU fuel in order to assess the computer codes employed in the neutronics calculations.

The critical experiments using MEU fuel in the KUCA were started in May 1981, as a first series of the MEU experiments in the world.[48,50] In this series of critical experiments, a mock-up core for a proposed high flux reactor was employed; namely, a light-water-moderated and heavy-water-reflected annular core with a central flux trap. The items of the KUCA critical experiments using MEU fuel were the measurements of (1) the criticality, (2) the control rod worth, (3) the reactivity effect of boron loaded side-plates, (4) the neutron flux distribution, (5) the kinetic parameter, (6) the void reactivity effect, and (7) the temperature effect on reactivity.[48-58] The experimental results are subsequently described in the following sections in comparison with those of the HEU core.

III-2. Description of the Cores Employed in the Critical Experiments

The KUCA is a multi-core type critical assembly, which has 3 core positions designated as A, B, and C.[78~84] Light-water is used as a moderator at the C-core position,[82] while the solid moderators such as polyethylene and graphite are used at the A-core and B-core positions. For the MEU critical experiments, the C-core position was utilized among the above 3 core positions. In an aluminum core tank of approximately 1.8 m in depth and 2 m in diameter at the C-core position, there is a grid plate onto which a fuel assembly is installed to form a core. Usually, light-water is dumped from the core tank and is stored in another aluminum tank located under the core tank. When the C-core is to be in operation, light-water is pumped up and fed to the core tank to form a light-water-moderated core.

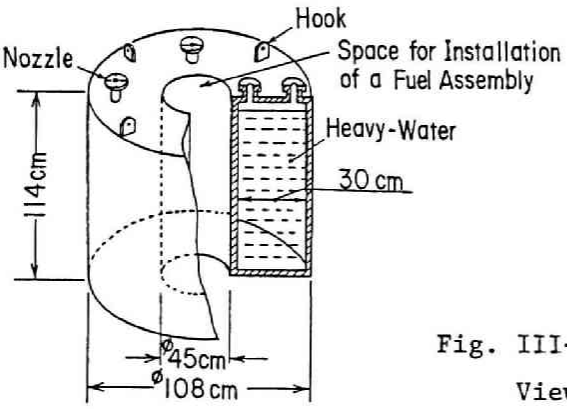

Fig. III-1
View of an Al Heavy-Water Tank

Figure III-1 shows an aluminum heavy-water tank which was employed in the present series of experiments as a container for a heavy-water reflector. This heavy-water tank of 45 cm in inner diameter and 108 cm in outer diameter was installed onto the grid plate in the C-core tank. Figure III-2 shows a view of the assembled fuel elements. This assembly was then installed in the center of the heavy-water tank to form a light-water-moderated and heavy-water-reflected core. Note here that each curved fuel

plate shown in Fig. II-3 can be inserted, one by one, between two side-plates shown in Fig. II-4 to form a fuel element, and the fuel elements are assembled in a cylindrical shape as shown in Fig. III-2.

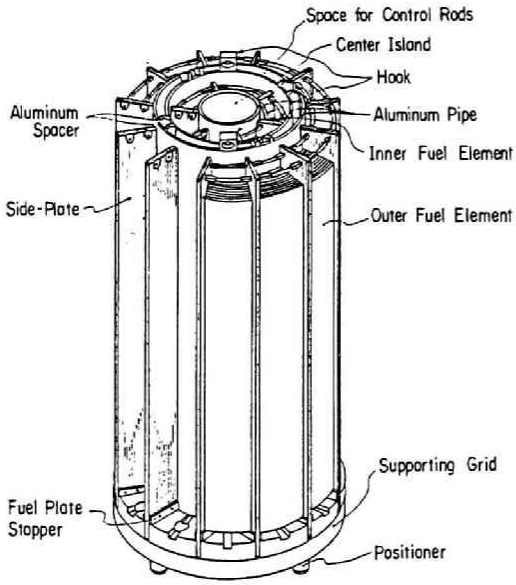

Fig. III-2 View of Assembled Fuel Elements

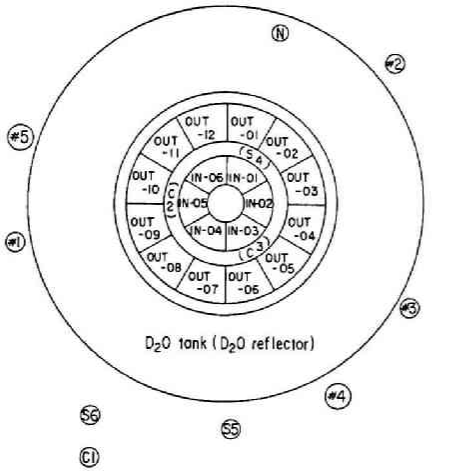

OUT-01 ~ OUT-12 : Outer fuel elements
IN-01 ~ IN-06 : Inner fuel elements
#1, #2, #3 : Start-up channels (FC)
#4, #5, #6 Lin-N, Log-N and Safety channels, respectively (UIC)
C1 ~ C3 : Control rods
S4 ~ S6 : Safety rods
N : Neutron source (Am-Be 2 Ci)

Fig. III-3
Typical Core Configuration Employed in the Experiments

The core had a cylindrical center island of light-water as a flux trap, and the fuel region was divided into two parts by an annular space

for the control rods. The inner fuel region consisted of 6 fuel elements which were numbered as IN-01, IN-02, ---, IN-06. The outer fuel region consisted of 12 elements numbered as OUT-01, OUT-02, ---, OUT-12, or EX-01, EX-02, ---, EX-12 depending on HEU or MEU fuel elements. The maximum of 15 fuel plates can be loaded into each inner fuel element and 17 plates into each outer fuel element.

A typical core configuration employed in the present series of experiments is shown in Fig. III-3. The criticality of the core was finally controlled by 3 control rods, namely C1, C2, and C3 rods, while all 3 safety rods (S4, S5, and S6) were fully withdrawn to their upper limit at every operation. The detectors for nuclear instruments (#1 through #6) were arranged around the heavy-water tank, under which a neutron source could be inserted.

III-3. Criticality Measurements

As a first step toward the criticality, all outer fuel elements were fully loaded with 17 fuel plates (204 fuel plates total). With use of the inverse multiplication method,[85] the criticality was approached by inserting fuel plates into the inner fuel elements from the outside toward the inside in order. At that time, all side-plates contained no boron. After the critical state of a core was achieved, the excess reactivity was measured by the positive period method.[85,86]

The experimental results are tabulated in Table III-1 in comparison with those of the HEU cores. Fuel loading patterns of the cores employed in the criticality measurements are shown in Fig. III-4. Note that the experimental error for the excess reactivity measurement in the KUCA

annular core is estimated to be approximately ± 0.005 %Δk/k from experience.

Table III-1 shows that the critical mass of ^{235}U in the MEU core is larger approximately 18 % than that of the HEU core. Table III-1 also shows that a minor change in fuel pitch from 3.84 mm to 3.80 mm evidently decreases the excess reactivities of both MEU and HEU cores. This indicates that both the HEU and MEU cores behave as under-moderated ones.

Table III-1 Measured Critical Mass and Excess Reactivity

	MEU Cores		HEU Cores		
No. of Fuel Plates	262		276		278
^{235}U Mass (g)	4165.7		3524.5		3542.5
U Total Mass (g)	9284		3784		3803
Al Pipe*	not used		used		not used
Fuel Loading Pattern	Fig.III-4(a)		Fig.III-4(b)		Fig.III-4(c)
Fuel Pitch (mm)	3.84	3.80	3.84	3.80	3.80
ρ_{ex} (%Δk/k)	0.211	0.077	0.468	0.129	0.165

* : This pipe separates the center island of light-water from the inner fuel elements (refer to Fig. III-2).

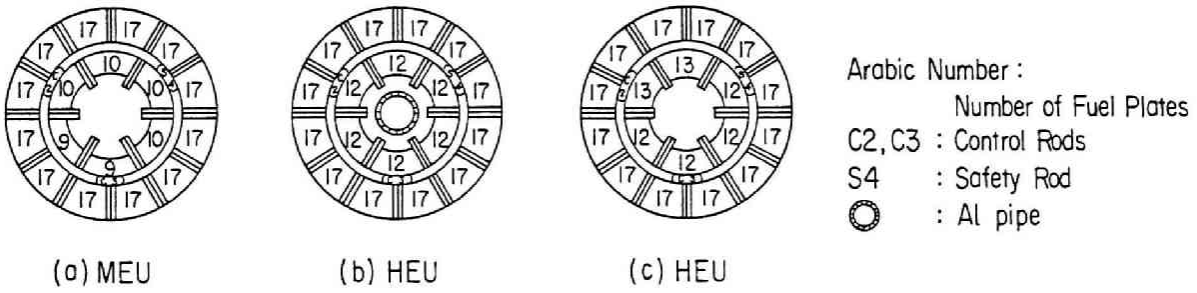

Fig. III-4 Fuel Loading Patterns Employed in the Criticality Measurements

Note here that an aluminum pipe shown in Fig. III-2, which separated the center island of light-water from the inner fuel elements was used in some of HEU cores, whereas this Al pipe was not used in any MEU core. The

reactivity effect of this Al pipe was positive from the experimental data listed in Table III-1. Namely, the critical states of the HEU cores with a 3.80 mm fuel pitch were achieved for both with and without this Al pipe. Therefore, from the consideration of this Al pipe effect mentioned above, the excess reactivity of the HEU core with a 3.84 mm fuel pitch would be less than the measured value and might possibly be negative (subcritical) when this Al pipe was not used. This Al pipe effect also indicates that the void reactivity effect in the central flux trap region is positive, since Al itself is often used as a void substitute.

III-4. Rod Worth Measurements

The safety and control rods in the KUCA basically consist of cadmium plates which absorb thermal neutrons. One can easily understand from the core configuration shown in Fig. III-3 that only 3 rods among 6 rods were worthy in the KUCA core, because only 3 rods located at the space for control rods and the other 3 rods located outside the heavy-water tank. Therefore, the reactivity worths of a safety rod (S4) and two control rods (C2 and C3) which located at the space for control rods were measured using the integral technique of the rod drop method.[85,86]

Note that there were two types of patterns for fuel loading in the KUCA cores. One was designated as Type-I, the other as Type-II. In the Type-I core, all outer fuel elements were fully loaded with 17 fuel plates and the criticality of the core was adjusted by inserting fuel plates into the inner fuel elements from the outside toward the inside in order. In the Type-II core to the contrary, all inner fuel elements were fully loaded with 15 fuel plates and the criticality was approached by inserting fuel

plates into the outer fuel elements from the inside toward the outside in order. These two types of fuel loading patterns were employed in the experiments to investigate the effects of the reflectors including the central flux trap of light-water, the light-water gap between the heavy-water reflector and the outer fuel region, and the heavy-water reflector. Furthermore, boron loaded side-plates were prepared for MEU cores. Therefore, the effects caused by the change in fuel loading pattern and the use of boron loaded side-plates on control rod worth were investigated in the measurements.

Table III-2 Reactivity Worths of Rods Measured by the Rod Drop Method in the Type-I Core Containing No Boron

	MEU Core		HEU Core
C2 Rod Worth (%Δk/k)	0.71	0.76	0.79
C3 Rod Worth (%Δk/k)	0.71	0.80	0.82
S4 Rod Worth (%Δk/k)	0.74	0.73	0.85
Total Rod Worth (%Δk/k)	2.16	2.29	2.46
Fuel Loading Pattern	Fig.III-5(a)	Fig.III-5(b)	Fig.III-5(c)
No. of Fuel Plates	262	263	278
Fuel Pitch (mm)	3.84	3.80	3.80

Table III-3 Reactivity Worths of Rods Measured by the Rod Drop Method in the Type-II Core Containing No Boron

	MEU Core	HEU Core
C2 Rod Worth (%Δk/k)	0.81	0.77
C3 Rod Worth (%Δk/k)	0.82	0.86
S4 Rod Worth (%Δk/k)	0.75	0.88
Total Rod Worth (%Δk/k)	2.37	2.50
Fuel Loading Pattern	Fig.III-5(d)	Fig.III-5(e)
No. of Fuel Plates	256	275
Fuel Pitch (mm)	3.80	3.80

The measured results are tabulated in Tables III-2, III-3, and III-4 in comparison with those of the HEU cores. Fuel loading patterns of the cores where the measurements were carried out are shown in Fig. III-5. Note that the experimental error for the total rod worth measurement in the KUCA annular core by the rod drop method is estimated to be less than 5 % from experience.

Table III-4 Reactivity Worths of Rods Measured by the Rod Drop Method in the Type-I MEU Core Containing Boron

	All Outer Side-Plates Containing Boron	All Inner Side-Plates Containing Boron
C2 Rod Worth (%Δk/k)	0.66	0.70
C3 Rod Worth (%Δk/k)	0.70	0.74
S4 Rod Worth (%Δk/k)	0.73	0.77
Total Rod Worth (%Δk/k)	2.09	2.21
Fuel Loading Pattern	Fig.III-5(f)	Fig.III-5(g)
No. of Fuel Plates	287	282
Fuel Pitch (mm)	3.80	3.80

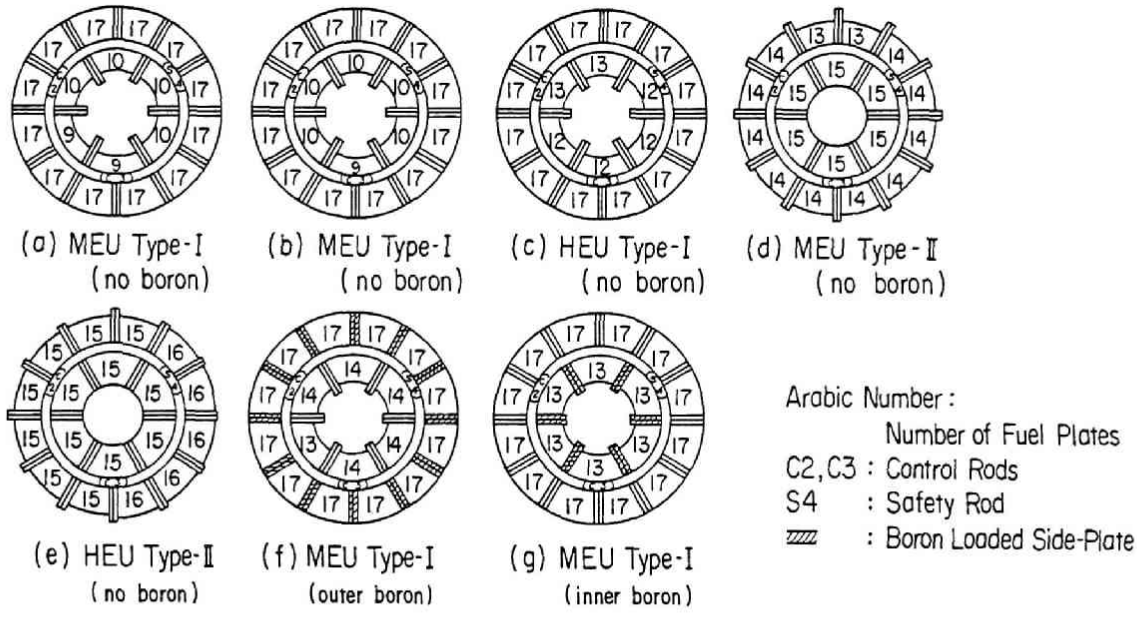

Fig. III-5 Fuel Loading Patterns Employed in the Rod Worth Measurements

Tables III-2, III-3, and III-4 show that the worth of each rod is sensitive to the minor change in fuel loading pattern and varied case by case. However, the total rod worth is considered to be not very sensitive to the minor change in fuel loading pattern. The direct comparison of the control rod worth between MEU and HEU cores and between MEU cores with and without boron loaded side-plates are difficult, since the numbers of fuel plates loaded in MEU and HEU cores are different with each other and the relative locations of the control rods in the cores are different accordingly. However, from Tables III-2 and III-3, it is indicated that the total rod worth in an MEU core is smaller than that of an HEU core. From Tables III-2 and III-4, it is also indicated that the total rod worth in a core with boron loaded side-plates is smaller than that of a core without boron loaded side-plates. These phenomena can be explained by the consideration that the thermal neutron flux in an MEU core is lower than that of an HEU core.

III-5. Measurements of the Boron Reactivity Effect

The side-plates containing natural boron was originally designed to act on a core as the burnable poison which suppresses the excess reactivity of the initial core loaded with fresh fuel for the purpose of obtaining a longer fuel life. The boron content in a side-plate was originally determined through the Phase B study of the ANL-KURRI joint study for the proposed KUHFR.[45] Note that a fuel element consists of two side-plates with or without boron and boron loaded side-plates are prepared only for MEU fuel plates.

The reactivity effects of boron loaded side-plates [BP effects] were measured in the following manner; by substituting a fuel element with boron for an element without boron one by one, the excess reactivity or subcriticality of the core was measured before and after the substitution. The excess reactivity was measured by the positive period method,[85] and the subcriticality was measured by the source multiplication method.[87] The BP effect was obtained from the difference between the reactivities measured before and after each substitution.[48,50]

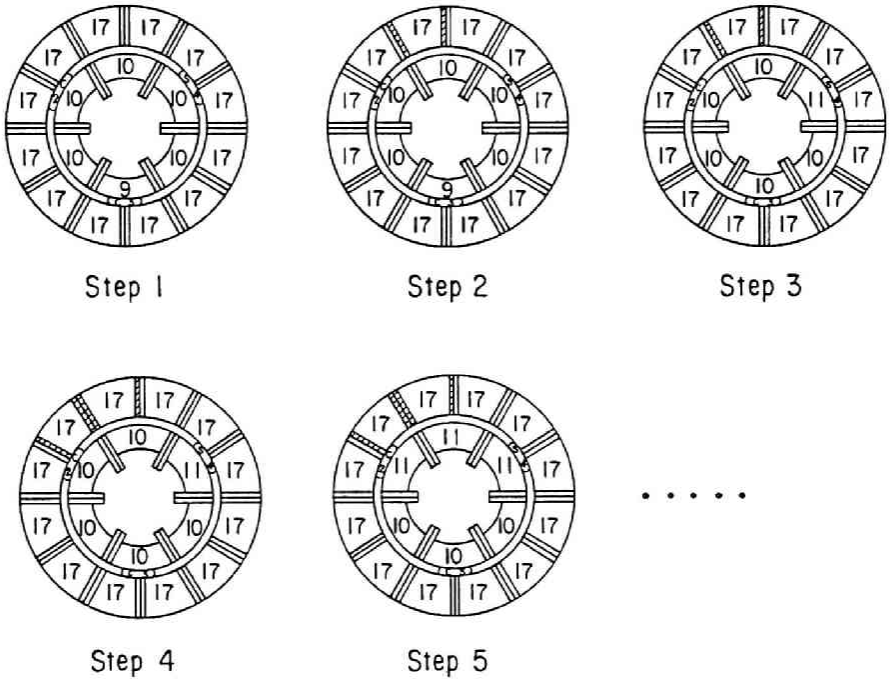

Fig. III-6 Experimental Procedure of the BP Effect Measurements in the Outer Fuel Region

In each measurement, an objective fuel element for a substitution was filled to its capacity with fuel plates. For the measurements of BP effects in the outer fuel region, a Type-I core was employed. Namely, all

outer fuel elements were loaded with 17 fuel plates and the criticality was essentially adjusted by the number of fuel plates inserted into the inner part of the inner fuel element. The experimental procedure for the BP effect measurements in the outer fuel region is shown in Fig. III-6.

On the other hand, for the BP effect measurements in the inner fuel region, a Type-II core was employed. Namely, all inner fuel elements were loaded with 15 fuel plates and the criticality was adjusted by the number of fuel plates inserted into the outer part of the outer fuel element. The experimental procedure for the BP effect measurements in the inner fuel region is shown in Fig. III-7.

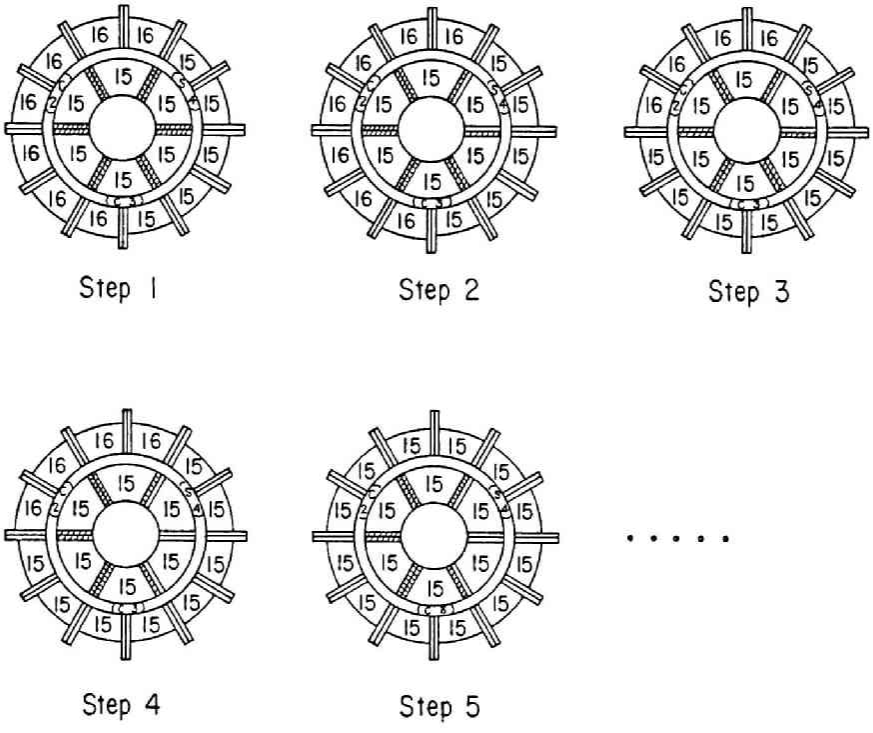

Fig. III-7 Experimental Procedure of the BP Effect Measurements in the Inner Fuel Region

Therefore, through the BP effect measurements, the mass reactivity effects of fuel plates were also obtained. Note that, in the BP effect measurements, the fuel pitch in the element with boron was 3.80 mm and the pitch in the element without boron was 3.84 mm.

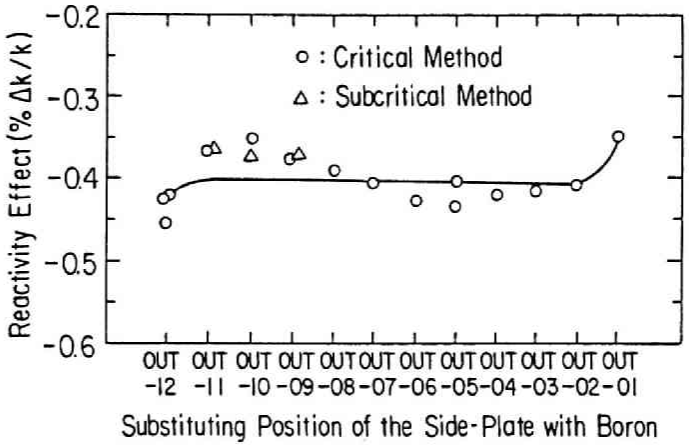

Fig. III-8 Reactivity Effects Caused by Each Substitution of a Fuel Element with Boron for an Element without Boron in the Outer Fuel Region

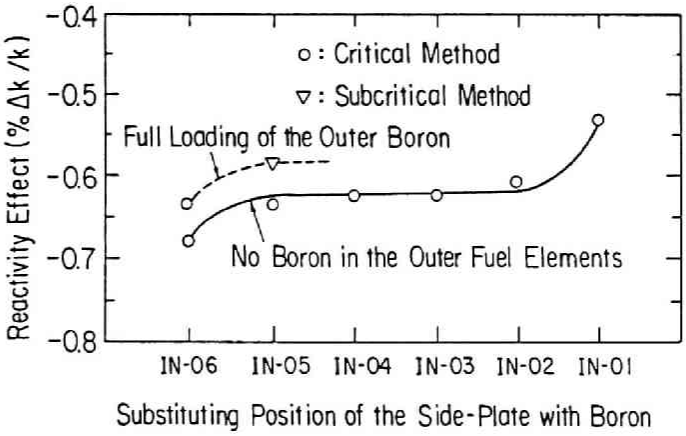

Fig. III-9 Reactivity Effects Caused by Each Substitution of a Fuel Element with Boron for an Element without Boron in the Inner Fuel Region

The results of the BP effect measurements are shown in Figs. III-8, III-9, and III-10, and are tabulated in Table IV-3 of Chapter IV together

with the results of the mass reactivity effects of fuel plates in comparison with the calculated results. The BP effects for the substitution were approximately -0.4 %Δk/k per outer fuel element and -0.6 %Δk/k per inner element, whereas ^{10}B mass in each outer side-plate was 117 mg and that of an inner side-plate was 104 mg. Therefore, on contrary to the fact that ^{10}B mass in an outer fuel element was heavier than that of an inner element, the BP effect in the outer fuel region was smaller than that of the inner fuel region. This indicates that the thermal neutron flux in the inner fuel region is higher than that of the outer fuel region. This conjecture is supported by the experimental data that the mass reactivity effects of fuel plates in the inner fuel region was larger than those of the outer fuel region (refer to Table IV-3 in Chapter IV). One can estimate the experimental error for the BP effect measurement from Fig. III-8, in which raw data are plotted. That is approximately ± 0.01 %Δk/k for each substitution.

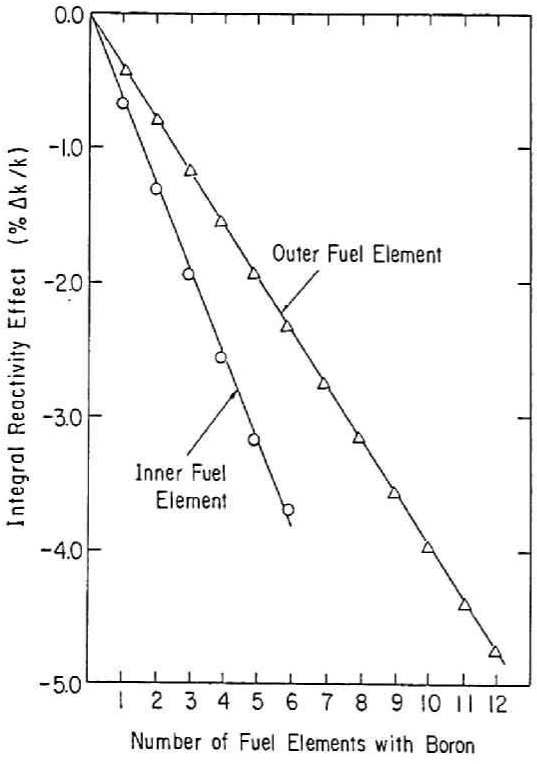

Fig. III-10
Integral Reactivity Effects of the Inner and Outer Elements Containing Boron

In addition, due to the interference effect between adjacent side-plates with boron, the reactivity effect of each substitution was not constant for each substitution. The total BP effects were approximately -4.7 %Δk/k in the outer fuel region when there was no boron loaded side-plate in the inner fuel region, and -3.7 %Δk/k in the inner fuel region when there was no boron in the outer fuel region. In consideration of the interference effect between the inner and outer side-plates with boron, which can be estimated from Fig. III-9 as approximately 0.05 %Δk/k per inner fuel element when all outer side-plates containing boron, the total BP effect would be approximately -8 %Δk/k for the whole core.

III-6. Measurements of the Neutron Flux Distribution

The neutron flux distributions in the MEU cores were measured using the foil activation technique.[85,88] Gold wires of 0.5 mm diameter, with and without cadmium sheath, were activated in various regions of the core.[51] The relative neutron flux distributions were obtained for various positions. Cadmium sheath of 0.5 mm thickness and 1 mm inner diameter was employed in order to obtain the thermal neutron flux distributions only in the vertical direction.

The irradiated positions of Au wires are shown in Figs. III-11 and III-12. The numerical symbols "1 ∿ 11" in Figs. III-11 and III-12 indicate the positions where Au wires were set vertically, whereas the alphabetical symbols "a ∿ p" indicate Au wires set horizontally. Two types of cores were employed for the measurements; namely, with and without an acrylic void tube of 9.2 cm inner diameter and 8 mm thickness at the central flux trap region of light-water. In the core with an acrylic void tube, the

horizontal neutron flux distributions were mainly measured and the thermal neutron flux distributions were obtained only at the positions "2" and "5" shown in Fig. III-11. In the core without void, the thermal neutron flux distributions were mainly measured along the vertical direction.

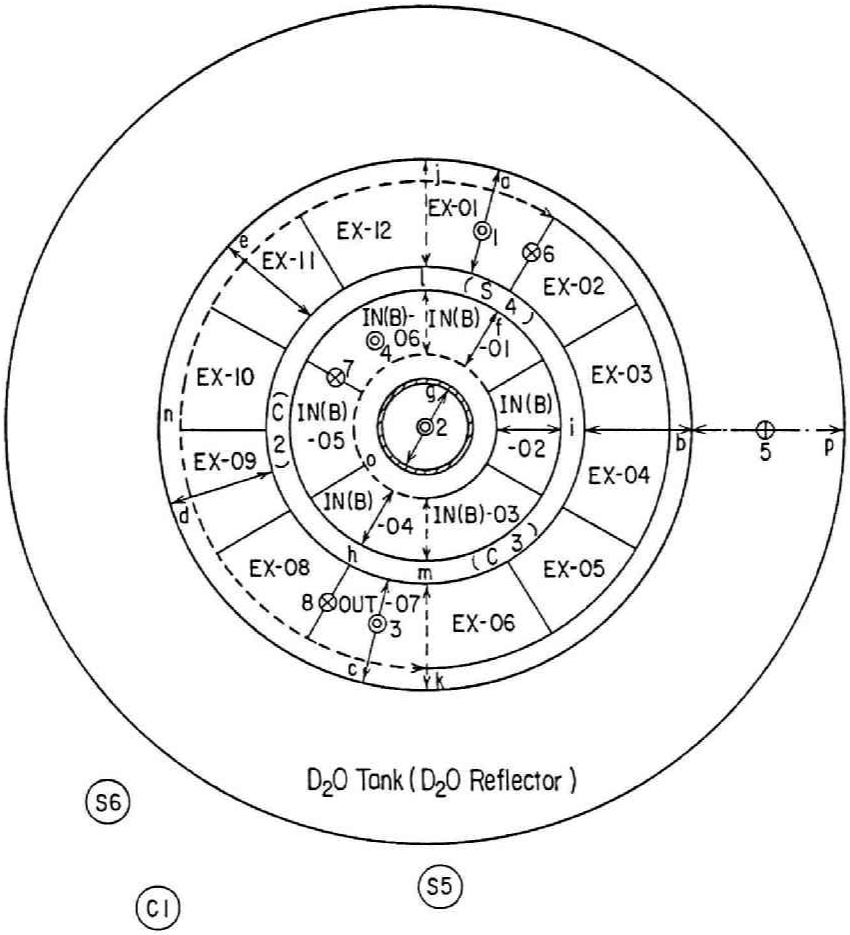

IN(B)-01~IN(B)-06 : Inner Fuel Elements (Containing Boron)
EX-01~06,08~12 : Outer Fuel Elements (〃 〃)
OUT-07 : Outer Fuel Elements (Containing no Boron)
C1~C3 : Control Rods
S4~S6 : Safety Rods
⊛ : Acrylic Void Tube
◎1,2,3,4,⊕5,⊗6,7,8 : Positions of Gold Wires (Vertical. Direction)
a~i : 〃 〃 (at the Top of Fuel Plate)
j~o : 〃 〃 (at the Middle of Fuel Plate)
p : 〃 〃 (at 44 mm Below the Middle of Fuel Plate)

Fig. III-11 Irradiated Positions of Au Wires in the MEU Core with a Central Void

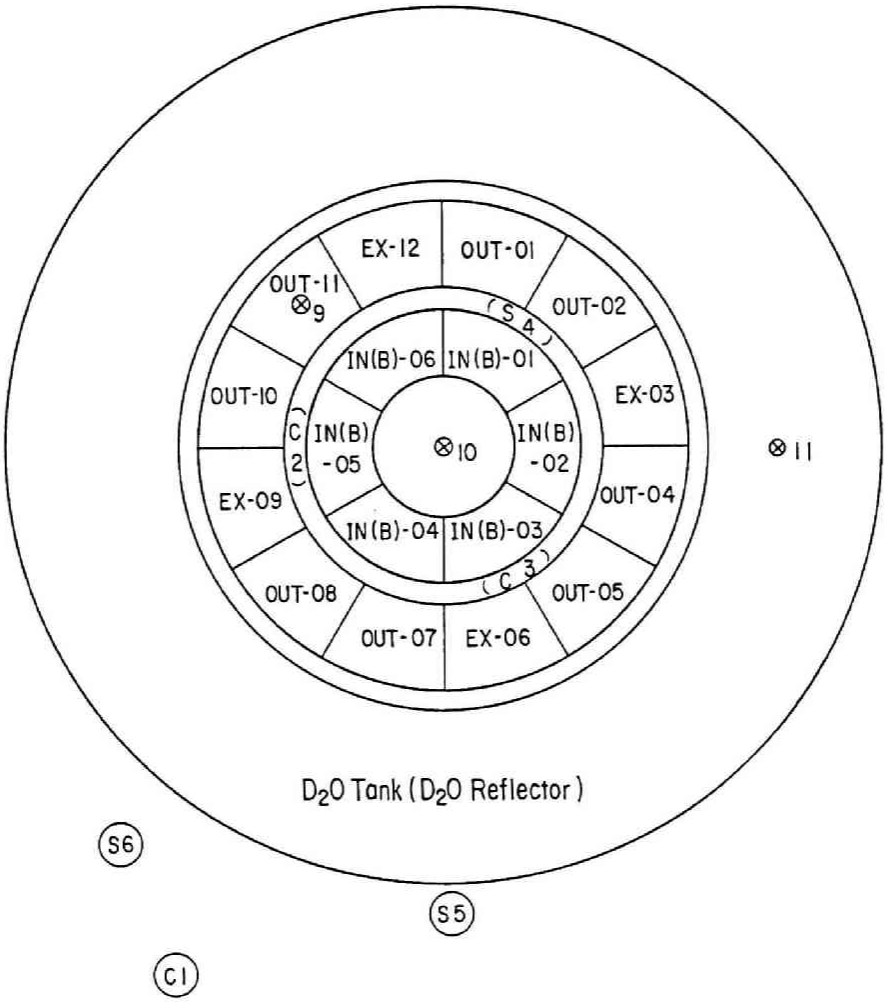

IN(B)-01~IN(B)-06: Inner Fuel Elements (Containing Boron)
EX-03,06,09,12 : Outer Fuel Elements (〃 〃)
OUT-01,02,04,05 07,08,10,11 : Outer Fuel Elements (Containing no Boron)
C1~C3 : Control Rods
S4~S6 : Safety Rods
⊗9,10,11 : Gold Wire Setting Positions (with and without Cadmium Sheath)

Fig. III-12 Irradiated Positions of Au Wires in the MEU Core without a Central Void

The MEU cores were fully loaded with 294 fuel plates in the measurements. Therefore, the criticality of cores were essentially adjusted by the number of fuel elements consisted of boron loaded side-plates. The Au wires were irradiated at a reactor power of approximately 1 W. Each irradiation time was 30 minutes. After the irradiation, Au wires were cut

into small pieces of 1 ∿ 2 cm length. The gamma-rays of 412 keV emitted from the decay of ^{198}Au were counted with an automatic sample changer (OKEN model S-1023) which consists of a well-type NaI(Tl) scintillator of 2" diameter and 3" length.

Horizontal Neutron Flux Distributions

Typical neutron flux distributions in the horizontal direction are shown in Figs. III-13, III-14, and III-15.

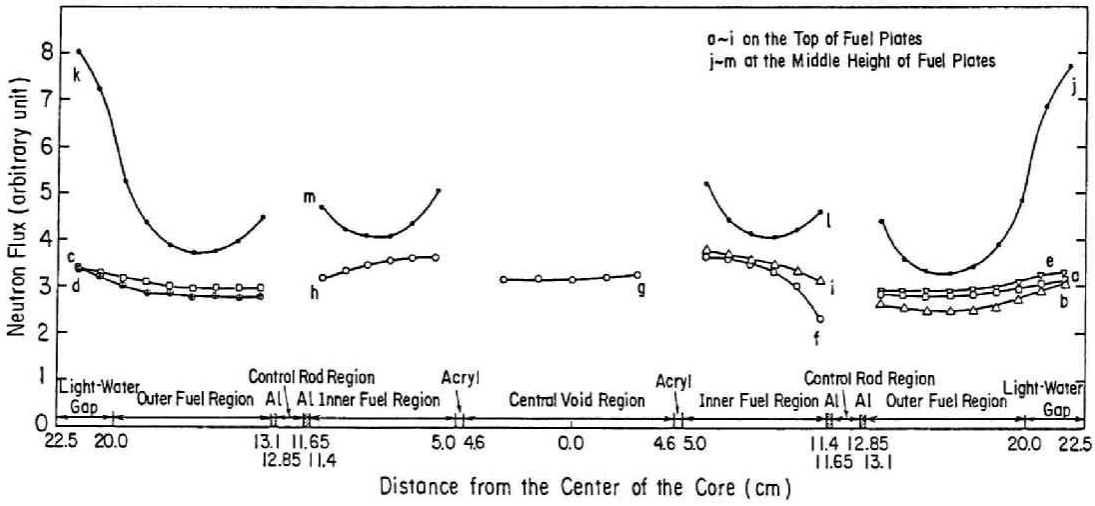

Fig. III-13 Horizontal Neutron Flux Distributions in the MEU Core with a Central Void at the Positions "a ∿ m" Shown in Fig. III-11

Figure III-13 shows the neutron flux distributions in the fuel region and in the central void tube. This figure shows that the thermal neutron flux in the inner fuel region is higher than that of the outer fuel region. Neutron flux distributions at the positions "j ∿ m", measured at the middle height of the fuel plates between the side-plates, have some depressions in the fuel region due to boron contained in the side-plates. Neutron flux distributions at the positions "j ∿ m" also indicate that there are flux

peaks at the central flux trap, at the control rod region, and at the light-water gap between the outer fuel elements and the heavy-water reflector caused by the existence of light-water. This figure shows that the neutron flux at the position "g" in the central void tube is flat, since there is no neutron scattering and absorbing material in a void region. At the outer part of the inner fuel region, the neutron flux at the position "f", which was measured on the top of fuel plates, is more depressed than that of the position "i". This is because the lower edge of the fully withdrawn safety rod S4 was near that position at the irradiation of Au wire.

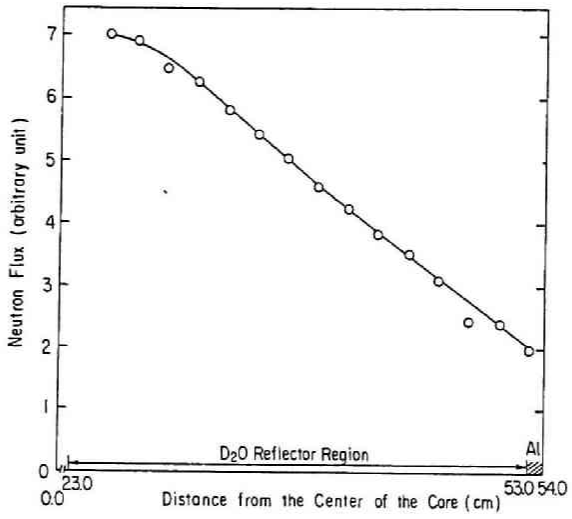

Fig. III-14 Horizontal Neutron Flux Distribution in the MEU Core with a Central Void at the Position "p" Shown in Fig. III-11

Figure III-14 shows the neutron flux distribution measured at 4.4 cm below the middle height of the fuel plates in the heavy-water reflector. This distribution has no peak and decreases rather rapidly with the distance from the center of core. This phenomenon is attributed to the facts that there is light-water gap of approximately 2.5 cm thickness between the outer fuel elements and the heavy-water reflector and a 30 cm thick heavy-

water layer is not sufficient enough for a neutron reflector. Although the horizontal neutron flux distributions have not been measured in an HEU core, it is considered that the similar feature to this can be observed in an HEU core, since the similar results to those in the MEU core was obtained in the HEU core for the vertical flux distributions (refer to Figs. III-20 and III-21).

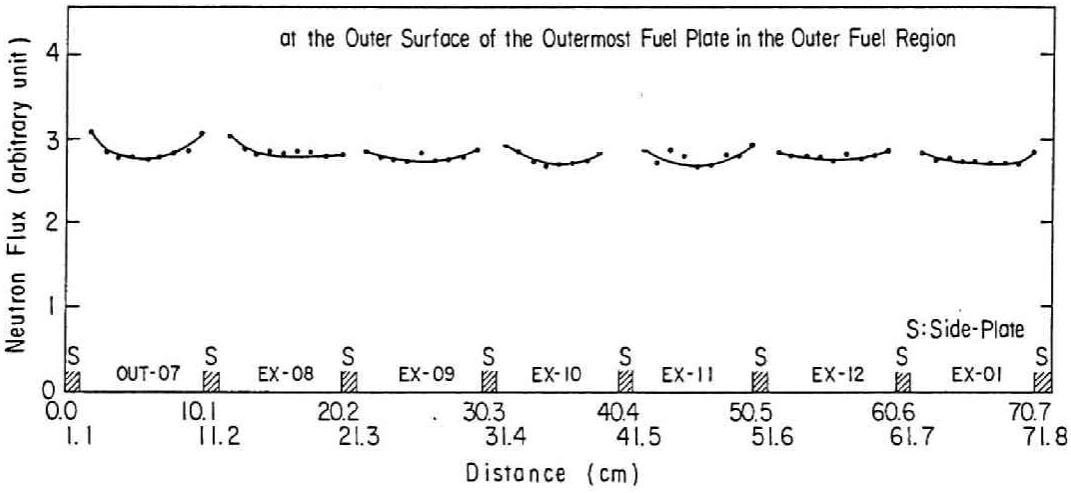

Fig. III-15 Horizontal Neutron Flux Distributions in the MEU Core with a Central Void at the Position "n" Shown in Fig. III-11

Figure III-15 shows the neutron flux distribution measured at the middle height of the fuel plates in the azimuthal direction at the outer surface of the outer fuel fuel region. Although most side-plates contain boron, there are flux peaks in the vicinities of side-plates regardless of with and without boron. However, the flux peaking is larger at the region without boron than that at the region with boron. This is attributable to the fact that a region in the vicinity of side-plates consists of not only aluminum but also light-water. One can find from this figure that the experimental error in the neutron flux measurement was around a few percent.

Vertical Neutron Flux Distributions

Typical neutron flux distributions in the vertical direction in the core with a central void are shown in Figs. III-16, III-17, and III-18, and those for the core without a central void are shown in Figs. III-19 and III-20.

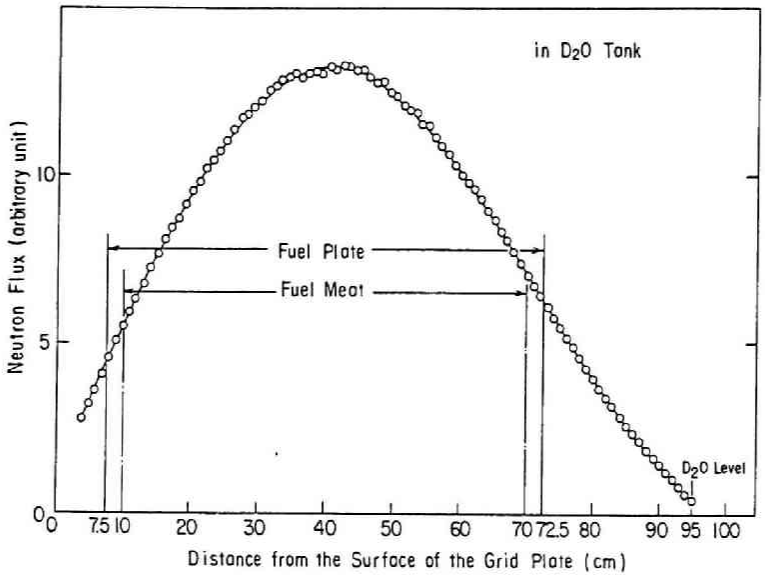

Fig. III-16 Vertical Neutron Flux Distribution in the MEU Core with a Central Void at the position "5" Shown in Fig. III-11

Figure III-16 shows the neutron flux distribution in the heavy-water reflector. The neutron flux at the height of the upper edge of fuel plates is higher than that of the lower edge. Similar asymmetric features can be observed in all of the vertical neutron flux distributions. The reason is that the thicknesses of light-water and heavy-water layers are not the same at the upper and lower sites. At the upper site, they are much thicker than those at the lower site. In addition, there are layers of other materials such as the aluminum basements of fuel elements and the stainless-steel grid plate of the core tank at the lower site. These materials

are not favorable in a view point of the neutron reflection and thermal neutrons are strongly absorbed by a stainless-steel layer.

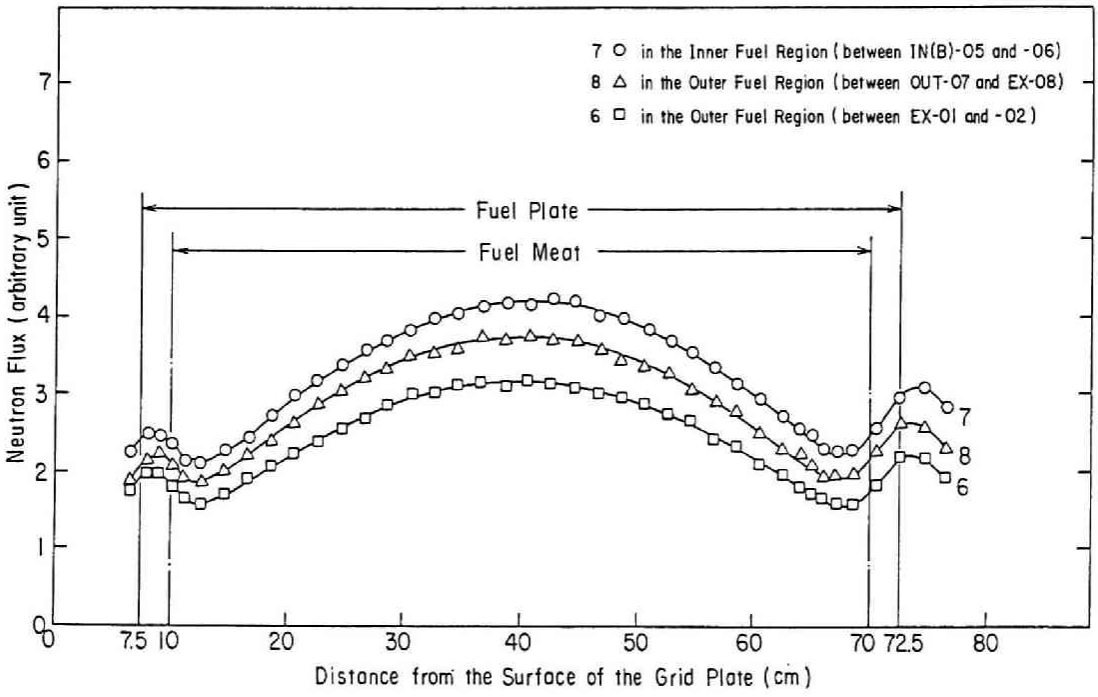

Fig. III-17 Vertical Neutron Flux Distributions in the MEU Core with a Central Void at the Positions "6 ∿ 8" Shown in Fig. III-11

Figure III-17 shows the neutron flux distributions between the side-plates in the fuel region. This figure shows that the neutron flux in the inner fuel region is higher than those of the outer fuel region. In the outer fuel region, the neutron flux at the position "8" is higher than that of the position "6". The difference between the positions "6" and "8" in the outer fuel region is attributed to that the position "6" is sandwiched between two boron loaded side-plates and the position "8" is sandwiched between side-plates with and without boron. At the upper and lower sites of the fuel plates, the neutron flux peaks can be observed due to the existence of the light-water reflectors.

Figure III-18 shows the neutron flux distributions along center axes of the central void, outer fuel, and inner fuel regions. This figure shows that the neutron flux in the central void is the highest, that of the inner fuel region is the second, and those of the outer fuel region are the third. In outer fuel region, the difference between fuel elements with and without boron is not so clear as that shown in Fig. III-17. In the fuel regions, the ratios of the neutron flux peaks at the upper and lower sites of the fuel plates to the neutron flux peaks at the middle of the fuel plates in Fig. III-18 are higher than those in Fig. III-17. The reason is that the neutron flux is measured at the side-plate region in Fig. III-17, whereas that is measured at the actually fueled region in Fig. III-18.

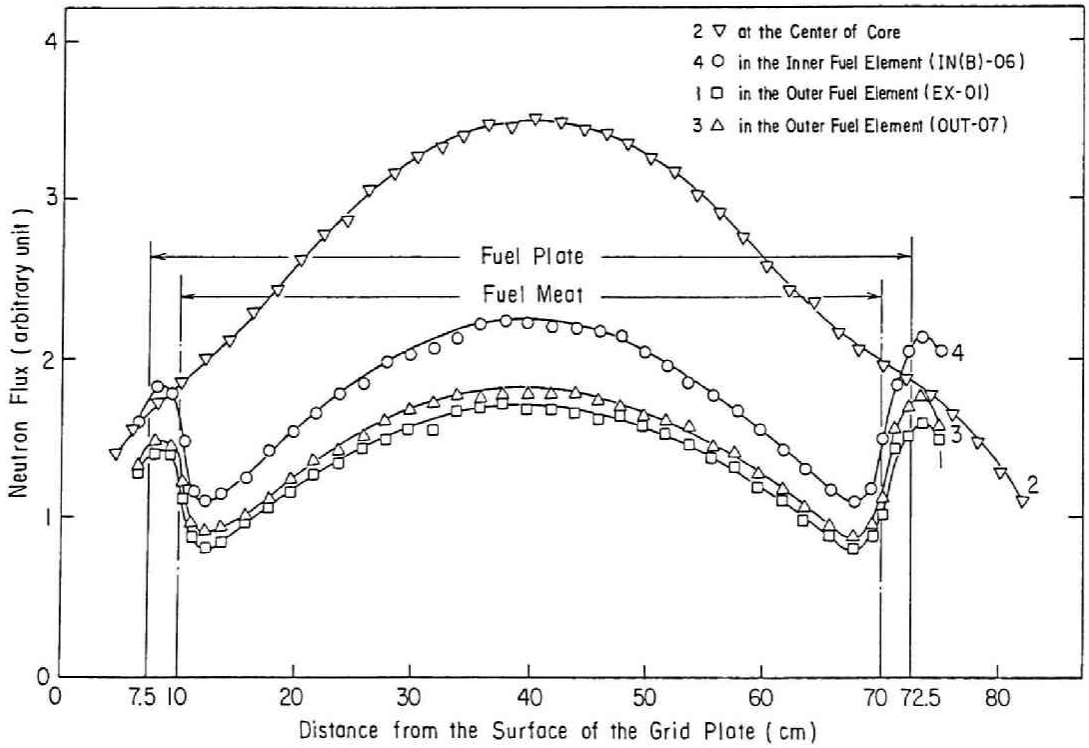

Fig. III-18 Vertical Neutron Flux Distributions in the MEU Core with a Central Void at the Positions "1 ∿ 4" Shown in Fig. III-11

The experimental data show that, in MEU core with a central void, the neutron flux in the heavy-water reflector is the highest, the second is that of the central void region, and the third is that of the side-plate region, and the lowest is that of the fuel region. Furthermore, the neutron flux in the inner fuel region is higher than that of the outer fuel region as suggested previously in Section III-5. The cadmium ratios in the central void and heavy-water regions were approximately 1.7 and 20 at the middle height of the fuel plate, respectively.

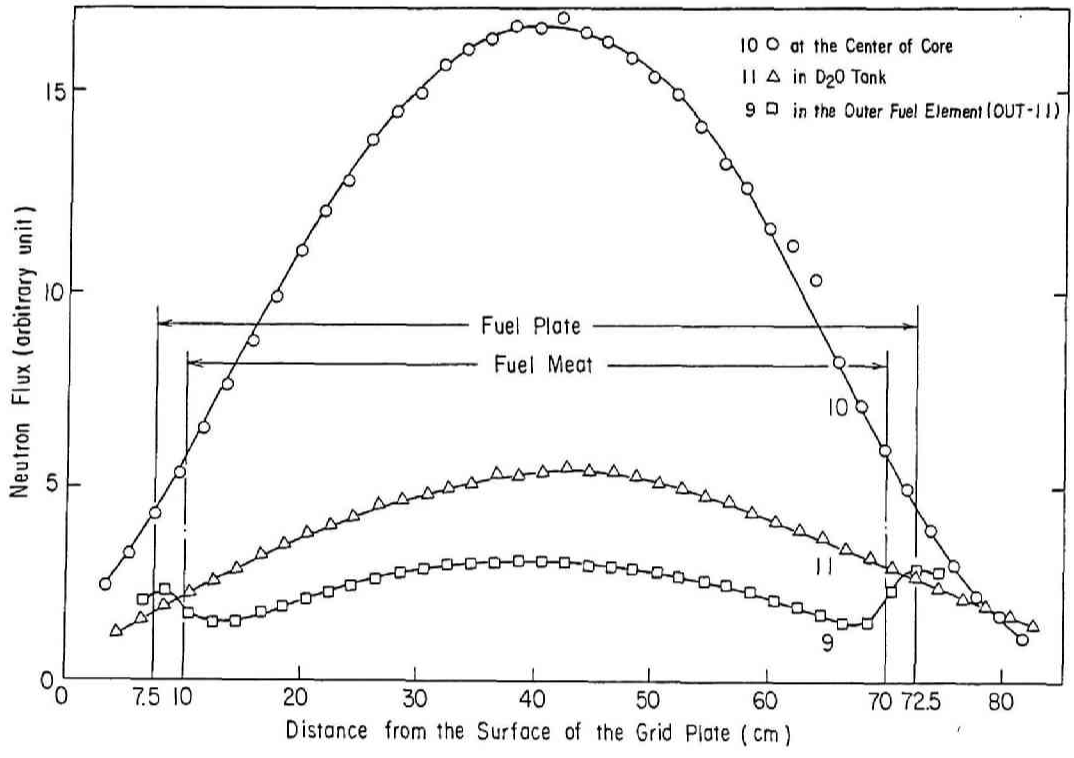

Fig. III-19 Vertical Neutron Flux Distributions in the MEU Core without a Central Void at the Positions "9 ∿ 11" Shown in Fig. III-12

Figure III-19 shows the neutron flux distributions along the center axes of the central flux trap of light-water, the outer fuel region, and the heavy-water reflector. The neutron flux in the central flux trap is distinctly higher than anywhere else and the neutron flux in the heavy-

water reflector is higher than that of the outer fuel region, whereas the neutron flux in the heavy-water reflector is the largest in the MEU core with a central void. This indicates that the central light-water region has a good capability as a neutron flux trap.

Figure III-20 shows the neutron flux distributions at the same positions as those shown in Fig. III-19. The cadmium ratios in the central flux trap, heavy-water reflector, and outer fuel regions were approximately 16, 30, and 3.0 at the middle height of the fuel plate, respectively. Therefore, the cadmium ratios in the central flux trap and heavy-water reflector regions in the core without void were larger than those of the core with a central void.

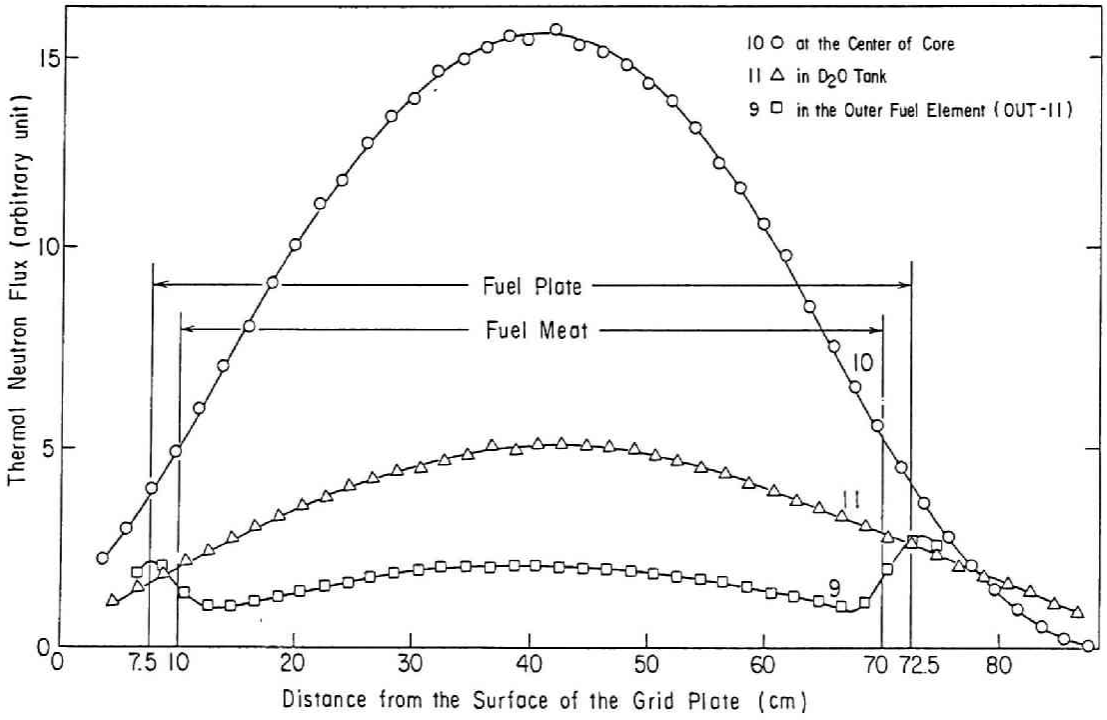

Fig. III-20 Vertical Flux Distributions of Thermal Neutrons in the MEU Core without a Central Void at the Positions "9 ∿ 11" Shown in Fig. III-12

In the HEU core, only the vertical neutron flux distributions were measured. Figure III-21 shows the thermal neutron flux distributions along the center axes of the central flux trap of light-water, the inner and outer fuel regions, and the heavy-water reflector. Note that the HEU core was not fully loaded with the fuel plates and had a wider central flux trap region of light-water. Moreover, the boron loaded side-plates were not utilized in the HEU core.

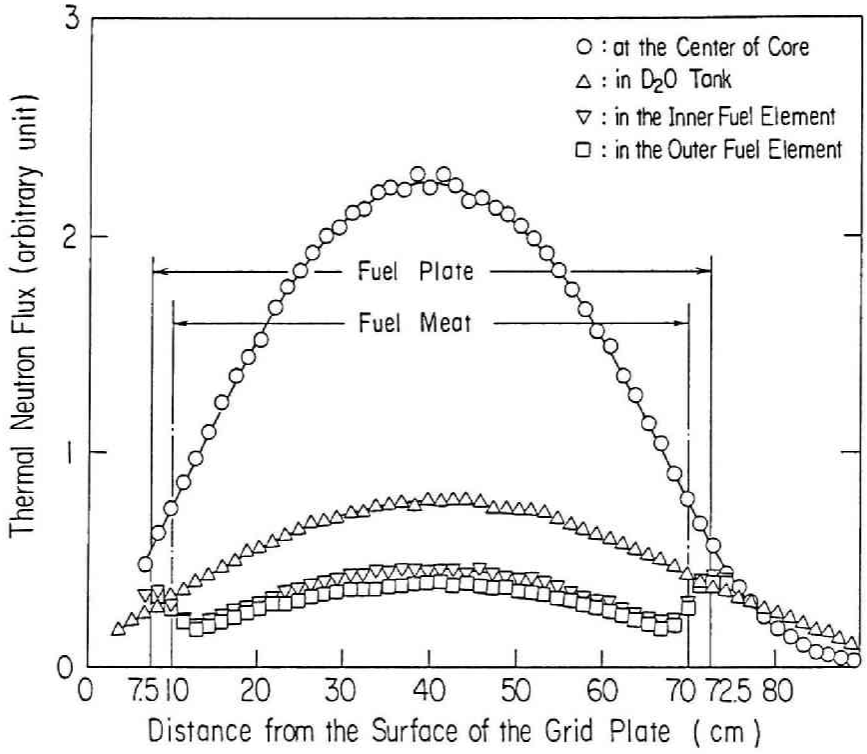

Fig. III-21 Vertical Flux Distributions of Thermal Neutrons in the HEU Core at the Central Flux Trap, Inner and Outer Fuel, and D_2O Reflector Regions

Figure III-21 shows that the neutron flux in the central flux trap is the highest, the second is that of the heavy-water reflector, the third is that of the inner fuel region, and the lowest is that of the outer fuel region. The neutron flux peaks are observed at the upper and lower sites of the fuel plate in the inner and outer fuel regions. These phenomena in

the HEU core are consistent with those in the MEU core. The cadmium ratios in the central flux trap, heavy-water reflector, outer fuel, and inner fuel regions in the HEU core without void were measured as approximately 18, 15, 3.8, and 3.6 at the middle height of the fuel plate, respectively. Hence, the cadmium ratios in the HEU core were larger than those of the MEU core except for the heavy-water reflector region. This indicate that the neutron spectra in an MEU core are harder than those of an HEU core.

From Fig. III-20, the neutron flux peaks in the central flux trap and heavy-water reflector regions are approximately 8 and 2.5 times larger than that of the outer fuel region. Whereas, in the HEU core, the neutron flux peaks in the central flux trap and heavy-water reflector regions were approximately 6 and 2 times larger than those of the outer fuel region, respectively, as shown in Fig. III-21. It is inadequate to compare these results directly, since there exists a difference between the configurations of MEU and HEU cores. However, the above results indicate that there is a recovery mechanism of the thermal neutron flux in a reflector including a flux trap for the reduction of the thermal neutron flux in a fuel region due to the reduction in ^{235}U enrichment.

Table III-5 Reflector Savings in the MEU and HEU Cores

Region	MEU Core	HEU Core
Heavy-Water Reflector	9.8 ± 0.3	9.8 ± 0.3
Outer Fuel Region	7.8 ± 0.1	8.3 ± 0.3
Inner Fuel Region	———	7.9 ± 0.1
Central Flux Trap	8.1 ± 0.1	8.3 ± 0.2

The thermal neutron flux distributions in the MEU core without void were fitted to cosine curves using the least square method in order to obtain vertical reflector savings.[7] The reflector saving is especially important to determine the transverse buckling of a core which should be

used in the two-dimensional calculations. The results are tabulated in Table III-5 in comparison with those of the HEU core. Since there exists a difference between the core configurations of the MEU and HEU cores, a direct comparison may not be adequate. However, the region dependent reflector savings in the MEU and HEU cores approximately agreed with each other.

III-7. Kinetic Parameter Measurements

Among the kinetic parameters, the ratio of the delayed neutron fraction β to the prompt neutron life time ℓ is especially important for the kinetics of a nuclear reactor and a value of β/ℓ is often used for the reactor safety calculations. Therefore, the kinetic parameter β/ℓ was measured in the MEU core using the Feynman-α method[85,89~95] and the pulsed neutron method.[85,86,96]

In the pulsed neutron experiments, fission chambers of 0.5" diameter were located at the center of the flux trap and at the middle of the heavy-water reflector and a pulsed neutron source of a handy type (KAMAN NUCLEAR model A-800/801) was located outside the heavy-water tank. With use of the Simmons and King technique,[96] the decay constants of the prompt neutrons α were measured for a few subcritical states of which reactivities were previously known. By plotting a curve of α versus the subcriticality, the curve was extrapolated to the critical state for determining a value of β/ℓ.

In the Feynman-α experiments, a BF_3 counter of 0.5" diameter was located at the center of the flux trap region and a ^3He counter of 0.5" diameter was located at the middle of the heavy-water reflector. At a

critical state, a value of α which corresponds to β/ℓ was measured by using a pulse rate analysis mode of a multi-channel analyzer (HITACHI 505A).[95]

The agreement between β/ℓ values measured by the above two methods was very good. The results are tabulated in Table III-6 in comparison with those of the HEU core. Note that only the Feynman-α method was employed in the HEU core and Type-I cores (refer to Section III-4) were used for the measurements.

Table III-6 β/ℓ Values in the MEU and HEU Cores

	MEU Cores		HEU Core
Number of Fuel Plates	262	294	277
Boron Loaded Side-Plates	not used	used	not used
β/ℓ (sec^{-1})	67 ± 2	79 ± 2	68 ± 3

A value of β/ℓ in a small sized core depends strongly on a core configuration. In the present core, it depends strongly on an effectiveness of a reflector including a flux trap. When the effectiveness of the heavy-water reflector grows higher, the value of β/ℓ would decrease. On contrary, when the flux trap of light-water grows more effective, β/ℓ would increase its value. This tendency can be seen in Table III-6. The effectiveness of the light-water flux trap for the neutron reflection grows higher with the increase in number of fuel plates loaded into the core, because the volume of flux trap becomes smaller and the neutron importance in the flux trap grows higher in the Type-I core. It is inadequate to compare directly β/ℓ values in the MEU and HEU cores, since the number of fuel plates loaded to the core is different from each other. It is indicated from the experimental results, however, that the difference between β/ℓ values in the MEU and HEU cores are small.

III-8. Measurements of the Void Reactivity Effect

The void reactivity effects were measured at several locations in a core, since the void reactivity is an important physical quantity in a research reactor both for the operation and for the safety analysis.

III-8-A. Void Reactivity Effects in the Water Regions

Firstly, with use of Al void pipes with several diameters and thicknesses, the void reactivity effects were measured in an MEU core at 4 locations; namely, (1) the center of the central flux trap of light-water, (2) the space for the control rods, (3) the light-water gap between the outer fuel elements and the heavy-water tank, and (4) the middle of heavy-water reflector.[50] The MEU core employed in this series of experiments was fully loaded with 294 fuel plates and one half of the outer fuel elements consisted of boron loaded side-plates. The excess reactivities were measured before and after pouring light-water or heavy-water into an Al void pipe by the positive period method. From the difference between the above two reactivities, the void effect was obtained.

The results were tabulated in Table III-7 in comparison with those of the HEU core. Note that the HEU core was not a fully loaded one and was a Type-I core loaded with 277 fuel plates.

Table III-7 shows that the void reactivity effects are negative in the space for the control rods and at the middle of heavy-water reflector, whereas they are positive at the other locations. Note that experimental error is estimated to be ± 0.005 %Δk/k for this void reactivity measurement from experience. In the MEU core, the void coefficients of reactivity are estimated to be approximately 1×10^{-5} $\Delta k/k/cm^3$ at the center of the flux

trap, -5×10^{-6} $\Delta k/k/cm^3$ at the space for the control rods, 2×10^{-6} $\Delta k/k/cm^3$ at the light-water gap between the outer fuel elements and the heavy-water tank, and -2×10^{-7} $\Delta k/k/cm^3$ at the middle of the heavy-water reflector, respectively. A direct comparison between the MEU and HEU cores is inadequate, because there is a difference in the volume of the central flux trap of light-water. However, the experimental results indicate that the void reactivity effect in the central flux trap of an MEU core is slightly larger than that of an HEU core.

Table III-7 Reactivity Effects of Al Void Pipes

Locations in the Core	Outer Diameter (cm)	Inner Diameter (cm)	Void Reactivity (%Δk/k) MEU Core	HEU Core
Center of the Central Flux Trap of H_2O	1.0	0.7	0.025	——
	2.5	1.9	0.17	0.15
	2.5	2.1	0.21	——
	2.5	2.2	0.23	——
	2.5	2.3	0.25	0.22
	4.0	3.38	0.54	——
Space for Control Rods	1.0	0.7	-0.011	——
H_2O Gap between the Outer Fuel Elements and D_2O Tank	1.0	0.7	0.004	——
	2.5	2.3	0.063	——
Middle of the D_2O Reflector	3.5	2.9	-0.010	——
	6.5	5.5	-0.030	——
	9.0	8.4	-0.078	——

III-8-B. Void Reactivity Effects in the Fuel Region

Secondary, the void reactivity effects in the fuel region of the MEU and HEU cores were measured with a gas bubbling technique,[97,98] since it was considered to be impractical to use an Al pipe in the narrow flow channels (2.4 mm) of the KUCA core.[58]

Measurement of Void Fraction

When determining the void reactivity coefficient, a direct measurement of the channel-averaged void fraction in the core is preferable. However, the following limiting conditions existed in the core:

(1) Adjacent fuel elements, control rods, heavy-water tank and other core components obstructed the access of equipment to the test section.

(2) Probes such as optical probes and anemometers could not be introduced into the test section due to its narrow channel width.

(3) Conductance probe techniques[99] could not provide sufficient sensitivity because of the high resistivity of the ion-exchanged light-water in the core tank.

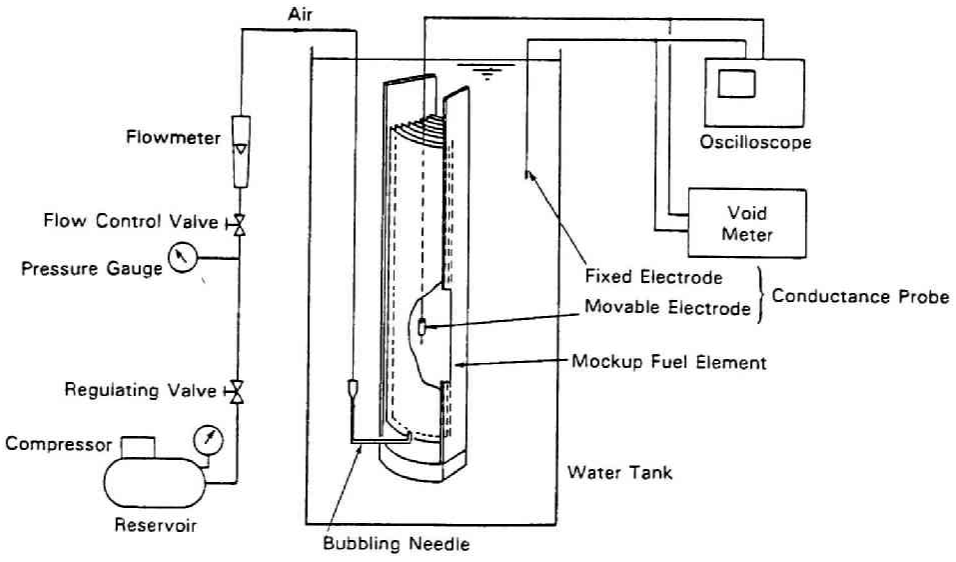

Fig. III-22 Schematic Drawing of the Equipment for the Out-of-Pile Experiment

For these reasons, it was decided to measure the void fraction in an out-of-pile experiment using a full-scale fuel element mock-up made of aluminum alloy. Figure III-22 shows the schematic drawing of the equipment for the out-of-pile experiment. A fuel element mock-up was set up in a

tank filled with tap water to approximately 30 cm above the top of the fuel mock-up in order to simulate the pressure condition in the core tank of the KUCA. Air was supplied by an air-compressor and introduced into the test channel through a small needle-like nozzle (stainless-steel tube of 1.0 mm inner diameter and 1.5 mm outer diameter) mounted at the bottom of the channel. The nozzle was placed upright at the center of the channel with the nozzle tip 1 cm above the bottom of the fuel plates. The flow rate of air was measured with a rotameter.

A two-phase flow measuring device based on the conductance probe technique,[100] can be utilized now to measure the local void fractions in the flow channels because of sufficient electric conductivity of tap water. The probe consisted of two electrodes; one was fixed in water and grounded, while the other was movable. When the tip of the movable electrode was in the water, a low-level voltage was obtained; when it was in air bubbles, a high-level voltage was obtained. Thus, the local void fraction could be determined by averaging a properly processed signal.

The calibration curve, i.e., the channel-averaged void fraction versus the air flow rate, was obtained by the following procedure:

(1) Place the movable electrode at a particular location and measure the local void fractions at air flow rates from 50 to 450 ℓ/h with an increment of 50 ℓ/h. Continue sampling for 20 sec and repeat 10 times under a given condition. Finally, average the measured void fractions to obtain a local void fraction.

(2) Repeat Step (1) at predetermined locations (24 to 36 points per channel) to obtain the void fraction profile. The locations of the calibrated channels are shown in Fig. III-23. For each channel (refer to Fig. III-23), one must calibrate the length of the arc centerlines of the channels, which varies from channel to channel even though the

gap of the channels remains unchanged.

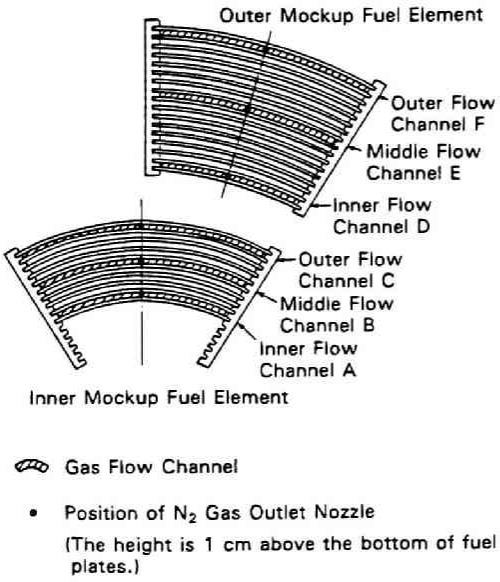

Fig. III-23
Cross Section of Mock-up Fuel Elements and the Position of the N_2 Gas Outlet Nozzle

(3) The channel-averaged void fraction at a given flow rate can be determined by averaging the void fraction profile over the channel at the same flow rate.

Since the local void fractions are measured only along the arc centerlines of the channels, some corrections for the average void fractions are necessary to take into account the radial profile of the local void fraction. Visual observations indicated that the bubbles were large enough to be taken as Taylor bubbles in the radial direction over the range of the gas flow rates in this work. Therefore, the modification was made by calculating the liquid film thickness along a Taylor bubble, using the equations by Özugü et al.[101]

Note also that the width of the channels was 2.44 mm in the out-of-pile experiment whereas the channel width for the in-pile experiment was 2.4 mm. In addition, air was used in the out-of-pile experiment whereas N_2 gas was injected into the core. It was assumed, however, that the calibration curves for the void fraction obtained from the out-of-pile experi-

ment were applicable to the in-pile experiment because the difference in the cross-sectional area of the channels was less than 3 % and the physical properties of air and nitrogen are very similar to each other.

Measurement of Void Reactivity

The in-pile experiment consisted of two parts. In the first series of experiments, bubbles were generated in a single channel to investigate the effects of the fuel enrichment, bubbling location and boron loaded in the side-plates on the void reactivity. In the second series, bubbles were generated in two separated channels as well as in two adjacent channels simultaneously to examine the additivity and the interference effect of the void reactivity.

Table III-8 Summary of the Cores Employed in This Experiment

Core	Number of Fuel Plates	^{235}U Loading (g)	Excess Reactivity* ($\times 10^{-3}$ $\Delta k/k$)
MEU Core without Boron	263	4176.4	1.5
MEU Core with Boron	267	4229.5	0.4
HEU core without Boron	278	3542.5	1.6

* : Measured when a needle-like nozzle is in the outermost channel of the outer fuel element.

Three types of Type-I cores were constructed in the first series of experiments, namely, the MEU core without boron, the MEU core with boron, and the HEU core without boron. The fuel loading and the excess reactivity of these cores are shown in Table III-8.

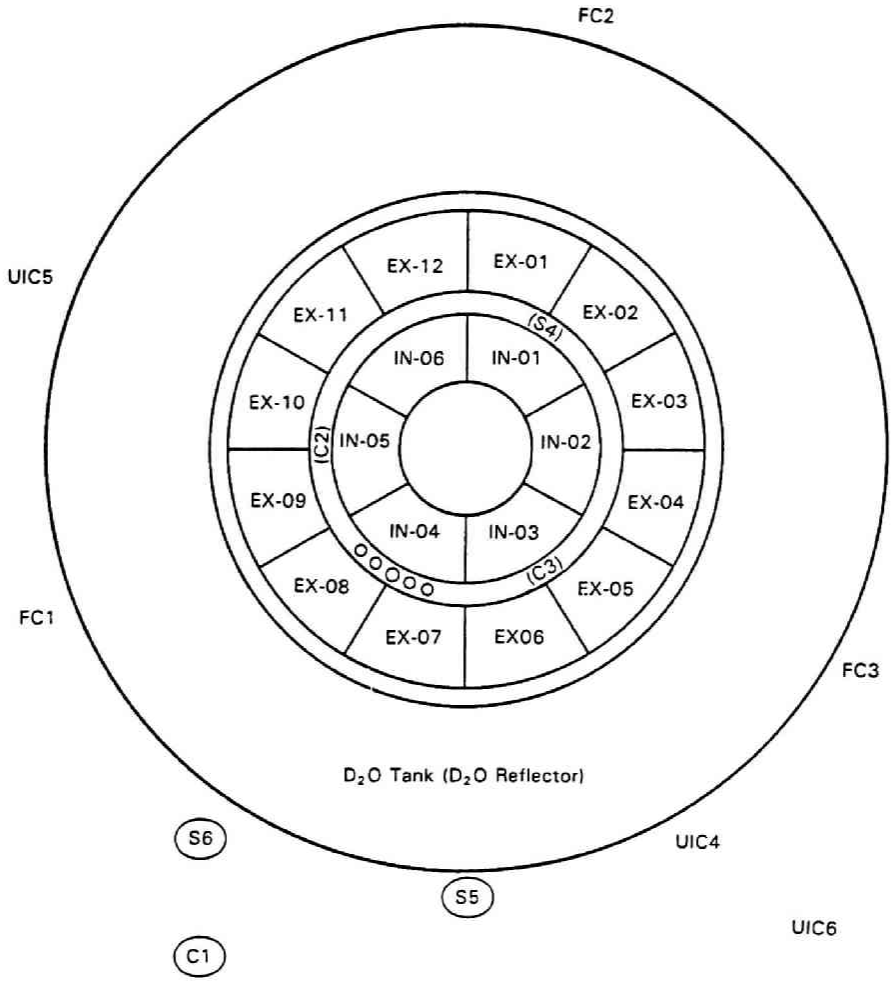

IN-01 to IN-06 = Inner Fuel Elements (Containing No Burnable Poison)
EX-01 to EX-12 = Outer Fuel Elements (Containing No Burnable Poison)
C1 to C3 = Control Rods
S4 to S6 = Safety Rods
FC1 to FC3 = Fission Chambers
UIC4 to UIC6 = Uncompensated Ionization Chambers
o o o o o o = Aluminum Tubes

EX-01 to EX-12 contain 17 fuel plates.
IN-01 to IN-05 contain 10 fuel plates
IN-06 contains 9 fuel plates
Total: 263 fuel plates.

The tenth, eleventh, and twelfth plates of IN-05 counted from the outside have been removed.

Fig. III-24 Configuration of the MEU Core without Boron

Figure III-24 shows the MEU core without boron. The reactivity was controlled with three control rods (C1, C2, C3) while three safety rods (S4, S5, S6) were held at their upper limit during normal operation. The fuel loading was such that the reactivity of void could be compensated for

using only the C2 rod, while the other rods were fully withdrawn. Small-diameter aluminum tubes were also inserted into the control rod region adjacent to the elements IN-04, EX-08 and EX-07 to adjust the excess reactivity. Voids were generated by bubbling N_2 gas in the elements IN-02 and EX-04. Locations of the channels where voids were generated are shown in Fig. III-25. Nitrogen was supplied from a gas bomb and the flow rate was measured with a rotameter.

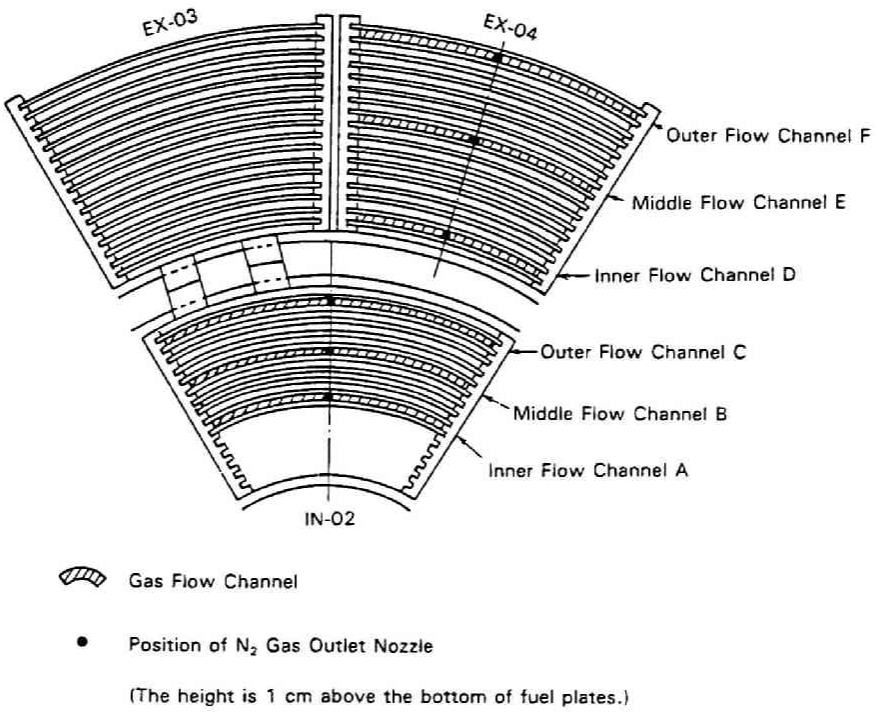

Fig. III-25 Positions of the Voided Channels in the MEU Core

The configuration of the MEU core with boron was almost the same as shown in Fig. III-24, except that the side-plates of the elements IN-02 and EX-04 contained boron. These elements were then referred to as IN(B)-02 and EX(B)-04, respectively.

Figure III-26 shows the HEU core without boron. In the HEU core, outer fuel elements are denoted by "OUT" instead of "EX" in order to distinguish the HEU core from the MEU core. As shown in Table III-8,

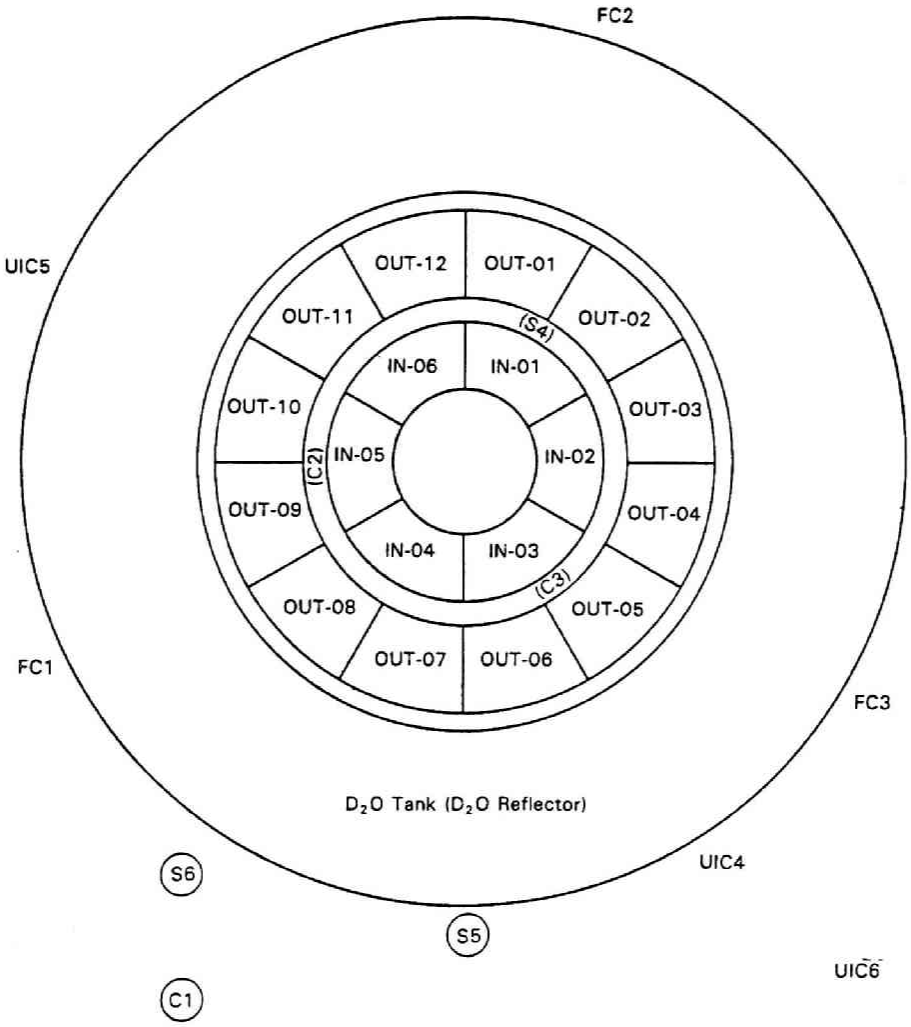

IN-01 to IN-06 = Inner Fuel Elements (Containing No Burnable Poison)
OUT-01 to OUT-12 = Outer Fuel Elements (Containing No Burnable Poison)
C1 to C3 = Control Rods
S4 to S6 = Safety Rods
FC1 to FC3 = Fission Chambers
UIC4 to UIC6 = Uncompensated Ionization Chambers

OUT-01 to OUT-12 contain 17 fuel plates.
IN-04 and IN-06 contain 13 fuel plates.
IN-01,02,03,05 contain 12 fuel plates.
Total: 278 fuel plates.

Fig. III-26 Configuration of the HEU Core without Boron

approximately 18 % less ^{235}U was needed in the HEU core without boron in order to produce approximately the same excess reactivity as in the MEU core without boron. Since the ^{235}U content is less in HEU fuel plates than

in MEU fuel plates, however, one or two extra fuel plates were loaded in each inner fuel elements of the HEU core without boron. For this reason, the void reactivity was measured in the extra channel G(H) in the inner element IN-02 as well as Channels A(H) through F(H) as shown in Fig. III-27.

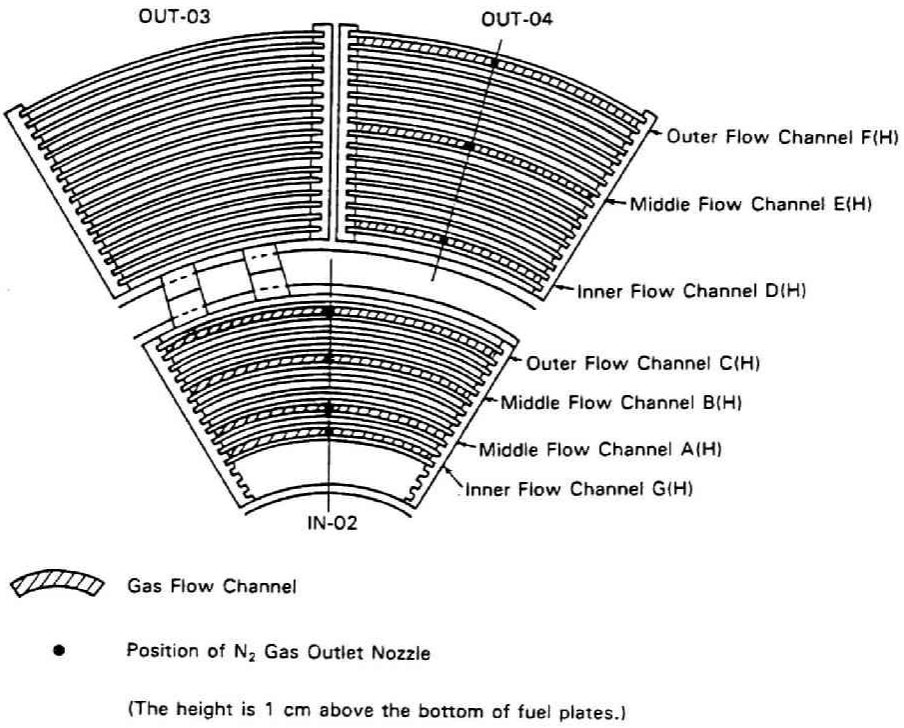

Fig. III-27 Positions of the Voided Channels in the HEU Core

In the second series of experiments in which bubbles were generated in two channels, a core configuration very similar to the MEU core shown in Fig. III-24 was employed. The following differences were that in the second series of experiments; (1) small aluminum tubes were not utilized, (2) ten fuel plates were inserted into the inner fuel element IN-05 in order from the outside, and (3) the location of the inner fuel element containing nine fuel plates was different. In the first run of the second series which is discussed later, the inner element with nine fuel plates was the element IN-04, while in the second run it was IN-03. Therefore, in

the second run, the core was symmetrical with respect to vertical plane P-Q as shown in Fig. III-28. The locations of voided channels during the second series of experiments are shown in Fig. III-28.

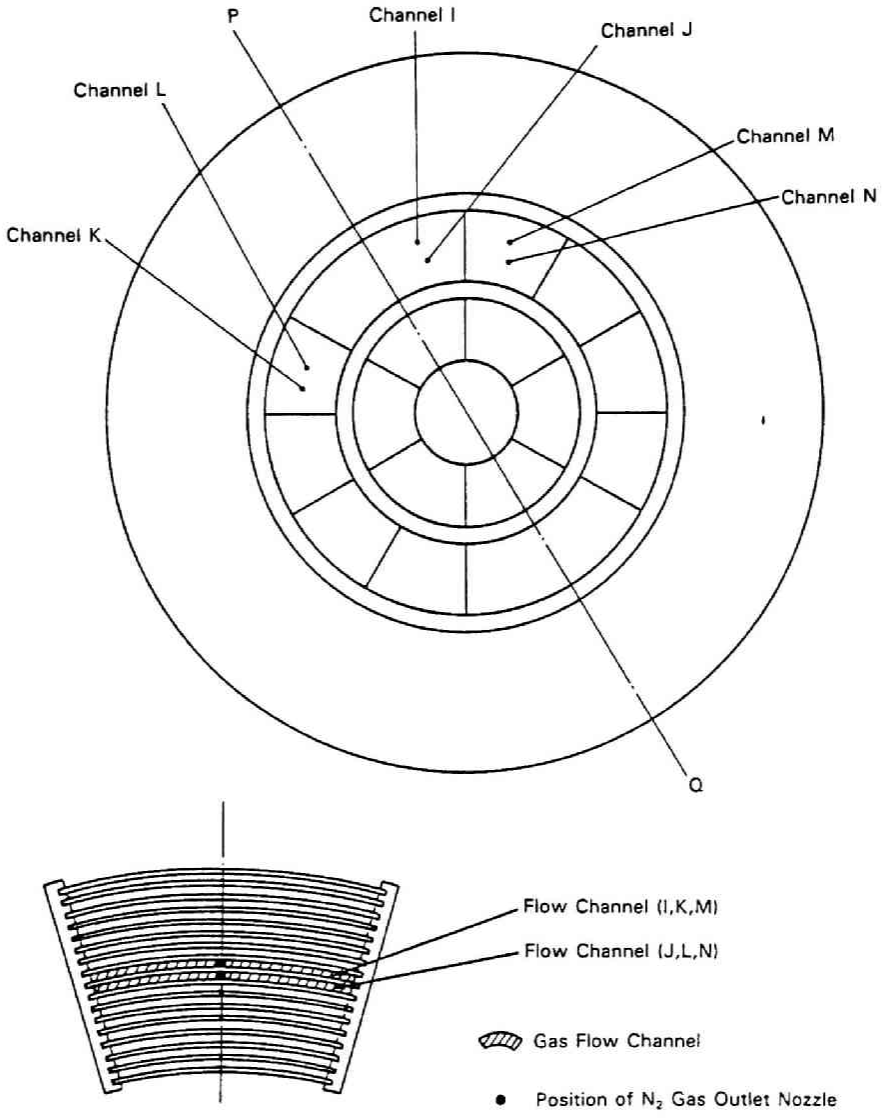

Fig. III-28 Positions of the Voided Channels in the Second Series of Experiments

A diagram of the N_2 gas supply system is shown in Fig. III-29. Nitrogen gas was supplied from a large gas bomb and introduced into the channels through the same needle-like nozzles used in the out-of-pile experiment, which were mounted at the bottom of the channels in the same

manner. The flow rate of N_2 gas was measured with a rotameter.

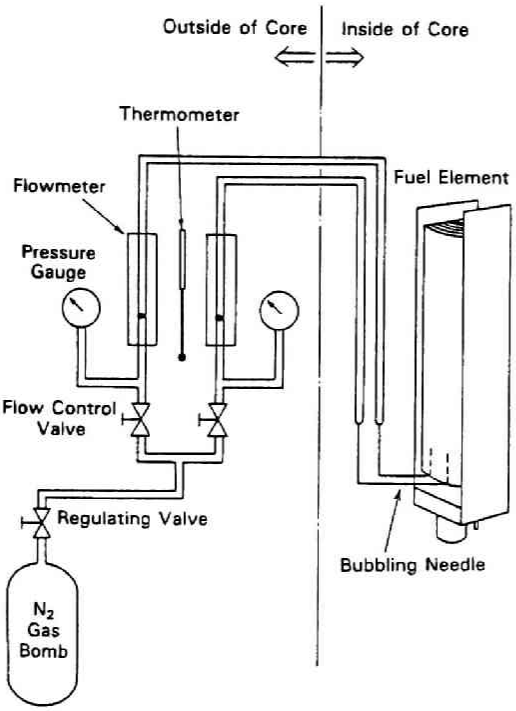

Fig. III-29
The N_2 Gas Supply System

In the first series of experiments, the void reactivity coefficient was measured by the following procedure:

(1) Place a needle-like nozzle at the bottom of the test channel so that the tip of the nozzle is positioned at the center of the cross section of the channel and 1 cm above the bottom of the fuel plates. Clamp the N_2 gas pipeline so that it will not move during the measurement. The locations of the test channels were shown in Figs. III-25 and III-27.

(2) Feed light-water to the core tank. Fill the pipeline with N_2 gas and purge any light-water from the pipeline before criticality is attained. Move the C2 rod to attain criticality while the other rods are fully withdrawn.

(3) Move the C2 rod to the upper limit and measure the stable period of

the increasing neutron level by using a multi-channel scaler, thus obtaining the excess reactivity of the core when the gas flow rate is zero.

(4) Set N_2 gas flow rate at 50 ℓ/hr and use the C2 rod to attain criticality. Measure the excess reactivity again in the same manner as step (3).

(5) Repeat step (4) at gas flow rates of 100, 200, 300 and 400 ℓ/hr.

(6) Calculate the void reactivity coefficient from the difference between the excess reactivities with and without voids.

In the second series of in-pile experiments, in which bubbles were generated in two channels simultaneously, the same basic procedure as in the first series, i.e., the positive period method, was used to measure the reactivity. To measure the small interference effect of void reactivity, however, two methods were employed.

In the first run of the second series, the reactivities were measured, voiding in adjacent channels I and J shown in Fig. III-28, both separately and simultaneously. Let $\rho_v(I)$ be the reactivity of voiding in Channel I, and $\rho_v(I+J)$ be that of voiding in Channels I and J simultaneously, then the interference effect can be measured by ρ_{int}, defined as

$$\rho_{int} = |\rho_v(I+J)| - |\rho_v(I) + \rho_v(J)| \quad . \qquad \text{(III-1)}$$

If $\rho_{int} = 0$, the additivity of reactivity with a single voided channel exists; otherwise, the interference effect exists. Channels I and J were chosen because in the first series of the experiment, the void reactivity for a given channel-averaged void fraction had a maximum absolute value (most negative) in those channels located at the middle of the outer fuel

element. Hence, the experimental error was expected to be minimum for those channels.

It turned out from the first run, however, that the interference effect was small enough to be within the experimental error even if any interference effect existed. Therefore, the following alternative tech nique was devised in the second run in order to reduce the experimental error which was attributed to the summing up of measured reactivities. In the second run, two pairs of adjacent channels (K, L and M, N) were chosen, as shown in Fig. III-28. From the viewpoint of fuel loading in the core, channels K and M are symmetrical to each other with respect to line P-Q, and likewise, channels L and N. Theoretically, this means that

$$\rho_v(K) = \rho_v(M) \quad , \tag{III-2}$$

and

$$\rho_v(L) = \rho_v(N) \quad . \tag{III-3}$$

It is assumed here that the separated channels of any pair were independent of each other in terms of the void reactivity. Then

$$\rho_v(K+N) = \rho_v(K) + \rho_v(N) \quad , \tag{III-4}$$

and

$$\rho_v(L+M) = \rho_v(L) + \rho_v(M) \quad . \tag{III-5}$$

Therefore, if one measures the reactivity of voiding two adjacent channels $\rho_v(K+L)$ or $\rho_v(M+N)$ and that of voiding two separated channels $\rho_v(K+N)$ or $\rho_v(L+M)$, one may obtain the interference effect as follows:

$$\begin{aligned} \rho_{int} &= |\rho_v(K+L)| - |\rho_v(K+N)| \quad , \\ &= |\rho_v(M+N)| - |\rho_v(L+M)| \quad . \end{aligned} \tag{III-6}$$

Results of Void Fraction Calibration

An example of the local void fraction profile is shown in Fig. III-30. The ordinate represents the local void fraction, the abscissa the distance from the centerline of the channel, and the oblique line the height measured from the bottom of the fuel plates. The names of the channels correspond to that shown in Fig. III-23.

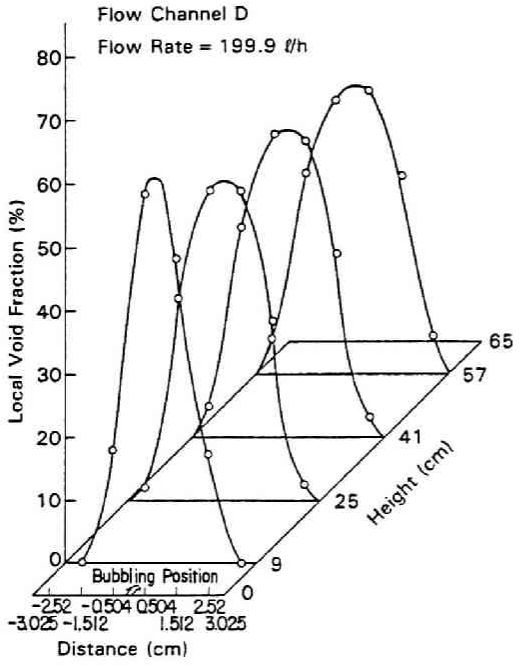

Fig. III-30
Profile of a Local Void Fraction at the Gas Flow Rate of 200 ℓ/hr in Channel D

Figure III-30 indicates that the horizontal profile of the local void fraction is similar to a Gaussian distribution with the shape becoming more blunt with increasing distance from the nozzle. Such a profile of the local void fraction was commonly observed through all conditions in the calibration of the void fraction.

The channel averaged void fraction is calculated by averaging the local void fraction profile. The result is given in Fig. III-31 as a function of the gas flow rate for all channels marked in Fig. III-23. These calibrated channels correspond to all the channels in Figs. III-25

and III-27 except channel G(H) in Fig. III-27. Taking advantage of the fact that the cross-sectional area of channel G(H) is in between that of channels A and D, the average void fraction for channel G(H) was estimated by a linear interpolation of the results for those channels.

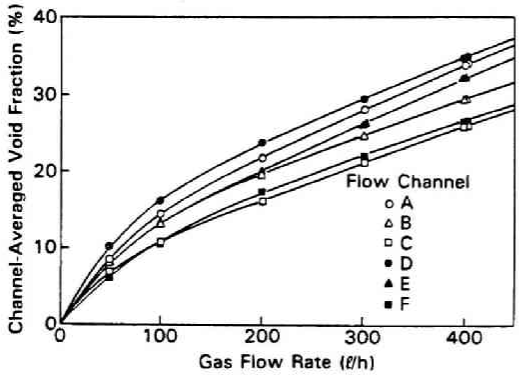

Fig. III-31
Calibration Curves for Void Fraction in Flow Channels A through F

Results of Void Reactivity in a Single Channel

The results of void reactivity versus gas flow rate in the first series of in-pile experiments are shown in Figs. III-32 and III-33. They indicate that the overall effect of voids on reactivity is negative in the fuel regions and the effect is maximum in the middle channels while it is minimum in the channels adjacent to the reflector. The result for channel G(H) is the exceptional case in which the void reactivity appears to be positive. Note, however, that the result for channel G(H) may not be reliable because the measured reactivities are very small and the error in the measurement is comparable to the measured values. Figure III-32 also indicates that the existence of boron loaded side-plates near the bubbling channel weakens the reactivity effect of void.

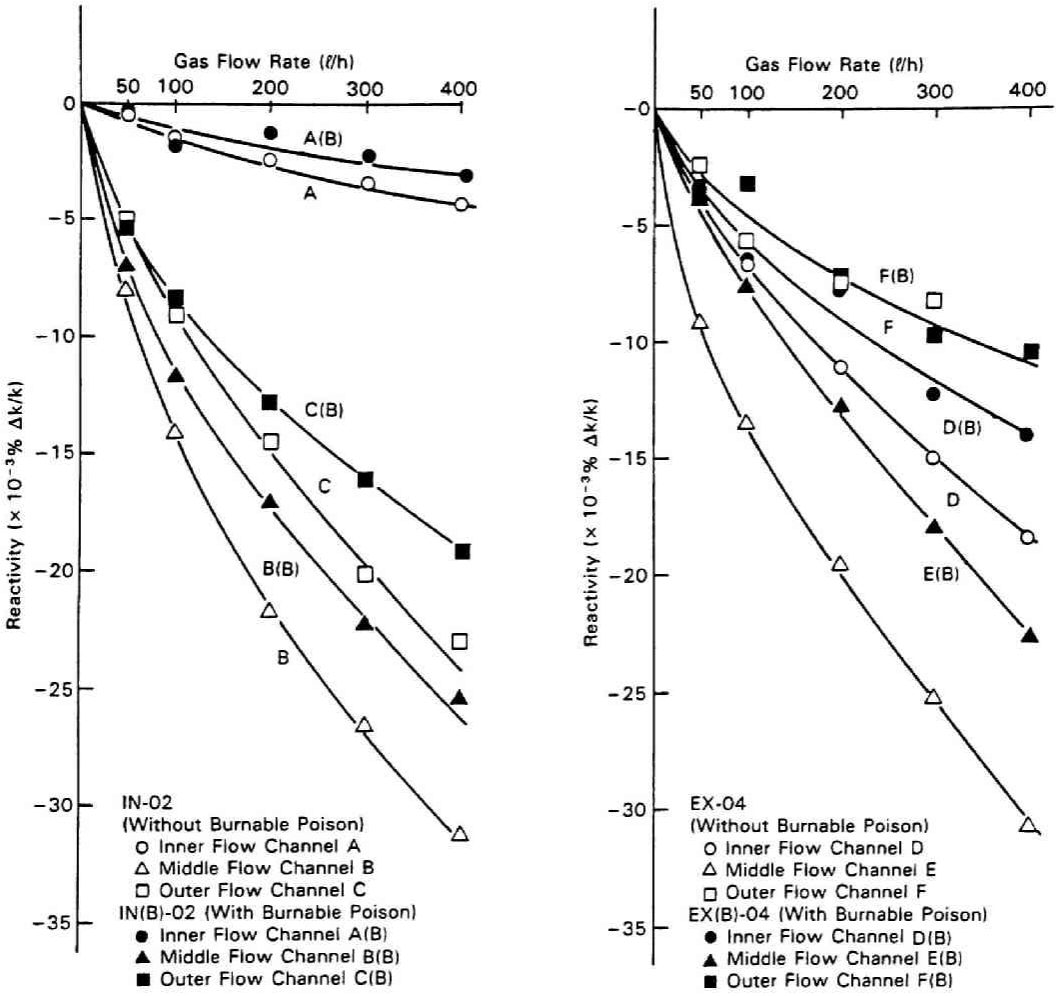

Fig. III-32 Measured Void Reactivity versus Gas Flow Rate for the MEU Cores with and without Boron

From the results shown in Figs. III-32 and III-33 and by using the calibration curves Fig. III-31, the relation between the void reactivity and the channel-averaged void fraction can be obtained. The overall void fraction, which is defined by the ratio of the void volume to the total light-water volume in the fueled regions, is calculated from the channel-averaged void fraction. The overall void reactivity is then obtained as a function of the overall void fraction. The results are shown in Figs. III-34, III-35, and III-36. Note here that the overall void coefficient thus obtained may be different from that for a homogeneous void over the

core even if the apparent overall void fraction is unchanged.

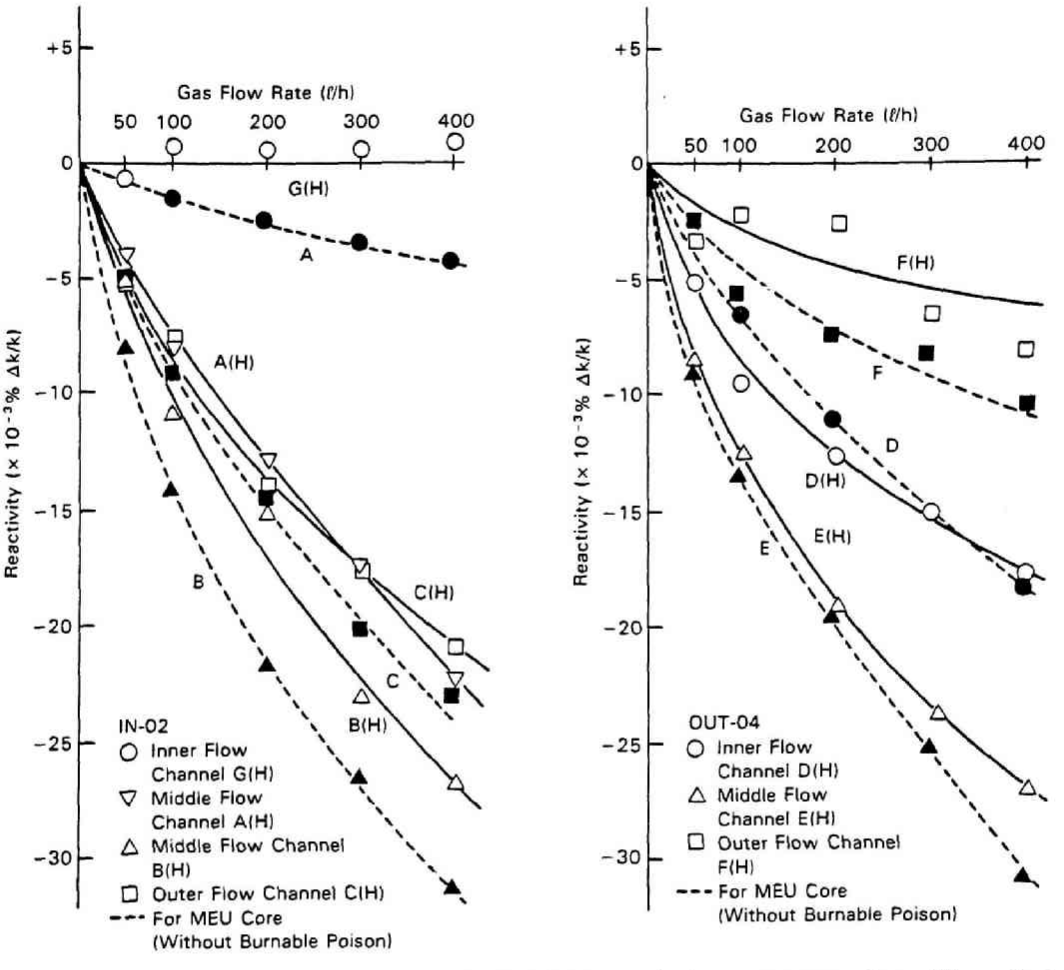

Fig. III-33 Measured Void Reactivity versus Gas Flow Rate for the HEU Core Compared with That of MEU Core

These figures indicate that the reactivity coefficient of voids is negative in the fueled regions, except in channel G(H), which was discussed previously, and strongly space-dependent. Comparing the results between the HEU and MEU cores, it can be seen that the void effect on reactivity is slightly larger (more negative) in the MEU core than in the HEU core, which can be attributed to several factors. This is consistent with the simple consideration on k_∞ value described in Section II-2 of the preceding chapter. In addition, the volume of the fueled regions is smaller in the MEU core, which means that the neutron importance at the voided channel is

larger in the MEU core. Moreover, the energy spectrum of neutrons is harder in the MEU core because of the larger fraction of ^{238}U in the fuel. These effects tend to increase the void effect in the MEU core. Further studies may be needed, however, in order to give a thorough explanation.

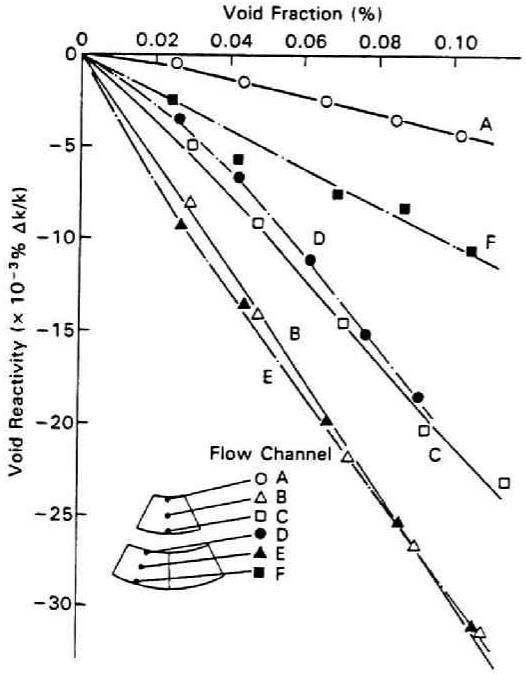

Fig. III-34
Void Reactivity versus Overall Void Fraction for the MEU Core without Boron

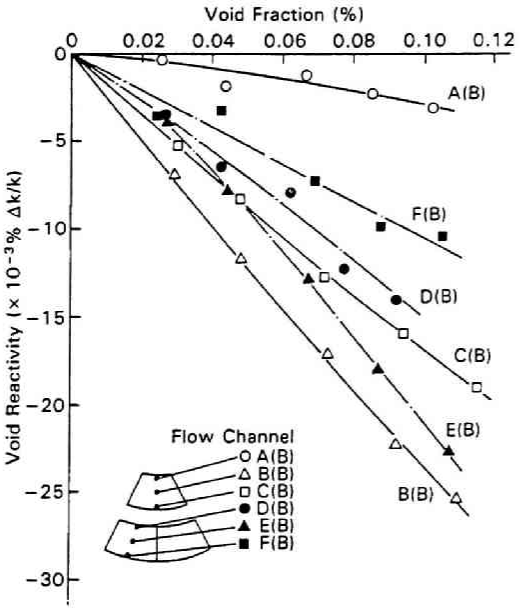

Fig. III-35
Void Reactivity versus Overall Void Fraction for the MEU Core with Boron

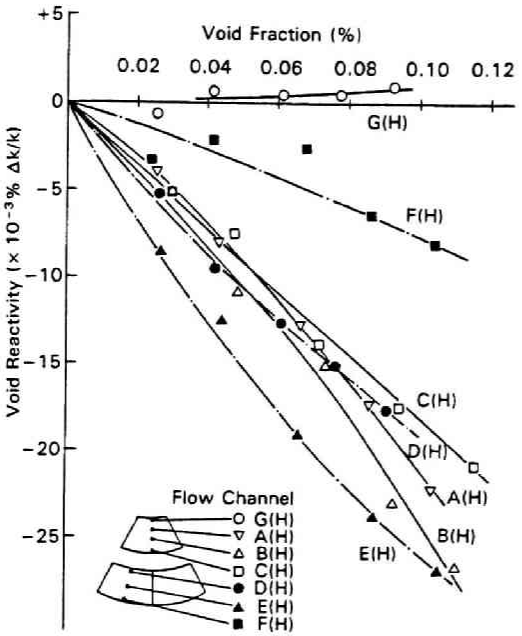

Fig. III-36
Void Reactivity versus Overall Void Fraction for the HEU Core without Boron

Results of Interference Effect of Void Reactivity

Table III-9 Results of Reactivity of Voiding Two Channels

Measurement	Voided Channel	Channel-Averaged Void Fraction (%)	Void Reactivity ($\times 10^{-3}$ Δk/k)
First Run	I	32	-0.30
	J	32	-0.31
	I and J	both 32	-0.62
Second Run	K and L	both 32	-0.67
	M and N	both 32	-0.71
	K and N	both 32	-0.64
	M and L	both 32	-0.66
	K and L	both 20	-0.45
	K and N	both 20	-0.45

The channel averaged-void fraction and the void reactivity in the second series of in-pile experiments are presented for each channel or each pair of channels in Table III-9. Based on the results, the interference effect ρ_{int} can be calculated by using Eq. (III-1) for channels I and J, and Eq. (III-6) for channels K, L, M, and N. Thus, ρ_{int} obtained from the

first run is $(0.01 \pm 0.04) \times 10^{-3}$ $\Delta k/k$ for a channel-averaged void fraction of 32 %, and that obtained from the second run becomes $(0.04 \pm 0.03) \times 10^{-3}$ $\Delta k/k$ for a channel-averaged void fraction of 32 % and zero for a channel-averaged void fraction of 20 %. Since the last result (0 $\Delta k/k$) was calculated from only one set of data, the statistical error is not estimated.

On the basis of experience in measuring the excess reactivity in the KUCA, the experimental error is estimated to be approximately $\pm 0.05 \times 10^{-3}$ $\Delta k/k$. Hence, the values of ρ_{int} obtained above are within the experimental error. Therefore, it may be concluded that the interference effect with two adjacent voided channels, whose channel-averaged void fraction is as high as 32 %, is within the experimental error if the interference effect even exists.

Conclusions

The results obtained from this work are summarized as follows.

(1) The reactivity coefficient of voids is negative in the fueled regions for all the core configurations employed here.

(2) The void effect is strongly space-dependent; the effect is maximum in the middle channels in the inner and outer fuel regions while it is minimum in the channels adjacent to the reflector.

(3) The reactivity coefficient is slightly larger (more negative) in the MEU core than in the HEU core.

(4) The void effect is weakened by the existence of boron loaded side-plates near the voided channel.

(5) The interference effect with two adjacent voided channels, whose channel-averaged void fraction is as high as 32 %, is within the experimental error.

III-9. Measurements of the Temperature Effect on Reactivity

The temperature coefficients of reactivity are important physical quantity concerned deeply with reactor operation and safety. Therefore, the measurements of the temperature effect on reactivity were performed. The purposes of the experiments are to investigate the dependencies of temperature reactivity effects on (1) the geometrical heterogeneity in the multi-region type core, (2) the ^{235}U enrichment of fuel, and (3) boron contained in the side-plates as a burnable poison.

III-9-A. Temperature Effect on Reactivity in a Full Loading MEU Core

Firstly, the temperature effects were measured in the MEU core fully loaded with 294 fuel plates under the conditions with and without a central acrylic void tube which was utilized in the neutron flux measurements (refer to Section III-6).[50] The reasons were as follows; (1) the experimental results of Al void pipe effects demonstrated that the void reactivity coefficient in the central flux trap of light-water was positive as described in Section III-8-A and (2) the feature of the neutron flux distribution was different from each other in the MEU cores with and without a central void as described in Section III-6. Therefore, it was interesting to investigate the effect of a central void on the temperature reactivity effects.

Then, the MEU cores with and without a central void were constructed in the KUCA. The criticality of the core was adjusted by the number of boron loaded side-plates. Note that, in this experiment, the fuel pitch in the fuel element with boron was 3.80 mm and the pitch in the element without boron was 3.84 mm. With use of heaters and stirrers, the

temperature of light-water and heavy-water were raised simultaneously and uniformly. At several temperatures in a range of 20 °C through 75 °C, the excess reactivities were measured by the positive period method.[85] The temperatures at several locations in the core were monitored with thermocouple type thermometers and the uniformity of temperature in the core was assured for each measurement.

Let $\rho(T)$ be the excess reactivity of the core at a temperature T (°C) and $\rho(T+\Delta T)$ be the excess reactivity at a temperature $(T+\Delta T)$ (°C). Then, the temperature coefficient $\alpha(T+\Delta T/2)$ can be obtained as,

$$\alpha(T+\Delta T/2) = [\ \rho(T+\Delta T) - \rho(T)\ ] / \Delta T \quad . \qquad \text{(III-7)}$$

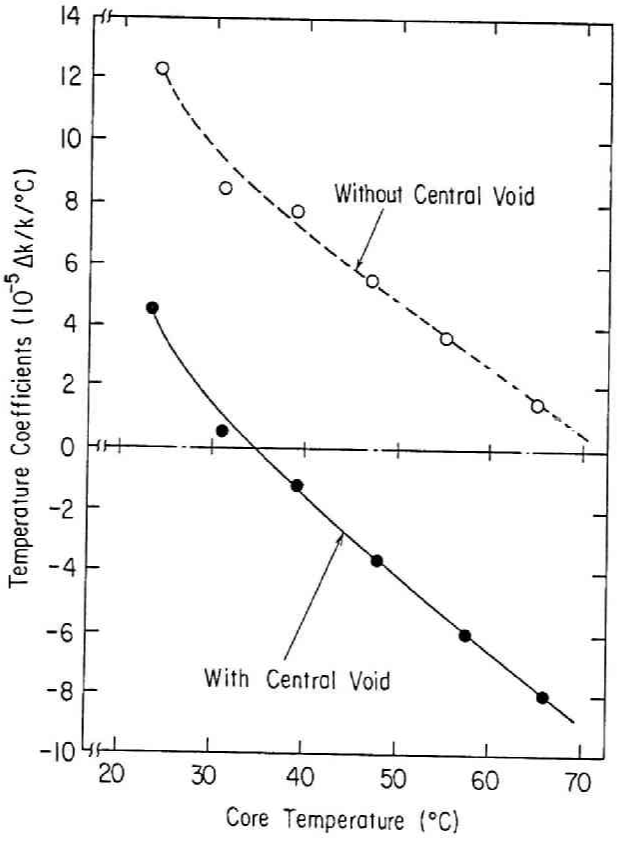

Fig. III-37 Temperature Coefficients of Reactivity for the MEU Cores with and without a Central Void

The results are shown in Fig. III-37. Figure III-37 shows that the temperature coefficient is positive below 70 °C for the core without a central void. On the other hand, in the core with a central void, the sign of the temperature coefficient changes from positive to negative at approximately 33 °C. Two curves of the temperature coefficients are almost parallel, however, the gradient for the core with a central void is slightly steeper than that of the core without a central void. The difference between two curves is approximately 9×10^{-5} $\Delta k/k/°C$. These results indicate that the thicker the light-water layer in the center of core becomes, the larger (more positive) the temperature coefficient grows. This indicates that the positive temperature coefficient of the core is mostly attributed to the positive temperature coefficient of the central flux trap of light-water. This also indicates that the temperature coefficient is strongly depend on the core configuration.

III-9-B. Temperature Effects on reactivity in the MEU and HEU Cores

Secondary, the temperature effects were measured in the MEU and HEU cores to investigate the effect of reduced ^{235}U enrichment. The Type-I and Type-II Cores (refer to Section III-4) were employed for both MEU and HEU cores to investigate the effect caused by a change in core configuration. In the Type-I MEU cores, the temperature effects in the cores with and without boron loaded side-plates were also measured to investigate the effect caused by an existence of boron. In this series of experiments, the fuel pitch was 3.80 mm for all cases. The fuel loading patterns of the cores employed in the experiments are shown in Figs. III-38 and III-39.

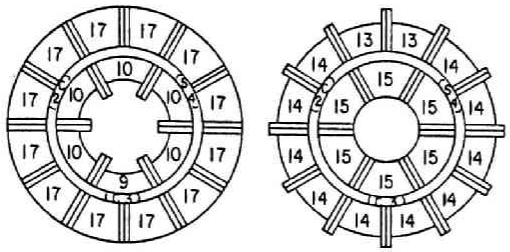

a) MEU - I (no BP) b) MEU - Ⅱ (no BP)

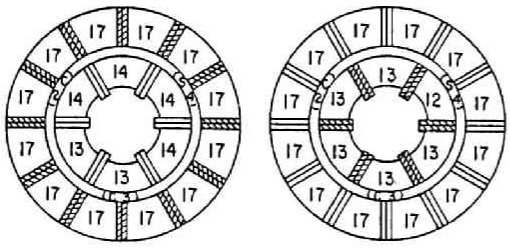

c) MEU - I (Outer BP) d) MEU - I (Inner BP)

▨ : Side Plate Containing BP
Arabic Number : Number of Fuel Plates
C2, C3 : Control Rods
S4 : Safety Rod

Fig. III-38
Fuel Loading Patterns of the MEU Cores Employed in the Temperature Effect Measurements

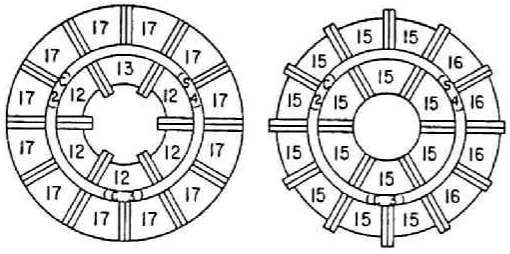

a) HEU - I (no BP) b) HEU - Ⅱ (no BP)

Arabic Number : Number of Fuel Plates
C2, C3 . Control Rods
S4 : Safety Rod

Fig. III-39
Fuel Loading Patterns of the MEU Cores Employed in the Temperature Effect Measurements

A heater and a stirrer were installed in the heavy-water tank, and several thermocouples and two quartz-type thermometers were settled at various locations in the C-core tank as shown in Fig. III-40. These

thermometers were used to check the uniformity of temperature in the core during the measurements. The temperature of light-water was raised using 3 heaters and a stirrer installed in the dump tank from which light-water was pumped up to the core just before the reactivity measurement.

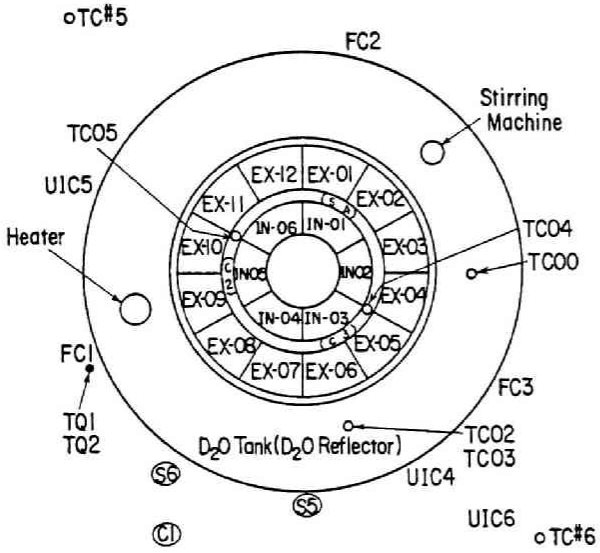

Thermometers	Height from the center of the fuel plate
TC#5	35.5 cm beneath
TC#6	44.5 cm above
TC00	7.0 cm beneath
TC02	30.0 cm beneath
TC03	27.0 cm above
TC04	0.0 cm
TC05	0.0 cm
TQ1	28.0 cm beneath
TQ2	46.5 cm above

IN-01~IN-06 : Inner Fuel Elements
EX-01~EX-12 : Outer Fuel Elements
C1~C3 : Control Rods
S4~S6 : Safety Rods
FC1~FC3 : Fission Chambers
UIC4~UIC6 : Uncompensated Ionization Chambers
TC#5, TC#6 : Thermocouples (Stationary)
TC00~TC05 : Thermocouples
TQ1, TQ2 : Quartz-Type Thermometers

Fig. III-40 Typical Core Configuration Employed in the Temperature Effect Measurements

When the temperatures of light-water and heavy-water reached the same level, the excess reactivity or subcriticality was measured using the positive period method[85] or the source multiplication method.[87] Thus, the temperature dependent excess reactivities at several temperatures were obtained in a range from 20 °C to 75 °C. The temperature coefficient was determined by two methods. One was calculated directly using the experimental data by Eq. (III-7). The other was calculated by fitting the experimental data to a quadratic curve,

$$\rho(T) = aT^2 + bT + c \ , \qquad \text{(III-8)}$$

where, a, b, c : constants,

using the method of least squares. Thus, the temperature coefficient was obtained as,

$$\alpha(T) = 2aT + b \ . \qquad \text{(III-9)}$$

Tables III-10 Temperature Effects on Reactivity in the MEU Cores

Designation of Core*	MEU-I (no BP)	MEU-II (no BP)	MEU-I (Outer BP)	MEU-I (Inner BP)
No. of Fuel Plates	263	256	286	281
Measured Excess Reactivity ρ_{ex} (%Δk/k)	0.073[25.1°C] 0.132[28.9°C] 0.212[35.1°C] 0.284[40.8°C] 0.389[49.7°C] 0.480[59.3°C] 0.546[69.7°C]	0.067[21.7°C] 0.156[27.4°C] 0.248[35.2°C] 0.318[41.8°C] 0.397[49.4°C] 0.451[59.2°C] 0.491[67.8°C]	-0.007[23.7°C] 0.064[30.1°C] 0.152[39.2°C] 0.222[49.0°C] 0.281[59.0°C] 0.317[71.2°C]	-0.001[22.0°C] 0.107[30.2°C] 0.209[39.7°C] 0.287[49.8°C] 0.332[59.2°C] 0.381[70.6°C]
Results of Least Square Fitting $\rho_{ex}=aT^2+bT+c$	a:-1.07×10^{-4} b: 2.08×10^{-2} c:-3.82×10^{-1}	a:-1.33×10^{-4} b: 2.10×10^{-2} c:-3.25×10^{-1}	a:-1.05×10^{-4} b: 1.68×10^{-2} c:-3.46×10^{-1}	a:-1.21×10^{-4} b: 1.89×10^{-2} c:-3.55×10^{-1}
Temperature Coefficient Calculated by using Eq.(III-7) α (10^{-4}Δk/k/°C)	1.55[27.0°C] 1.29[32.0°C] 1.27[38.0°C] 1.18[45.3°C] 0.94[54.5°C] 0.63[64.5°C]	1.56[24.6°C] 1.18[31.3°C] 1.05[38.5°C] 1.04[45.6°C] 0.55[54.3°C] 0.47[63.5°C]	1.11[26.9°C] 0.97[34.7°C] 0.71[44.1°C] 0.59[54.0°C] 0.30[65.1°C]	1.32[26.1°C] 1.07[35.0°C] 0.77[44.8°C] 0.47[54.5°C] 0.43[64.9°C]

Note : A value in [ ] shows a temperature T (°C).
* : Refer to Fig. III-38.

The results are tabulated in Tables III-10 and III-11. The results shows that the temperature coefficients are positive in the measured temperature range for all the cores employed in this series of experiments. This is expected from the results of the Section III-8-A, because the cores had no central void. However, this also indicated that, in a high temperature region above 100 °C, the temperature coefficient becomes negative for

all the cores employed in this series of experiments.

Table III-11 Temperature Effects on Reactivity in the HEU Cores

Designation of Core*	HEU-I (no BP)	HEU-II (no BP)
No. of Fuel Plates	277	274
Measured Excess Reactivity ρ_{ex} (%Δk/k)	-0.044 [22.4°C] 0.009 [26.6°C] 0.108 [35.2°C] 0.152 [39.8°C] 0.238 [49.7°C] 0.286 [57.8°C] 0.337 [66.3°C]	0.009 [24.4°C] 0.129 [33.5°C] 0.192 [39.4°C] 0.251 [48.1°C] 0.316 [57.3°C] 0.344 [66.4°C]
Results of Least Square Fitting $\rho_{ex} = aT^2 + bT + c$	a : -0.98×10^{-4} b : 1.73×10^{-2} c : -3.82×10^{-1}	a : -1.40×10^{-4} b : 2.06×10^{-2} c : -4.08×10^{-1}
Temperature Coefficients Calculated by Using Eq.(III-7) α (10^{-4}Δk/k/°C)	1.25 [24.5°C] 1.15 [30.9°C] 0.97 [37.5°C] 0.87 [44.8°C] 0.60 [53.8°C] 0.60 [62.1°C]	1.33 [29.0°C] 1.06 [36.5°C] 0.68 [43.8°C] 0.70 [52.7°C] 0.31 [61.9°C]

Note : A value in [ ] shows a temperature T (°C).
* : Refer to Fig. III-39.

The results of least square fitting shown in Tables III-10 and III-11 indicate some features of the temperature effects on reactivity. In a low temperature region (refer to values of "b" in Tables III-10 and III-11), the temperature coefficient decreases with the increase in number of fuel plates loaded to the core, regardless of the Type-I and Type-II and of with and without boron for both the HEU and MEU cores. In other words, the smaller is the critical mass, the larger (more positive) the temperature coefficient grows up in a low temperature region. Therefore, the temperature coefficient grows more positive with the increase in effectiveness of a light-water reflector including a flux trap. This indicates that the temperature coefficient of a light-water reflector is positive. Whereas that of a fuel region is usually negative, because the neutron leakage from the fuel region becomes large with the increase of temperature. Note here

that, although the core employed in this experiment was a mock-up of a light-water-moderated and heavy-water-reflected annular core with a central flux trap of light-water, the actual core had a more than 2.5 cm thick light-water gap between the heavy-water tank and the outer fuel elements.

The gradient of the temperature coefficient (refer to values "a" in Tables III-10 and III-11) of the Type-II core is steeper than that of the Type-I. This means that the temperature coefficient of the Type-II core grows smaller (more negative) than that of the Type-I in a high temperature region. This may be attributed to the size of the central flux trap and the thickness of the light-water gap between the heavy-water tank and the outer fuel elements. This is also consistent with the results of the preceding section which indicate that the less is the volume of central light-water, the steeper the gradient of the temperature coefficient becomes. However, in the MEU cores with boron, the slope in the MEU core with inner boron is steeper than that of the core with outer boron regardless of the size of central light-water. This may be attributed to the boron effect. The difference between values "a" or "b" in the Type-I and Type-II MEU cores is smaller than that between the HEU cores. This indicates that, in the HEU core, the temperature coefficient depends more strongly on the core configuration than in the MEU core. This may be attributed to the effect of reduced ^{235}U enrichment.

Further experimental study may be necessary to obtain a thorough explanation of the temperature effects on reactivity. However, the experimental results indicate that the temperature effects depends strongly on the core configuration rather than on the ^{235}U enrichment or the existence of boron.

III-10. Conclusions

The results obtained through the critical experiments are summarized as follows:

(1) The number of fuel plates needed to attain criticality in the MEU core is less than that in the HEU core. The critical mass of the MEU core is approximately 18 % larger in ^{235}U mass than that of the HEU core.

(2) The total reactivity worth of the control rods is around 10 % smaller in the MEU core than the HEU core. The control rod worth decreases further with the introduction of the boron loaded side-plates.

(3) In the MEU core, the total reactivity effect of the boron loaded side-plate is approximately -8 %Δk/k. The reactivity effect of a boron loaded side-plate in the inner fuel region is larger than that in the outer fuel region. The interference effects are observed between two adjacent boron loaded side-plates.

(4) The neutron spectrum in the MEU core is harder than that in the HEU core. The ratio of the thermal neutron flux in the reflector including the central flux trap to that in the fuel region of the MEU core is larger than the ratio in the HEU core. This ratio changes remarkably with the introduction of a central void. For both the MEU and HEU cores, a high peak of the thermal neutron flux is observed in the central flux trap of light-water. On the other hand, there is no flux peak in the heavy-water reflector, because the KUCA core has rather thick light-water layer between the heavy-water reflector and the fueled region. The vertical reflector saving in the MEU core is almost the same as that in the HEU core.

(5) The kinetic parameter β/ℓ in the MEU core is almost the same as that in the HEU core. The value of β/ℓ is in the middle of that in a light-water moderated and reflected core, and that in a heavy-water moderated and reflected core. The value of β/ℓ depends strongly on the core configuration.

(6) In the central flux trap of light-water and in the light-water gap between the heavy-water reflector and the outer fuel elements, the void reactivity effects are positive, whereas those are negative in the other regions. In the fuel region, the void reactivity in the MEU core is slightly more negative than that in the HEU core, and the void effect is slightly weakened by the existence of the boron loaded side-plates. At the middle flow channel of the fuel element, the void effect has the most negative value. The interference effect of void reactivity between two adjacent flow channels in the fueled region is negligibly small.

(7) The temperature effects on reactivity is positive for both the MEU and HEU cores with the central flux trap of light-water in a range of 20 °C through 70 °C. The temperature coefficients of reactivity depends more strongly on the core configuration rather than on the ^{235}U enrichment and the existence of boron. The temperature effects become negative with the introduction of a central void.

IV. ANALYSES OF THE CRITICALITY AND THE BORON REACTIVITY EFFECT

IV-1. Introduction

The determination of the critical mass provides the most essential base for reactor physics. In order to design a new reactor including a core conversion in accordance with the use of REU fuel, one should predict the effective multiplication factor as accurate as possible through the neutronics calculations. Therefore, it is important to assess the accuracy of the neutronics calculations in comparison with the experimental data. Moreover, in order to estimate a reactivity effect, the criticality calculation should provide an accurate value of k_{eff}, since the reactivity is defined from a difference between k_{eff} values. It is also important to estimate the boron reactivity effect accurately, since boron is often utilized as a material for the control rod or burnable poison.

The main objective of the present study is to establish a self-consistent system for the neutronics calculations in the KUCA through the analyses of the critical experiments using HEU and MEU fuels. Since the KUCA experiments have provided the only benchmark data for the use of MEU fuel in a light-water-moderated and heavy-water-reflected annular core, it is significantly important to assess a method of the neutronics calculations for an MEU core as well as an HEU core.

As a first step to establish a self-consistent system for the neutronics calculation, an assessment is made through the analyses of the experimental data using the ANL code system consisted of the conventional codes,[65] because this code system has provided good results for the benchmark calculations in the RERTR program[4,6] and commonly used as a standard

code system for the neutronics calculations of research reactors. Therefore, it is important to assess quantitatively its capability for the KUCA core loaded with MEU fuel, since the KUCA core has a remarkable heterogeneity in geometry which is difficult to model precisely with use of the conventional codes based on the finite-difference method. The assessment includes analyses on (1) the criticality data of HEU and MEU cores and (2) the reactivity effect data of boron for MEU cores.[65] The ANL code system employed in this study consists of two codes: (1) the EPRI-CELL code[67] for the generation of few-group constants and (2) the DIF3D code[68] for diffusion calculations.

The present assessment also includes results from a finite-element diffusion code, 2D-FEM-KUR,[69] which was developed in a cooperative research program between KURRI and JAERI. Since this code provides the capability for mocking-up a complex core configuration, it is especially important to assess this code for the KUCA core. Therefore, with use of the same group constants generated by the EPRI-CELL code, the 2D-FEM-KUR code was applied to the analysis of the KUCA experiments and the results were compared with those from the DIF3D code. Through this comparison, the merits and demerits of the 2D-FEM-KUR and DIF3D codes, which are based on the finite-element and finite-difference methods, respectively, can be clarified for the analyses of the KUCA experiments. The finite-element method employed in the 2D-FEM-KUR code is considered to be advantageous for the detailed analysis on the measurements of the boron reactivity effect [BP effect].

IV-2. Calculations

IV-2-A. Description of the Computer Codes

Microscopic broad-group cross sections were generated using the EPRI-CELL code.[67] This code combines a heterogeneous P_1 GAM[102] type treatment in the fast and resonance ranges with a heterogeneous integral-transport treatment [THERMOS][103] in the thermal range. The P_1 GAM type treatment includes (1) an interpolation over tabulated groupwise-resonance integrals as a function of temperature and potential scattering for the resonance self-shielding, (2) resonance overlap corrections, (3) an optional buckling search, and (4) several other refinements. The code also provides a cell depletion calculation using the CINDER code for each THERMOS space point in a depletable zone. Cell-averaged cross sections at any time step in a depletion history can be obtained in either a 2-, 3-, 4- or 5-group structure. A flow diagram of the EPRI-CELL code is shown in Fig. IV-1.

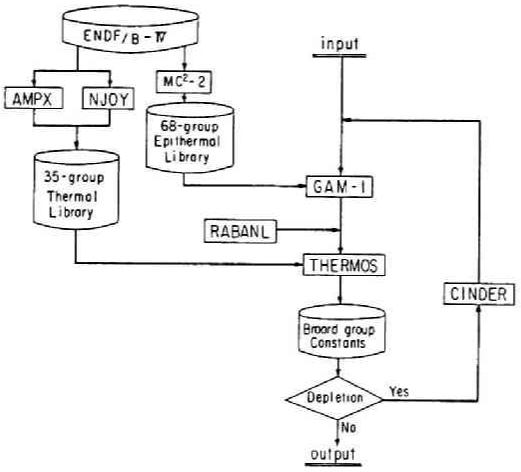

Fig. IV-1 Flow Diagram of the EPRI-CELL Code

The EPRI-CELL libraries are mostly based on the ENDF/B-IV data file.[104] The 68 group fast library was generated using MC^2-2[105] and the integral transport RABANL option in the MC^2-2 code can be used to calculate the resonance self-shielding parameters. The 35-group thermal library was generated using the AMPX[106] or NJOY codes with an $S_{\alpha,\beta}$ treatment for hydrogen and deuterium in light-water and heavy-water, respectively.

The diffusion calculations were performed using the DIF3D and 2D-FEM-KUR codes. The DIF3D code has the capability for one- through three-dimensional diffusion calculations for several geometries based on the conventional finite-difference method.[68] In the present study, a two-dimensional option of the code [DIF3D(2D)] was adopted. The 2D-FEM-KUR code is a two-dimensional diffusion code based on the finite-element method.[69]

IV-2-B. Generation of Group Constants

The core employed in the KUCA critical experiments was divided into 10 regions for the MEU core (refer to Fig. IV-6) and into 11 regions for the HEU core. For the MEU core, these regions were: (1) the inner and (2) the outer fuel regions, (3) the inner and (4) the outer side-plate regions, (5) the light-water region at the center of core, (6) the control rod region, (7) the outer vessel region between the outer fuel elements and the heavy-water reflector, (8) the heavy-water reflector region, (9) the outer wall region of the aluminum heavy-water tank, and (10) the light-water reflector region outside the heavy-water tank. For the HEU core, (11) the inner vessel region including the Al pipe which separated the inner fuel elements from the central flux trap of light-water (refer to Fig. III-2) was also modeled.

For generating the group constants, the EPRI-CELL code with a one-dimensional slab geometry was used for each of the above regions. The upper energy boundaries of the five-group structure used in this study were: 10 MeV, 0.821 MeV, 5.53 keV, 1.855 eV and 0.625 eV.

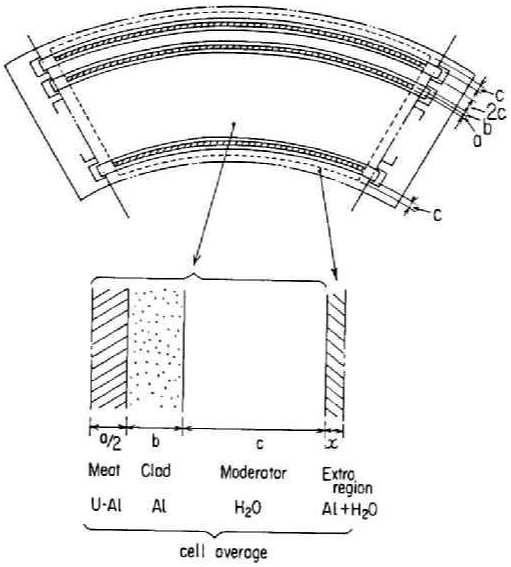

Fig. IV-2 Model for the Fuel Region Used in the Unit Cell Calculation

For the inner (1) and outer (2) fuel regions shown in Fig. IV-2, the materials between two side-plates (an enclosed area with double dotted dash lines in Fig. IV-2) were modeled as a unit cell using a slab geometry for a fully loaded fuel element. The fuel meat, aluminum clad and light-water moderator were modeled preserving their thicknesses as shown in Fig. IV-2. The effect of a residual region between two side-plates (an enclosed area with double dotted dash lines and dash lines in Fig. IV-2) was considered by using an artificial extra region. With homogenizing materials (aluminum and light-water) in the residual region, the thickness of the artificial extra region, x (cm), was assumed as:

$$x = \frac{d / 2}{S_t / S_r - 1} , \qquad \text{(IV-1)}$$

where, d : fuel pitch (cm),

S_t : total area of the region between two side-plates (cm^2),

S_r : area of the residual region between two side-plates (cm^3).

RABANL[105] corrections were applied for the resonance self-shielding.

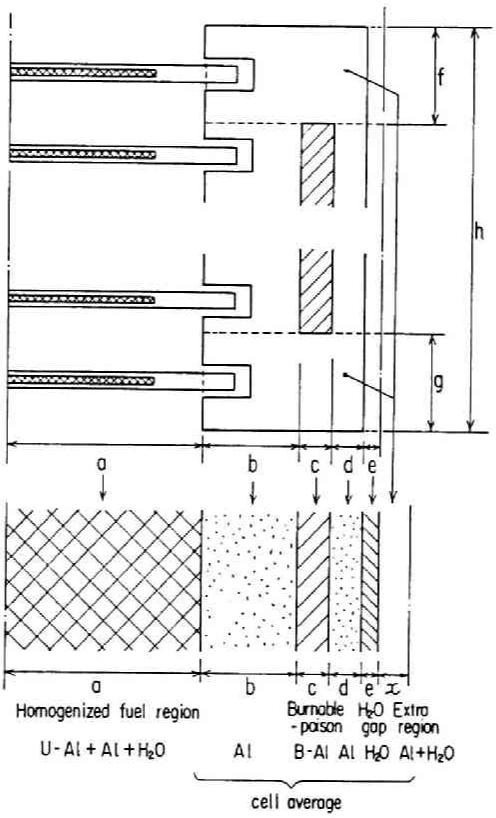

Fig. IV-3 Model for the Side-Plate Region with Boron Used in the Cell Calculation

For the inner (3) and outer (4) side-plate regions shown in Fig. IV-3, the treatment was different for the side-plates with and without boron. In each case, the small portion of light-water in the grooves for fuel plate insertion into the side-plates was ignored, but the light-water in a gap between two adjoining side-plates was taken into account. For the side-plates with boron, the spectrum for collapsing the cross-sections was generated using a homogenized core source in order to consider the effect

of leakage neutron spectrum from the actual fuel region. On the other hand, for the side-plates without boron, a simple ^{235}U fission spectrum was assumed without attaching any special source region. For the side-plates with boron, all regions were represented preserving their thicknesses, and the effect of end sections of the side-plates containing no boron were taken into consideration by using an artificial extra region shown in Fig. IV-3.

For regions (5) through (11), a ^{235}U fission spectrum was employed for collapsing the cross sections. In the control rod region (6), aluminum spacers, aluminum sheaths for the control rod insertion and all other aluminum support structures were homogenized. On the other hand, in the inner (11) and the outer (7) vessel regions which consisted of aluminum and light-water, geometrical heterogeneities were taken into account. For the outer tank wall region (9), the group constants prepared for aluminum in the outer vessel region (7) were utilized. In the central light-water (5) and the light-water reflector (10) regions, the group constants were generated for a 10 cm thick light-water layer assuming the same thickness for both regions.

IV-2-C. Diffusion Calculations

The experimental results gave the axial reflector savings in the MEU core as 8.1 ± 0.1 cm in the central light-water region, 7.8 ± 0.1 cm in the outer fuel region and 9.8 ± 0.3 cm in the heavy-water reflector region, respectively (refer to Table III-5 in Section III-6). In the present study, the experimental values of the axial reflector savings were adopted to calculate the transverse buckling employed in the two-dimensional diffusion calculations.

In the DIF3D(2D) code, one quarter of the core was modeled in X-Y geometry as shown in Fig. IV-4. In the inner part of the core, a mesh of approximately 0.25 × 0.25 cm was employed. In the heavy-water reflector and in the heavy-water tank regions, a 1 × 1 cm mesh was basically used. In the light-water reflector region, a 2 × 2 cm mesh was mainly adopted.

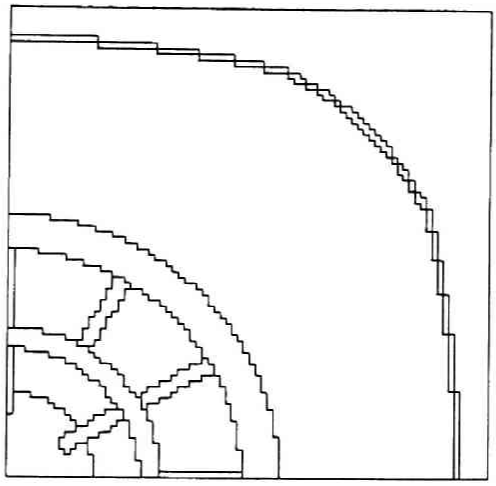

Fig. IV-4 Example of a Jagged X-Y Approximation for One Quarter of the MEU core Used in the DIF3D(2D) Code

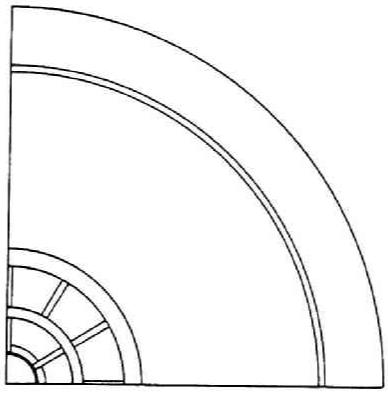

Fig. IV-5 Example of a Explicit Representation for One Quarter of the HEU Core Used in the 2D-FEM-KUR Code for the Comparison with the DIF3D(2D) Code

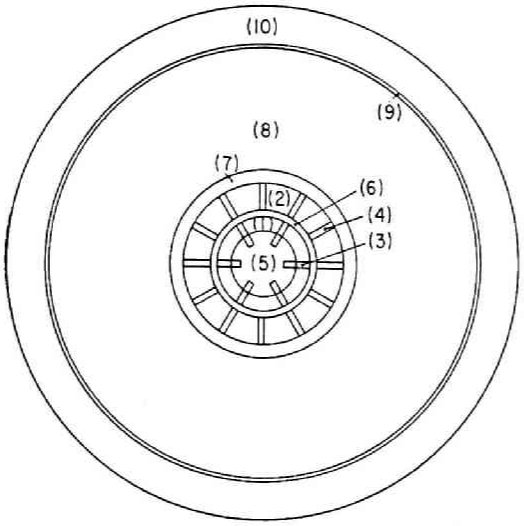

(1) Inner fuel region
(2) Outer fuel region
(3) Inner side-plate region
(4) Outer side-plate region
(5) Light-water region at center of core
(6) Control rod region
(7) Outer vessel region
(8) Heavy-water reflector region
(9) Outer wall region of aluminum heavy-water tank
(10) Light-water reflector region

Fig. IV-6 Example of a Explicit Representation of the Full MEU Core Used in the 2D-FEM-KUR Code for the Detailed Analysis on the Boron Reactivity Effects

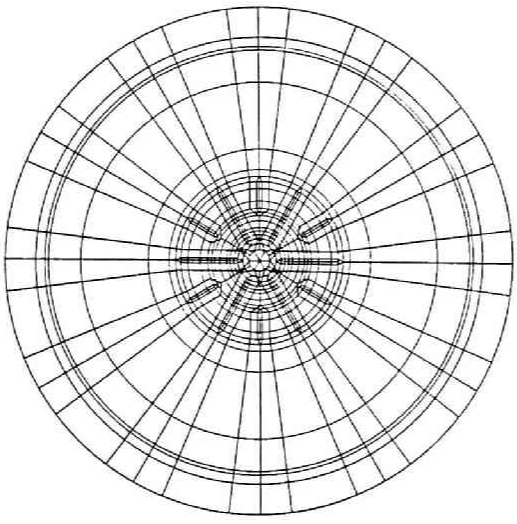

Fig. IV-7 Example of the Finite-Elements Used in the 2D-FEM-KUR Code

Figure IV-5 shows the core configuration simulated by the 2D-FEM-KUR code for the comparison with the DIF3D(2D) code. For the detailed analysis on the boron effect measurements, the full core was explicitly modeled by the 2D-FEM-KUR code as shown in Fig. IV-6, by taking advantage of the finite-element method for the capability of the precise geometrical representation. Figure IV-7 shows an example of the finite-elements used in the detailed analysis on the boron effect measurements.

IV-3. Results and Discussion

Results of the calculations are tabulated in Tables IV-1 through IV-3 together with the experimental results. Table IV-1 shows a comparison between the DIF3D(2D) and 2D-FEM-KUR codes for the criticality measurements. Table IV-2 makes the same comparison for the boron effect measurements. Table IV-3 shows the results from the 2D-FEM-KUR code for the detailed analysis on the boron effect measurements. Figure IV-8 shows the reactivity effect caused by the substitution of a fuel element with boron for a fuel element without boron in the outer fuel region, and Fig. IV-9 shows the BP effect for the inner fuel region. Note that experimental errors for the excess reactivity and BP effect measurements in the KUCA annular core are estimated to be 5×10^{-5} and 1×10^{-4} $\Delta k/k$ from experience, respectively.

Tables IV-1 through IV-3 show that differences between the results of calculations and experiments were less than 2 % in C/E ratios for eigenvalues. The calculated eigenvalues were always higher than the experimental values. One reason for this tendency was due to the unit cell model employed for the fuel region in generating the group constants. In the

present study, an artificial extra region was employed as shown in Fig. IV-2 so that the effect of the area surrounding the actually fueled region was taken into account. The extra region which consisted of light-water and aluminum tended to increase the apparent $H/^{235}U$ ratio in the actually fueled region. This caused a shift from an under-moderated fuel region to a more moderated region and led to the over-estimation of the eigenvalues.

Table IV-1 Eigenvalue for the Critical State without Boron

	Pitch (mm)	Number of plates	k_{exp}	k_{cal}		C/E	
				DIF3D(2D)	2D-FEM-KUR	DIF3D(2D)	2D-FEM-KUR
MEU (44.88%)	3.80	262	1.0008	1.0112	1.0111	1.0104	1.0103
MEU (44.88%)	3.84	262	1.0021	1.0112	1.0122	1.0091	1.0101
HEU (93.14%)	3.84	276	1.0047	1.0198	1.0204	1.0150	1.0157

Table IV-2 Boron Reactivity Effect for the MEU Core

(a) DIF3D(2D) code

	Pitch (mm)	Number of plates	Eigenvalue			Reactivity effect of BP		
			k_{exp}	k_{cal}	C/E	ρ^{exp} (%$\Delta k/k$)	ρ^{cal} (%$\Delta k/k$)	C/E
Inner SP without BP Outer SP with BP	3.84 3.80	288	1.0047	1.0188	1.0140	−4.74	−4.408	0.93
All SP without BP	3.84	288	—	1.0667	—			
All SP with BP	3.80	294	~0.984	0.9939	~1.010	(−8)†	−7.666	(0.96)
All SP without BP	3.84	294	—	1.0759	—			

(b) 2D-FEM-KUR code

Inner SP without BP Outer SP with BP	3.84 3.80	288	1.0047	1.0190	1.0142	−4.74	−4.227	0.89
All SP without BP	3.84	288	—	1.0649	—			
All SP with BP	3.80	294	~0.984	0.9940	~1.010	(−8)†	−7.616	(0.95)
All SP without BP	3.84	294	—	1.0754	—			

SP: Side-plate, † Estimated from experiments

Another calculation was performed to examine the effect of the extra region mentioned above for generating the group constants in the fuel region. Namely, in this calculation, the extra region was completely excluded from the unit cell model. It was found that the calculation using the group constants generated exclusive of the extra region led to the

under-estimation of the eigenvalue. The reason is considered that, with excluding the extra region, the actually fueled region becomes a less moderated region, since the effect of the region containing light-water next to the fuel region is neglected.

Table IV-3 Substitution Effects of Boron Loaded Side-Plates in the MEU core

No. of fuel plates	Number of element with BP†		Eigenvalue			BP effect ($\%\Delta k/k$)			Mass effect†† ($\%\Delta k/k$)		
	Inner	Outer	k_{exp}	k_{cal}	C/E	$\Delta\rho_{exp}$	$\Delta\rho_{cal}$	C/E	$\Delta\rho_{exp}$	$\Delta\rho_{cal}$	C/E
263	0	0	1.0047	1.0143	1.0096						
						−0.44	−0.39	0.88			
263	0	1	1.0004	1.0104	1.0100						
						−0.36	−0.39	1.07			
263	0	2	0.9965	1.0064	1.0099				0.40	0.45	1.13
265	0	2	1.0008	1.0110	1.0102						
						−0.37	−0.38	1.02			
265	0	3	0.9969	1.0072	1.0103				0.38	0.41	1.08
267	0	3	1.0010	1.0114	1.0103						
						−0.37	−0.38	1.04			
267	0	4	0.9969	1.0075	1.0106				0.85	0.87	1.02
271	0	4	1.0055	1.0164	1.0109						
						−0.39	−0.38	0.97			
271	0	5	1.0015	1.0125	1.0110				0.36	0.38	1.06
273	0	5	1.0052	1.0164	1.0112						
						−0.41	−0.39	0.96			
273	0	6	1.0011	1.0124	1.0113				0.41	0.44	1.06
275	0	6	1.0052	1.0169	1.0116						
						−0.43	−0.41	0.96			
275	0	7	1.0009	1.0127	1.0118				0.36	0.33	0.92
277	0	7	1.0045	1.0161	1.0115						
						−0.42	−0.42	1.02			
277	0	8	1.0003	1.0118	1.0115				0.56	0.58	1.04
280	0	8	1.0059	1.0177	1.0118						
						−0.41	−0.43	1.03			
280	0	9	1.0017	1.0134	1.0116				0.38	0.38	1.02
282	0	9	1.0055	1.0173	1.0118						
						−0.41	−0.44	1.06			
282	0	10	1.0014	1.0128	1.0115				0.37	0.38	1.03
284	0	10	1.0051	1.0168	1.0116						
						−0.40	−0.43	1.07			
284	0	11	1.0011	1.0123	1.0113				0.37	0.37	1.01
286	0	11	1.0047	1.0161	1.0113						
						−0.34	−0.37	1.09			
286	0	12	1.0013	1.0123	1.0110						
					Total	−4.74	−4.80	1.01	4.44	4.60	1.04
258	0	0	1.0084	1.0238	1.0153						
						−0.68	−0.60	0.88			
258	1	0	1.0016	1.0176	1.0160				0.61	0.55	0.91
262	1	0	1.0077	1.0233	1.0155						
						−0.64	−0.56	0.88			
262	2	0	1.0013	1.0175	1.0162				0.61	0.57	0.93
266	2	0	1.0074	1.0235	1.0159						
						−0.63	−0.56	0.89			
266	3	0	1.0011	1.0177	1.0165				0.60	0.57	0.96
270	3	0	1.0072	1.0239	1.0166						
						−0.62	−0.55	0.88			
270	4	0	1.0009	1.0179	1.0170				0.63	0.57	0.91
274	4	0	1.0073	1.0239	1.0165						
						−0.61	−0.53	0.88			
274	5	0	1.0011	1.0183	1.0172				0.48	0.42	0.89
277	5	0	1.0059	1.0228	1.0167						
						−0.53	−0.48	0.90			
277	6	0	1.0006	1.0178	1.0172						
					Total	−3.70	−3.28	0.88	2.93	2.70	0.92

† : Fuel pitch is 3.80 mm in the side-plate with BP and that is 3.84 mm in the side-plate without BP.
†† : Mass reactivity effect to the fuel plate

Table IV-1 also shows that the C/E ratio for the HEU core was slightly higher than that for the MEU core. The neutron spectrum in the fuel region

of the MEU core is harder than that of the HEU core, since the $H/^{235}U$ ratio in an essential lattice cell of the MEU core is lower than that of the HEU core. Therefore, the neutron reflection effect by the region containing light-water in the vicinity of the fuel region is considered to be larger in the MEU core than in the HEU core. The neutron reflection effect causes to soften the neutron spectrum in the lattice cell, that is analogous to the effect caused by the increase in $H/^{235}U$ ratio of the lattice cell. This indicates that the use of an artificial extra region is more adequate in the MEU core than in the HEU core. This is considered to be a main reason why the C/E ratio for the HEU core was slightly larger than that for the MEU core. In order to attain better C/E ratio, however, it might be necessary to investigate further the method generating the few-group constants or to check the cross section library itself.

It should be noted that the number of fuel plates in the MEU core at the critical state was less than that for the HEU core as shown in Table IV-1. This fact indicates that MEU fuel has a slightly higher reactivity worth in comparison with HEU fuel, in other words, MEU fuel is not exactly equivalent to HEU fuel, in spite of the original intention. Originally, the specification of MEU fuel was determined through the Phase A calculation of the ANL-KURRI joint study using the ANL code system,[29,30] so that MEU fuel would be equivalent to HEU fuel. The procedure of the Phase A calculation is cited here for reference: (1) the eigenvalue was calculated for the proposed KUHFR core loaded with HEU fuel, and (2) varying the uranium content in the UAl_x-Al of MEU fuel under the condition preserving all dimensions of the structures in the core, the eigenvalue was calculated for the KUHFR core loaded with MEU fuel until the same eigenvalue as calculated for the KUHFR's HEU core was achieved. In the Phase A calculation which is described in Section II-4, the U density of HEU fuel meat

was assumed as 0.72 g/cc that corresponds to the U density in U-Al alloy itself (refer to Tables II-1 and II-2). Whereas, the effective U density of the HEU fuel meat utilized in the KUCA is 0.64 g/cc due to a limitation in the fuel fabrication technique (refer to Table II-4). Therefore, a k_{eff} value of an HEU core in the Phase A calculation was larger than k_{eff} of an actual core due to the increase in ^{235}U mass loaded into a core. Accordingly, a reactivity worth of MEU fuel grows higher than that of actual HEU fuel. For reference, the U density of MEU fuel used in the Phase A calculation was 1.7 g/cc as shown in Table II-2 and the effective U density of the MEU fuel meat utilized in the KUCA is 1.68 g/cc as indicated from Table III-3.

In Table IV-1, the 2D-FEM-KUR code well follows the experimental result that the excess reactivity of the MEU core with a 3.84 mm fuel pitch was slightly higher than that with 3.80 mm fuel pitch. For example, the difference between measured excess reactivities for the above two fuel pitches was clearly confirmed through several experiments examining the reproducibility (refer to Table III-1 in Section III-3). On the other hand, for such a minor change in the fuel pitch, the DIF3D(2D) code could not follow the experimental result due to the poorer geometrical representation than the 2D-FEM-KUR code. For this reason, it was decided that the 2D-FEM-KUR code was to be applied to a detailed analysis of the experiments measuring the boron effects. For reference, in the present study, the CPU time for the 2D-FEM-KUR code was approximately one quarter of that for the DIF3D(2D) code.

In general, Tables IV-1 and IV-2 show that the agreement between the results obtained using the DIF3D(2D) code and the 2D-FEM-KUR code was excellent. Therefore, it demonstrates that both the 2D-FEM-KUR code with its precise geometrical representation and the DIF3D(2D) code with a jagged

X-Y approximation for the core can be applicable for the neutronics design calculation of a complex core similar to the KUHFR.

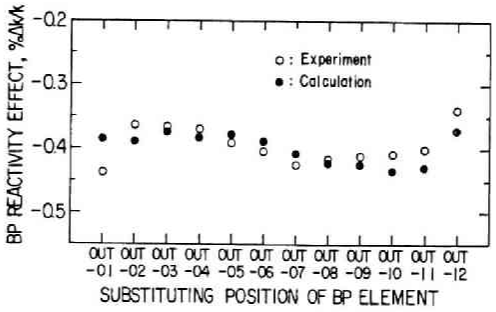

Fig. IV-8 Reactivity Effects Caused by a Substitution of a Fuel Element with Boron for a Element without Boron in the Outer Fuel Region

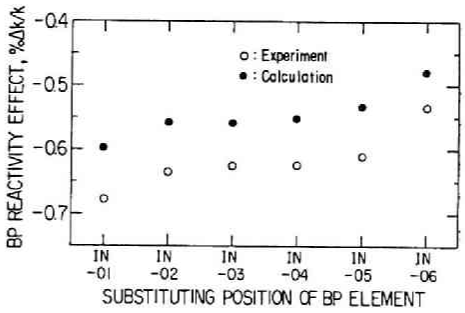

Fig. IV-9 Reactivity Effects Caused by a Substitution of a Fuel Element with Boron for a Element without Boron in the Inner Fuel Region

Table IV-3 shows that differences between the results of calculations and experiments were less than 12 % for the boron reactivity effects and less than 13 % for the mass reactivity effects of the fuel plate. In the outer fuel region, however, the agreement between the calculation and experiment was fairly good for the total boron reactivity effect and the total mass reactivity effect in the analysis of the boron substitution effects. These agreements are remarkable considering the difficulty to calculate such effects based on diffusion theory. Figures IV-8 and IV-9 show that the calculation well reproduced the qualitative dependence

observed in the experiments of the boron substitution effect upon the substituting position. For the outer elements, the boron substitution effects were well simulated except for some positions. On the other hand, for the inner fuel elements, calculations led to the systematic underestimation of the boron substitution effects by around 12 %, which is caused by the fact that the inner fuel region has more curved geometry and higher neutron importance than the outer fuel region. In other words, a curved geometry was approximated to a slab geometry in the generation procedure of the group constants in the present study. Therefore, a model used in the group constant generation is poorer in the inner fuel region than in the outer fuel region, that may lead to an inaccurate result of calculation. Moreover, when the inaccurate group constants are used in a region having higher neutron importance, a calculated result becomes more inaccurate. This is considered to be one reason for the above underestimation, however, further investigation would be necessary to clarify thoroughly the reason.

Although further investigation would be necessary to obtain more accurate results of calculations, confidence has been gained through the present study that the 2D-FEM-KUR code is an excellent tool for the analysis of the KUCA MEU experiments. In the next step, the use of the SRAC code system[71] is to be anticipated for the generation of the group constants, since the SRAC system has a capability of a two-dimensional treatment for the generation of group constants.

IV-4. Conclusions

The results obtained through this study are summarized as follows:

(1) Differences between the results of calculations and experiments are less than 2 % in C/E ratios for eigenvalues, with use of the ANL code system which is widely used in the RERTR program.

(2) The agreement between the results obtained using the DIF3D(2D) code and the 2D-FEM-KUR code is excellent. The 2D-FEM-KUR code is more advantageous than the DIF3D(2D) code in the precise geometrical representation and in the CPU time for a complex core configuration.

(3) With use of the 2D-FEM-KUR code, the calculated results of the boron and mass reactivity effects approximately agreed with the experiments. The agreement is good for the boron and mass reactivity effects in the analyses of the boron substitution effects in the outer fuel region.

(4) One should be careful, when an artificial extra region is attached in the cell calculation. A special attention should be paid in a generation process of the group constants to take into account the geometrical heterogeneity of a core. Further study would be necessary to generate the proper group constants for the boron loaded side-plates especially in the inner fuel region, where the neutron importance is the highest and a strongly curved geometry is used.

V. ANALYSES OF THE VOID REACTIVITY

V-1. Introduction

Since the void reactivity coefficient is a physical quantity closely related to the safety of liquid-moderated reactors, which are commonly used as research reactors, it is important to investigate this quantity. Especially in water-moderated research reactors which utilize plate type fuel, the void reactivity effect in the fuel region is designed to provide the most dominant negative feedback which could terminate a power excursion due to an accidental introduction of positive reactivity. Therefore, to submit an application of safety review (the Reactor Installation License by the Government) for a reactor construction including a core conversion in accordance with the use of REU fuel, it is significantly important to develop a method for calculating accurately the void reactivity in either core loaded with HEU fuel or REU fuel.

Through the KUCA experiments described in Section III-8-B, the void reactivity effects were measured at various locations in the fuel region of an annular core loaded with HEU fuel or MEU fuel. These data on the void reactivity effect have provided useful benchmark data not only for the use of MEU fuel but also for water-moderated reactors, since there was only few data obtained by injecting real voids in the fuel region.[97,98]

Main objectives of the present study was to develop a method for calculating the localized void reactivity and to assess the developed method of calculation in comparison with the experimental results.[66] The method for calculating the void reactivity was developed with use of current codes for the generation of the few-group constants and for the

diffusion calculation including the perturbation calculation. In order to establish a self-consistent system for the neutronics calculations in the KUCA, the assessment was performed through the following examinations:

(1) Whether the developed method of calculation can reproduce the observed spatial dependence of the void reactivity in the fuel region, in other words, how large the discrepancy between the measured and calculated void reactivities is.

(2) What is the most dominant nuclear feature (diffusion, absorption, moderation or generation of neutrons) affecting the reactivity change due to the injection of voids into a flow channel.

(3) Whether the method of calculation can be applied to the MEU core as well as the HEU core and to the MEU cores with and without boron.

(4) Whether the method is applicable to calculating the reactivity effect of bubbling in a pair of flow channels.

V-2. Calculations

V-2-A. Description of the Computer Codes

The calculation has been performed using SRAC[71] and the 2D-FEM-KUR code,[69] since SRAC has been applied to several benchmark problems and has provided good results.[27,28,72,107-110] SRAC was employed to generate the few-group constants for the subsequent diffusion calculation, since a two-dimensional transport calculation as well as a one-dimensional diffusion calculation was thought to be necessary to take into account the heterogeneity of the complex core constructed in the KUCA as suggested in Section IV-3. 2D-FEM-KUR was employed for both the criticality and void

reactivity calculations, since this code is assessed to be adequate for the analysis of the KUCA experimental data.

SRAC,[71] which stands for "Standard Reactor Analysis Codes", has been developed at JAERI as a code system for the analysis and design of a thermal nuclear reactor. It consists of neutron cross section libraries, auxiliary processing programs, neutron spectrum routines, one- and two-dimensional transport routines, one- through three-dimensional diffusion routines, dynamic parameters and cell burn-up routines. The user can select either cell or core calculation; fixed source or eigenvalue problem; transport (collision probability or S_n) theory or diffusion theory. Moreover, smearing and collapsing of macroscopic cross sections can be performed separately at the user's discretion. Special attention is paid to a two-dimensional treatment of heterogeneities when performing cell calculations. Various techniques are employed to access the data storage and to optimize the internal data transfer.

The 2D-FEM-KUR code[69] is a two-dimensional diffusion code employing the finite-element method which facilitates the precise modelling of complex core configurations, and has a capability for eigenvalue and perturbation calculations. The routine for the perturbation calculation can compute each contribution of the diffusion, moderation, absorption and generation of neutrons, to the reactivity change.

V-2-B. Procedure of the Calculation

The void reactivity was calculated by the following procedures:

(i) Generate 4-group constants for the subsequent calculations.

(ii) Perform the eigenvalue calculation using diffusion theory.

(iii) Calculate the void reactivity using perturbation theory.

The flow chart for the calculation is shown in Fig. V-1.

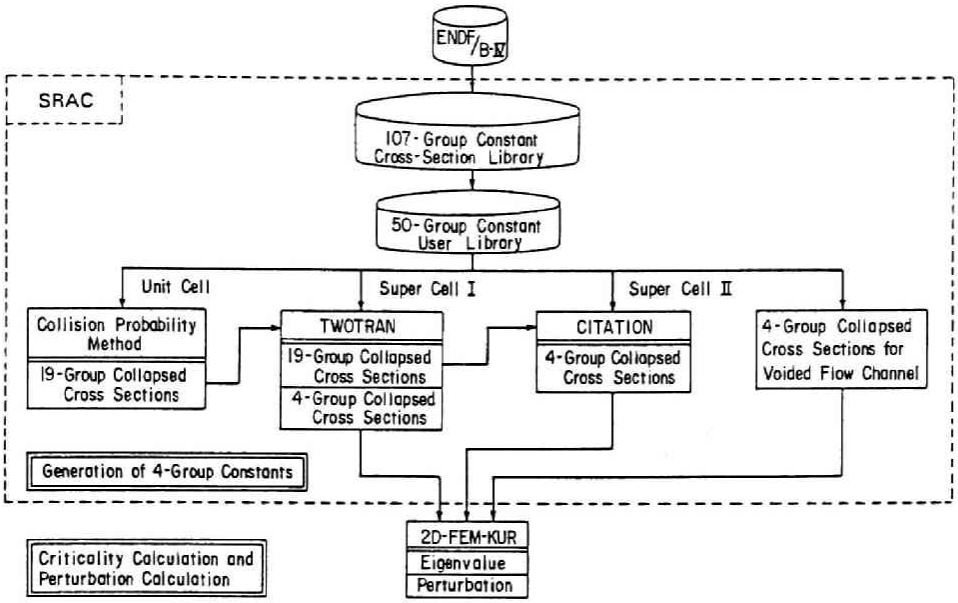

Fig. V-1 Flow Chart for the Calculation

(i) Generation of Four-Group Constants

The cylindrical core loaded with MEU or HEU fuel, in which the void reactivity measurements were performed, was divided into the following 10 regions including the reflector regions, as shown in Fig. V-2:

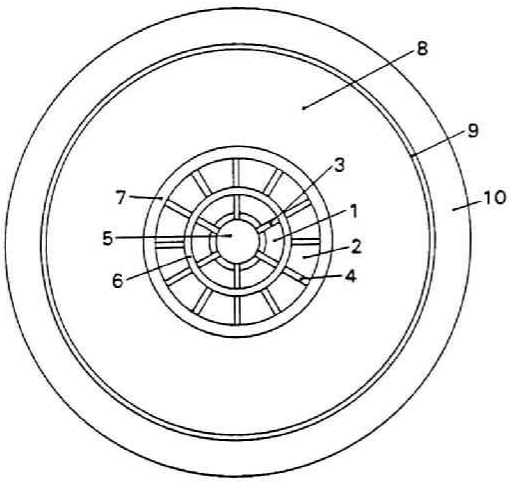

Fig. V-2
Core Configuration Used in the Diffusion Calculation

(1) Inner fuel regions.

(2) Outer fuel regions.

(3) Inner side-plate regions.

(4) Outer side-plate regions.

(5) Light-water region in the center of the core.

(6) Control rod region.

(7) Outer light-water region between the outer fuel elements and the heavy-water reflector, including the inner wall of the annular heavy-water tank made of aluminum.

(8) Heavy-water reflector region.

(9) Outer wall region of the heavy-water tank.

(10) Light-water reflector region outside the heavy-water tank.

To generate 4-group constants whose upper energy boundaries are 10 MeV, 497.87 keV, 5.53 keV and 0.68256 eV (thermal cut-off), the following three serial steps were performed with use of SRAC to take the heterogeneity of the core into account:

Step I : "Unit Cell" calculation,

Step II : "Super Cell I" calculation, and

Step III: "Super Cell II" calculation.

Each step will be described below in detail.

The fundamental library of group constants was produced mainly from the ENDF/B-IV nuclear data file[104] with 107 energy groups. The transport cross-sections for the P_0 transport calculation were calculated by the B_1 approximation, and the diffusion coefficients were obtained assuming $D = 1/(3\Sigma_{tr})$. The resonance absorption for heavy nuclides was calculated by two methods: a table look-up method for the neutron energy $E \geq 130.07$ eV, and a collision probability method using the ultra-fine energy points of 4600 for 130.07 ev $\geq E \geq$ 0.68256 eV. Thus, the user library was construct-

ed with a structure of 50 energy groups (23 fast groups and 27 thermal groups), as shown in Table V-1.

Table V-1 Energy Group Structure

Group Number		Fast Energy (eV)	Group Number		Thermal Energy (eV)
Fine	Coarse		Fine	Coarse	
1	1	0.10000E+8[a]	24	11	0.68256E+0
2		0.47237E+7	25		0.41399E+0
3	2	0.22313E+7	26		0.34206E+0
4		0.10540E+7	27	12	0.29792E+0
5	3	0.49787E+6	28		0.25683E+0
6		0.23518E+6	29		0.21878E+0
7	4	0.11109E+6	30	13	0.18378E+0
8		0.52475E+5	31		0.15183E+0
9	5	0.24788E+5	32		0.13700E+0
10		0.11709E+5	33	14	0.12293E+0
11	6	0.55308E+4	34		0.10963E+0
12		0.26126E+4	35		0.97080E−1
13	7	0.12341E+4	36	15	0.85397E−1
14		0.58295E+3	37		0.74276E−1
15	8	0.27536E+3	38		0.64017E−1
16		0.13007E+3	39	16	0.54520E−1
17		0.61442E+2	40		0.45785E−1
18	9	0.29023E+2	41		0.37813E−1
19		0.13710E+2	42	17	0.30602E−1
20		0.64760E+1	43		0.24154E−1
21	10	0.30590E+1	44		0.18467E−1
22		0.18554E+1	45	18	0.13543E−1
23		0.11253E+1	46		0.93805E−2
		0.68256E+0	47		0.59804E−2
			48	19	0.33423E−2
			49		0.14663E−2
			50		0.35238E−3
					0.10000E−4

[a]Read as 0.10000×10^8.

Step I : "Unit Cell" Calculation

The "Unit Cell" calculation was performed to obtain cell-averaged cross sections for the so-called fuel meat region, which is composed of fuel meat (UAl alloy in HEU fuel and UAl_x-Al dispersion aluminide in MEU fuel), aluminum cladding and light-water moderator. Assuming a fixed source problem, this calculation was performed with use of the collision probability routine in SRAC. Although the actual fuel plate has a curved geometry, it was approximated by a slab geometry as shown in Fig. V-3. In this step, the above 50 groups were collapsed to 19 groups (10 fast groups

and 9 thermal groups as shown in Table V-1).

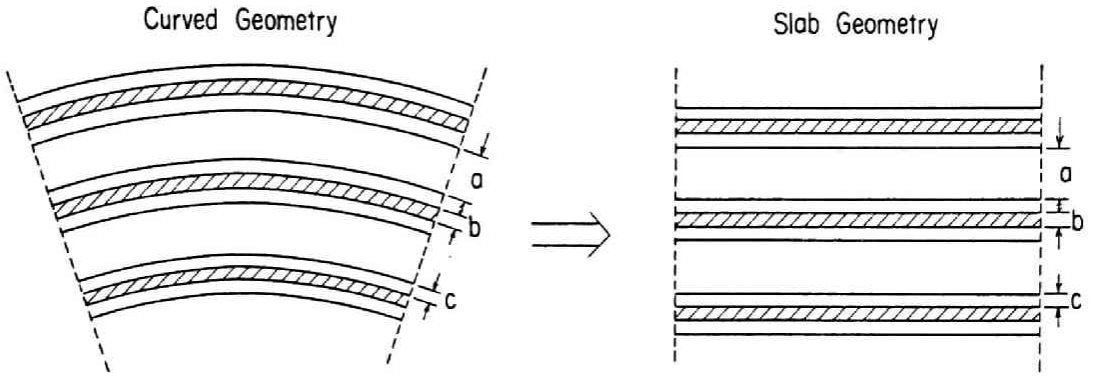

a. Thickness of Light-Water Moderator
b. Thickness of Fuel Meat
c. Thickness of Aluminum Cladding

Fig. V-3 Simplified Model of the Fuel Meat Region for the "Unit Cell" Calculation

Step II : "Super Cell I" Calculation

The "Super Cell I" calculation was performed with use of the TWOTRAN code (two-dimensional S_n transport calculation code)[97] in SRAC. Using TWOTRAN, a P_0 and S_4 calculation was performed in order to take into account the neutron flux distribution in the azimuthal direction, especially the effect of a flux tilt due to natural boron (a strong absorber) contained in some of the side-plate regions.

In this step, the cell-averaged 19-group constants of the so-called fuel region were generated by collapsing spatially over regions D and E described below (refer to Fig. V-4), with use of the 19-group constants for the fuel meat region (Region E) obtained in Step I. The 4-group constants of the side-plate region, which consisted of regions A through C described below, were also generated for use in the subsequent diffusion calculation. It should be noted here that, for regions other than the fuel meat region, the 19-group constants were generated in advance of the calculation by collapsing the 50-group constants (user library) with use of the standard

spectrum (fission + 1/E + Maxwellian) installed in SRAC.

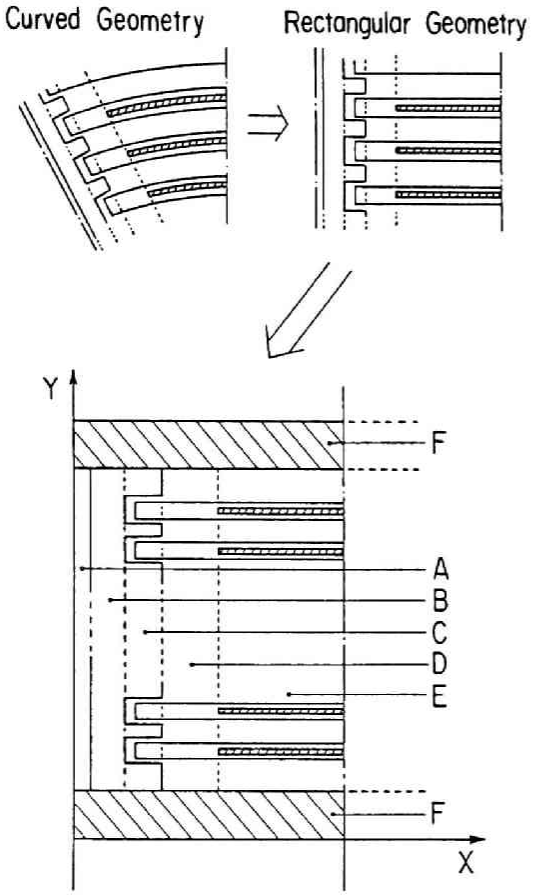

A. Light-Water Gap Between Side-Plates
B. Aluminum Plate Region of the Side-Plate
C. Groove Region of the Side-Plate
D. Part of the Fuel Plate without Fuel Meat
E. Part of the Fuel Plate with Fuel Meat
F. Extra Light-Water Region

Fig. V-4
"Super Cell I" Model without Boron

For simplicity, a curved geometry of the fuel element was approximated by a rectangular one, where the average arc length and the cross sectional area of the fuel region were preserved. An example of the model for the calculation in this step is shown in Fig. V-4. The area was divided into the following 5 regions along the X-axis:

Region A : light-water gap region between adjacent side-plates,

Region B : aluminum plate region of the side-plate,

Region C : groove region of the side-plate,

Region D : part of the fuel plate region without fuel meat, and

Region E : part of the fuel plate region with fuel meat.

When the side-plates contained boron, Region B was subdivided into 3 regions.

In the Y direction in Fig. V-4, extra water regions were attached to both ends of the fuel element in order to consider the effect of reflection by light-water in those regions. The axial buckling obtained from the neutron flux measurement, which tabulated in Table V-2, was used to take into account the effect of neutron leakage in the vertical direction. A reflective boundary condition was assumed for all boundaries.

Table V-2 Vertical Buckling

Region No.*	Buckling, B^2 ($10^{-3}cm^{-2}$) MEU	HEU
5	1.6966	1.6867
1 ∿ 4, 6, 7	1.7289	1.6201
8 ∿ 10	1.5595	1.5577

* : Refer to Fig. V-2.

Step III : "Super Cell II" Calculation

In consideration of the neutron flux distribution in the radial direction, the "Super Cell II" calculation was performed with use of the CITATION code (multi-dimensional diffusion calculation code)[112] in SRAC. One-dimensional cylindrical geometry was employed with the 19-group constants including the group constants for the fuel region obtained through Step I and II as shown in Fig. V-5.

In the vertical direction, the axial buckling tabulated in Table V-2 was used. Through this step, the 19 groups were collapsed to 4 groups, and the 4-group constants of the various regions in the core were obtained (except for the side-plate region where the group constants were previously

obtained in Step II).

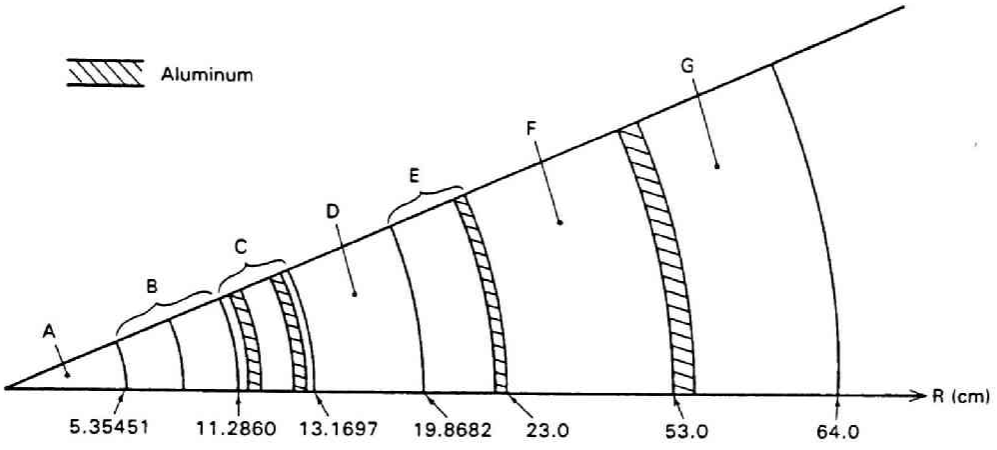

A. Light Water Region in the Center of Core
B. Inner Fuel Region
C. Control Rod Region
D. Outer Fuel Region
E. Outer Vessel Region Between the Outer Fuel Elements and the Heavy Water Reflector
F. Heavy Water Reflector Region
G. Light Water Reflector Region Outside of the Heavy Water Tank

Fig. V-5 "Super Cell II" Model for the MEU Core

(ii) Eigenvalue Calculation for the Effective Multiplication Factor

Employing the 2D-FEM-KUR code, two-dimensional diffusion calculations based on the finite-element method were performed with use of the 4-group constants obtained in the "Super Cell I and II" calculations. In the vertical direction, the buckling tabulated in Table V-2 was used. The model of the core configuration used for this calculation was shown in Fig. V-2.

(iii) Perturbation Calculation for the Void Reactivity

For the calculation of void reactivity, it was assumed that the voids were mixed homogeneously with light-water in the flow channel. Four-group constants for this mixture were obtained with use of SRAC. To collapse the

energy groups, the standard fission spectrum and 1/E spectrum + a Maxwellian distribution were assumed in the fast and thermal energy regions, respectively. Then, using the neutron flux and adjoint flux distributions obtained through the previous eigenvalue calculation, a perturbation calculation was performed to obtain the void reactivity with use of the 2D-FEM-KUR code.

V-3. Results and Discussion

V-3-A. Results of the Calculations

Void Reactivity with a Single Voided Channel in the MEU Core with Boron

The void reactivity with a single voided channel in the MEU core with boron was measured as described in Section III-8-B. The core configuration is shown in Fig. V-6. The side-plates of the fuel elements IN(B)-02 and EX(B)-04 contained boron loaded side-plates. Voids were generated by injecting N_2 gas into the fuel elements IN(B)-02 and EX(B)-04 as shown in Fig. V-7.

Table V-3 Effective Multiplication Factor in the Core without Void

Core	Measured Excess Reactivity, ρ_{ex} ($10^{-3}\Delta k/k$)	Effective Multiplication Factor, k_{eff}		C/E
		Experiment	Calculation	
MEU Core with Boron	0.4	1.0004	1.0033	1.0029
HEU Core without Boron	1.6	1.0016	1.0038	1.0022
MEU Core without Boron	1.9	1.0019	1.0058	1.0039

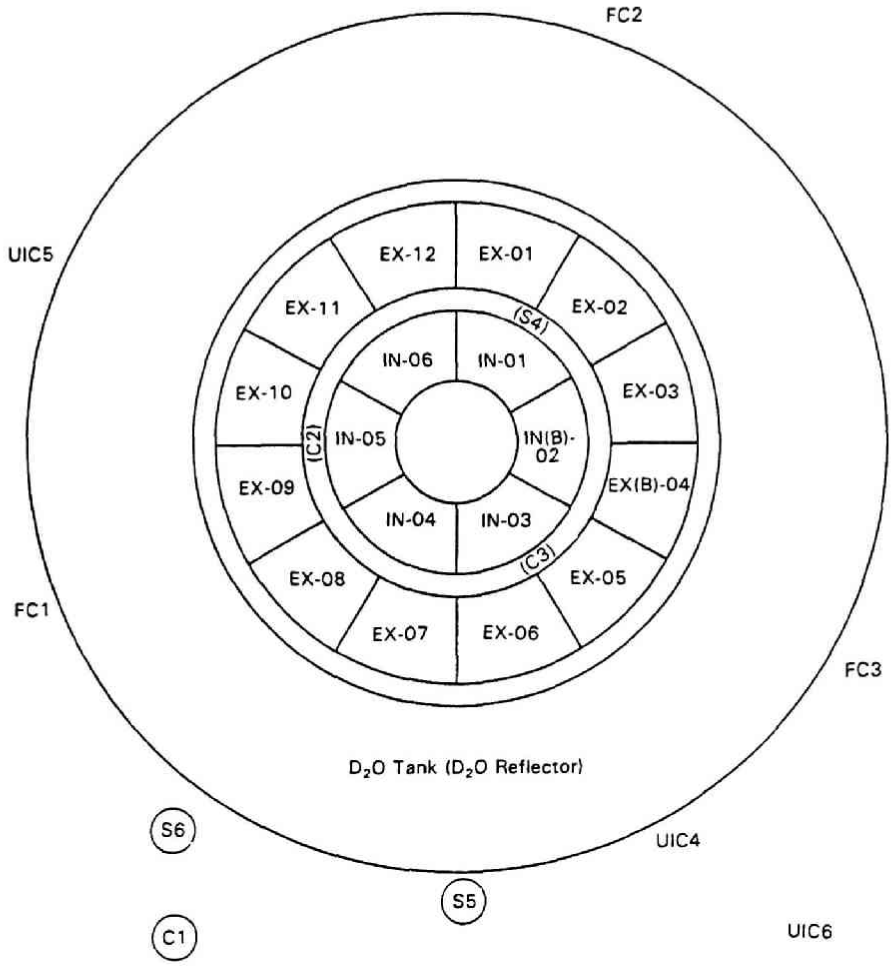

IN-01 and
IN-03 to IN-06 = Inner Fuel Elements (Containing No Burnable Poison)
IN(B)-02 = Inner Fuel Element (Containing Burnable Poison)
EX-01 to EX-03 and
EX-05 to EX-12 = Outer Fuel Elements (Containing No Burnable Poison)
EX(B)-04 = Outer Fuel Elements (Containing Burnable Poison)
C1 to C3 = Control Rods
S4 to S6 = Safety Rods
FC1 to FC3 = Fission Chambers
UIC4 to UIC6 = Uncompensated Ionization Chambers
EX-01 to EX-12 contain 17 fuel plates.
IN-03 to IN-05 contain 11 fuel plates.
IN-01, IN(B)-02, and IN-06 contain 10 fuel plates.
Total: 267 fuel plates.

Fig. V-6 Configuration of the MEU Core with Boron

The effective multiplication factor (k_{eff}) of the core without voids was calculated to be 1.0033, while the measured value was 1.0004, then a C/E ratio is 1.0029 as shown in Table V-3. The measured and calculated void reactivities are shown in Fig. V-8. The results of the calculation

for the void reactivities are also presented in Table V-4 in comparison with the experimental data.

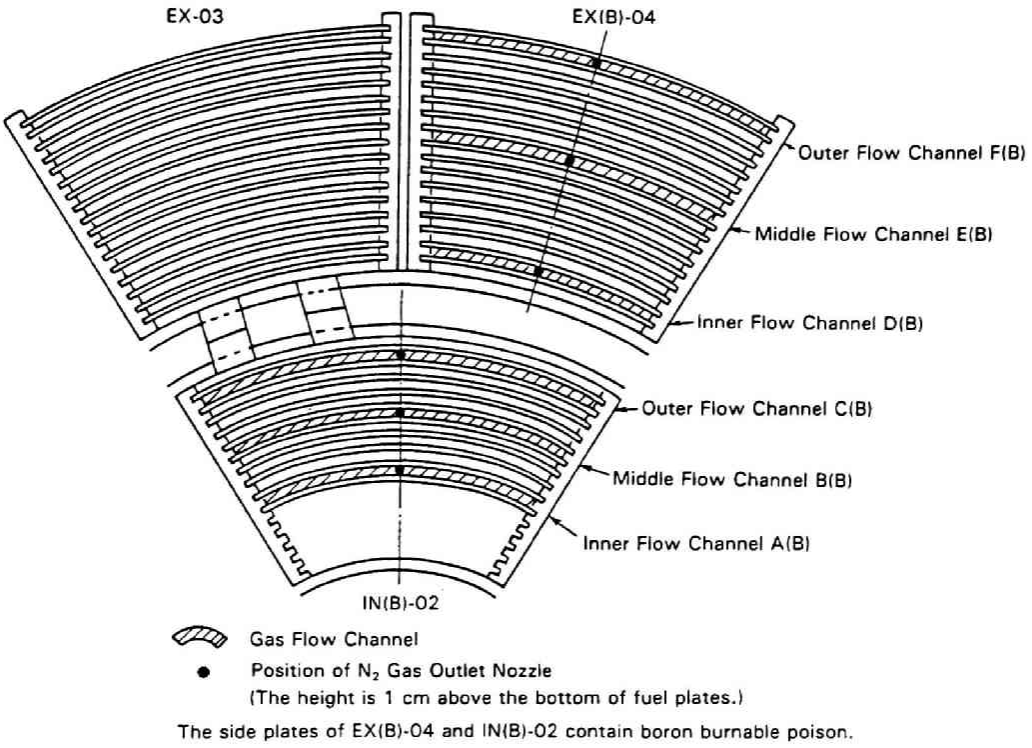

Fig. V-7 Cross-sectional View of Voided Flow Channels in Fuel Elements for the MEU Core with Boron

The discrepancy between the calculated and measured void reactivities is less than 0.04×10^{-3} $\Delta k/k$. The calculation approximately reproduces the dependence of void reactivity upon the location of the voided flow channel except in channels B(B) and F(B).

Figure V-8 shows that the measured void reactivities in Channel B(B) are larger than in Channel C(B), which are contrary to the calculated results. Figure V-8 also shows that the measured void reactivities in Channel F(B) are very close to those in Channel D(B) with which the calculated ones agree well as shown in Table V-4.

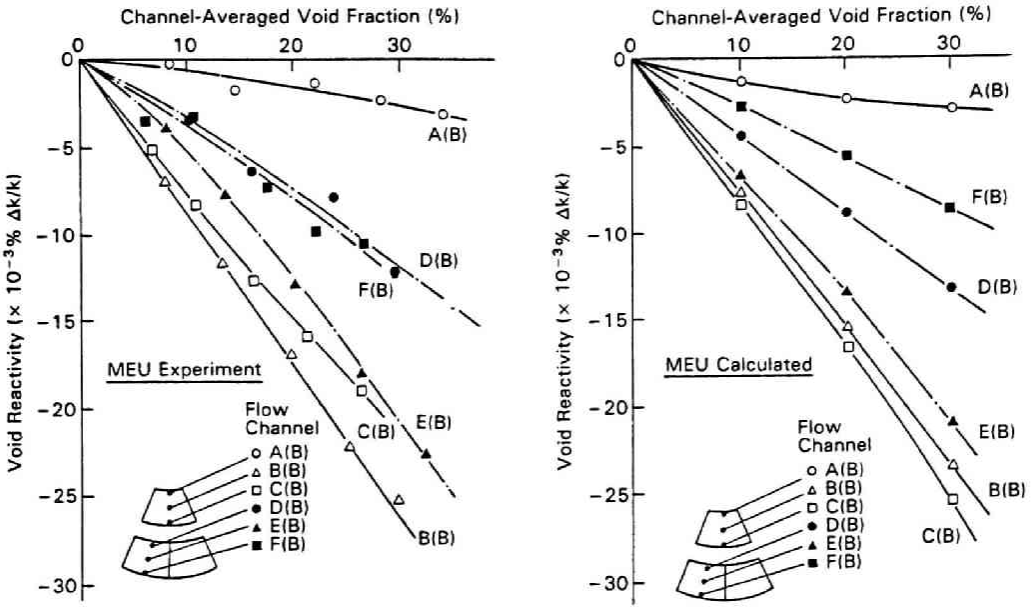

Fig. V-8 Measured and Calculated Void Reactivities versus Channel-Averaged Void Fraction for the MEU Core with Boron

Table V-4 Calculated Results of Void Reactivity in the MEU Core with Boron

Voided Channel Location	Void Fraction (%)	Void Reactivity ($\Delta k/k$)		Contribution of Nuclear Features ($\Delta k/k$)				
		Experiment[a]	Calculation	Diffusion[b] (Total)	Diffusion[c] (Vertical)	Diffusion[d] (Horizontal)	Absorption[e]	Degradation[f] (Moderation)
A(B)	10	−0.5E−5[g]	−1.3831E−5	1.2020E−5	−7.5781E−6	1.9598E−5	3.4074E−5	−5.9924E−5
	20	−1.6E−5	−2.4600E−5	2.7103E−5	−1.6988E−5	4.4091E−5	6.8145E−5	−1.1985E−4
	30	−2.7E−5	−3.0960E−5	4.6594E−5	−2.8981E−5	7.5575E−5	1.0221E−4	−1.7977E−4
B(B)	10	−9.0E−5	−7.7980E−5	−7.9482E−6	−9.7790E−6	1.8308E−6	3.4681E−5	−1.0471E−4
	20	−18.0E−5	−1.5787E−4	−1.7803E−5	−2.1920E−5	4.1170E−6	6.9358E−5	−2.0943E−4
	30	−27.1E−5	−2.4044E−4	−3.0348E−5	−3.7400E−5	7.0522E−6	1.0403E−4	−3.1413E−4
C(B)	10	−7.9E−5	−8.3856E−5	−8.8275E−6	−1.1406E−5	2.5785E−6	4.2008E−5	−1.1704E−4
	20	−15.4E−5	−1.6979E−4	−1.9725E−5	−2.5570E−5	5.8447E−6	8.4013E−5	−2.3407E−4
	30	−22.2E−5	−2.5859E−4	−3.3499E−5	−4.3620E−5	1.0121E−5	1.2601E−4	−3.5110E−4
D(B)	10	−3.4E−5	−4.4412E−5	−3.8795E−6	−4.8210E−6	9.4154E−7	2.0086E−5	−5.9619E−5
	20	−7.5E−5	−9.0002E−5	−1.0943E−5	−1.3050E−5	2.1160E−6	4.0171E−5	−1.1924E−4
	30	−12.2E−5	−1.3724E−4	−1.8638E−5	−2.2260E−5	3.6217E−6	6.0254E−5	−1.7885E−4
E(B)	10	−5.4E−5	−6.7311E−5	−1.4246E−6	−5.9090E−6	−8.3374E−6	1.8463E−5	−7.1528E−5
	20	−13.0E−5	−1.3807E−4	−3.1937E−5	−1.3250E−5	−1.8687E−5	3.6925E−5	−1.4306E−4
	30	−21.4E−5	−2.1365E−4	−5.4453E−5	−2.2590E−5	−3.1863E−5	5.5385E−5	−2.1458E−4
F(B)	10	−3.8E−5	−2.7302E−5	−9.2360E−6	−4.8860E−6	−4.3500E−6	2.4189E−5	−4.2255E−5
	20	−8.0E−5	−5.6650E−5	−2.0517E−5	−1.0956E−5	−9.5610E−6	4.8377E−5	−8.4510E−5
	30	−13.0E−5	−8.8746E−5	−3.4548E−5	−1.8694E−5	−1.5854E−5	7.2563E−5	−1.2676E−4

[a]The void reactivities obtained by the fitted curves to the experimental data (see Fig.V8).
[b]The perturbed reactivity by change in the diffusion length in both the vertical and the horizontal directions.
[c]The perturbed reactivity by change in the diffusion length only in the vertical direction.
[d]The perturbed reactivity by change in the diffusion length only in the horizontal direction.
[e]The perturbed reactivity by change in the rate of neutron absorption.
[f]The perturbed reactivity by change in the degradation of the moderation effect.
[g]Read as -0.5×10^{-5}.

Void Reactivity with a Single Voided Channel in the HEU Core without Boron

The void reactivity with a single voided channel in the HEU core without boron was also measured as described in Section III-8-B. The core configuration is shown in Fig. III-26. Voids were generated in the fuel elements IN-02 and OUT-04, as shown in Fig. III-27.

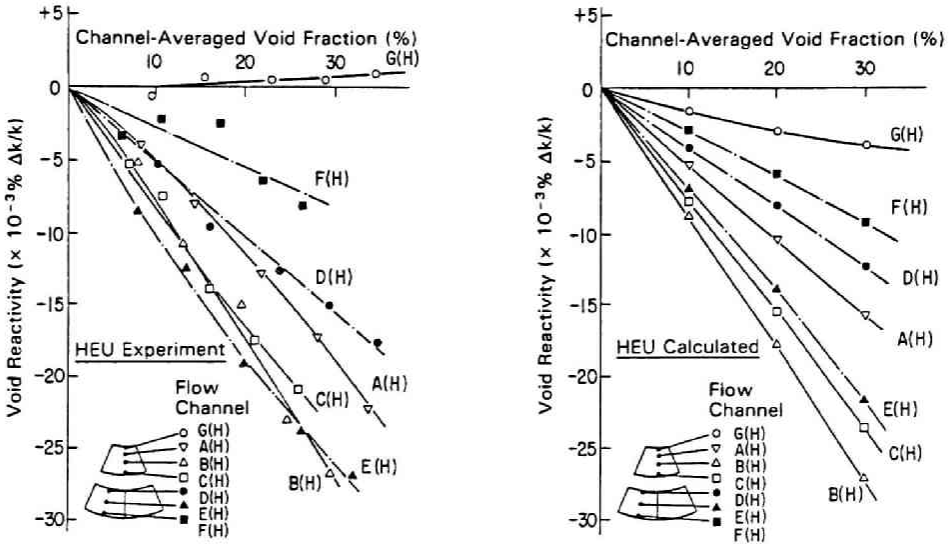

Fig. V-9 Measured and Calculated Void Reactivities versus Channel-Averaged Void Fraction for the HEU Core

As shown in Table V-3, the calculated K_{eff} in the core without voids was 1.0038, while the measured one was 1.0016, then a C/E ratio is 1.0022. Figure V-9 shows the measured and calculated void reactivity versus the channel-averaged void fraction. The results of the perturbation calculation for void reactivities are tabulated in Table V-5 in comparison with the experimental data.

The discrepancy between the calculated void reactivities and the measured ones was less than 0.05×10^{-3} $\Delta k/k$. The calculation approximately reproduced the spatial dependence of the void reactivity in the fuel region except in channels E(H) and G(H).

Table V-5 Calculated Results of Void Reactivity in the HEU Core

Voided Channel Location	Void Fraction (%)	Void Reactivity ($\Delta k/k$)		Contribution of Nuclear Features ($\Delta k/k$)				
		Experiment[a]	Calculation	Diffusion[b] (Total)	Diffusion[c] (Vertical)	Diffusion[d] (Horizontal)	Absorption[e]	Degradation[f] (Moderation)
G(H)	10	0.0	−1.5689E−5[g]	1.0212E−5	−7.5101E−6	1.7722E−5	4.1026E−5	−6.6926E−5
	20	0.4E−5	−2.8775E−5	2.3029E−5	−1.6839E−5	3.9868E−5	8.2049E−5	−1.3385E−4
	30	0.7E−5	−3.8104E−5	3.9602E−5	−2.8728E−5	6.8330E−5	1.2307E−4	−2.0078E−4
A(H)	10	−5.0E−5	−5.2447E−5	−2.1380E−6	−8.6420E−6	6.5040E−6	4.1271E−5	−9.1581E−5
	20	−11.8E−5	−1.0537E−4	−4.7480E−6	−1.9373E−5	1.4625E−5	8.2540E−5	−1.8361E−4
	30	−18.8E−5	−1.5893E−4	−8.0000E−6	−3.3050E−5	2.5050E−5	1.2381E−4	−2.7474E−4
B(H)	10	−8.0E−5	−8.8636E−5	−9.8077E−6	−1.0581E−5	7.7327E−7	4.5389E−5	−1.2422E−4
	20	−17.6E−5	−1.7963E−4	−2.1972E−5	−2.3720E−5	1.7479E−6	9.0775E−5	−2.4844E−4
	30	−27.6E−5	−2.7394E−4	−3.7455E−5	−4.0470E−5	3.0154E−6	1.3616E−4	−3.7265E−4
C(H)	10	−8.6E−5	−7.7542E−5	−7.0989E−6	−1.1952E−5	4.8531E−6	5.5756E−5	−1.2620E−4
	20	−16.8E−5	−1.5670E−4	−1.5802E−5	−2.6790E−5	1.0988E−5	1.1151E−4	−2.5240E−4
	30	−24.0E−5	−2.3806E−4	−2.6723E−5	−4.5720E−5	1.8997E−5	1.6726E−4	−3.7859E−4
D(H)	10	−5.2E−5	−4.0333E−5	−3.5896E−6	−5.9760E−6	2.3864E−6	2.6764E−5	−6.3507E−5
	20	−10.4E−5	−8.1527E−5	−8.0369E−6	−1.3399E−5	5.3621E−6	5.3527E−5	−1.2702E−4
	30	−15.6E−5	−1.2392E−4	−1.3685E−5	−2.2860E−5	9.1748E−6	8.0287E−5	−1.9052E−4
E(H)	10	−10.4E−5	−6.8523E−5	−1.6160E−5	−5.9130E−6	−1.0247E−5	2.3698E−5	−7.6061E−5
	20	−19.0E−5	−1.4095E−4	−3.6220E−5	−1.3250E−5	−2.2970E−5	4.7395E−5	−1.5212E−4
	30	−26.2E−5	−2.1887E−4	−6.1780E−5	−2.2610E−5	−3.9170E−5	7.1090E−5	−2.2818E−4
F(H)	10	−1.8E−5	−2.7955E−5	−1.1809E−5	−4.8620E−6	−6.9470E−6	2.8391E−5	−4.4538E−5
	20	−5.6E−5	−5.8580E−5	−2.6285E−5	−1.0901E−5	−1.5384E−5	5.6781E−5	−8.9076E−5
	30	−8.4E−5	−9.2831E−5	−4.4390E−5	−1.8601E−5	−2.5789E−5	8.5168E−5	−1.3361E−4

[a]The void reactivities obtained by the fitted curves to the experimental data (see Fig.V-9).
[b]The perturbed reactivity by change in the diffusion length in both the vertical and the horizontal directions.
[c]The perturbed reactivity by change in the diffusion length only in the vertical direction.
[d]The perturbed reactivity by change in the diffusion length only in the horizontal direction.
[e]The perturbed reactivity by change in the rate of neutron absorption.
[f]The perturbed reactivity by change in the degradation of the moderation effect.
[g]Read as -1.5689×10^{-5}.

Figure V-9 shows that the calculated void reactivities in Channel E(H) are the third largest in absolute value for a given channel-averaged void fraction, whereas the measured ones were the first or second largest. Figure V-9 also shows that the measured void reactivities in Channel E(H) are close to those in Channel B(H) with which the calculated ones agree very well as shown in Table V-5. Figure V-9 shows that the calculated void reactivities in Channel G(H) are negative, whereas the measured ones are slightly positive. Therefore, it is indicated that Channel G(H) was treated as an under-moderated region in the calculation, whereas it was found to be a slightly over-moderated region in the experiment.

Void Reactivity with Two Voided Channels in the MEU Core without Boron

As described in Section III-8-B, void reactivities were measured in the unpoisoned MEU core with two adjacent or two separated voided channels, the locations of which are shown in Fig. III-28. These measurements were analyzed in order to examine the further application of the computational method developed for the analysis on the void reactivity of a single voided channel. It should be noted that the method of calculation is unable to estimate the interference effect of two adjacent voided channels on the reactivity, because the method employed was based on perturbation theory.

The calculated k_{eff} in the core without voids was 1.0058, while the measured one was 1.0019, then a C/E ratio is 1.0039 as shown in Table V-3.

Table V-6 Calculated Results for the First Run of the Second Series of Experiments

Channel-Averaged Void Fraction (%)	Void Reactivity ($\times 10^{-3}\ \Delta k/k$)	
	Calculation	Experiment
10	−0.17	---
20	−0.35	---
30	−0.53	---
32	−0.57[a]	−0.62
35	−0.63	---

[a]This void reactivity was obtained by interpolation between the void reactivities at the void fraction of 30 and 35%.

As for the first run in the second series of experiments Table V-6 and Fig. V-10 show the comparison between the calculated and measured void reactivities with two adjacent voided channels (channels I and J). The discrepancy between the measured value and the calculated one was 0.05×10^{-3} $\Delta k/k$ at a channel-averaged void fraction of 32 %.

In the second run, Table V-7 shows the calculated and the measured void reactivities for a given channel-averaged void fraction when the voids were generated in two adjacent or two separated flow channels. Figure V-11

shows the comparison between the calculated and measured void reactivities for the two adjacent voided channels (channels K and L or channels M and N), and Fig. V-12 shows that for the two separated voided channels (channels K and N or channels L and M). The discrepancy between the average of the measured void reactivities and the calculated ones was approximately 0.10×10^{-3} $\Delta k/k$ for both cases.

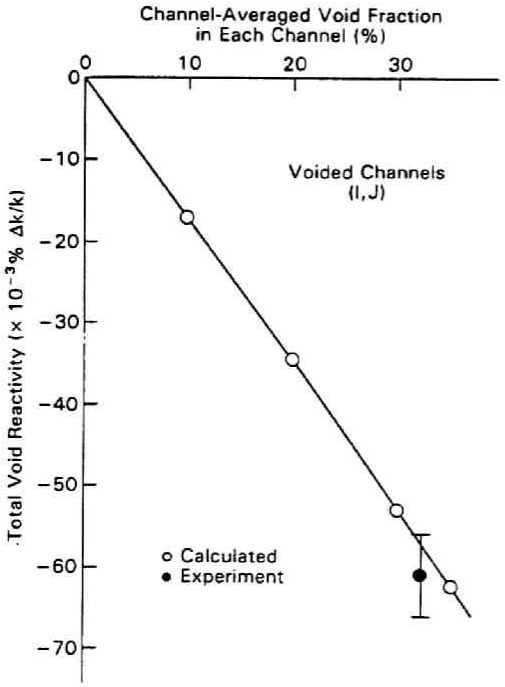

Fig. V-10 Void Reactivity versus Channel-Averaged Void Fraction for the MEU Core with Two Voided Channels (The first run in the second series experiments)

Table V-7 Calculated Results for the Second Run of the Second Series of Experiments

Channel-Averaged Void Fraction (%)	Void Reactivity ($\times 10^{-3}$ $\Delta k/k$)		
	Calculation	Experiment	
		Two Adjacent Voided Flow Channels	Two Separated Voided Flow Channels
10	−0.17	---	---
20	−0.35	−0.45	−0.45
30	−0.53	---	---
32	−0.57[a]	−0.69	−0.65
35	−0.63	---	---

[a]This void reactivity was obtained by interpolation between the void reactivities at the void fraction of 30 and 35%.

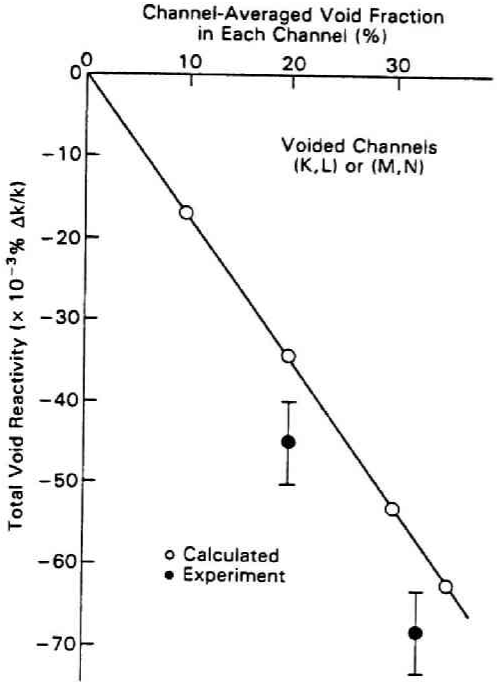

Fig. V-11

Void Reactivity versus Channel-Averaged Void Fraction for the MEU Core with Two Adjacent Voided Channels (The second run in the second series of experiments)

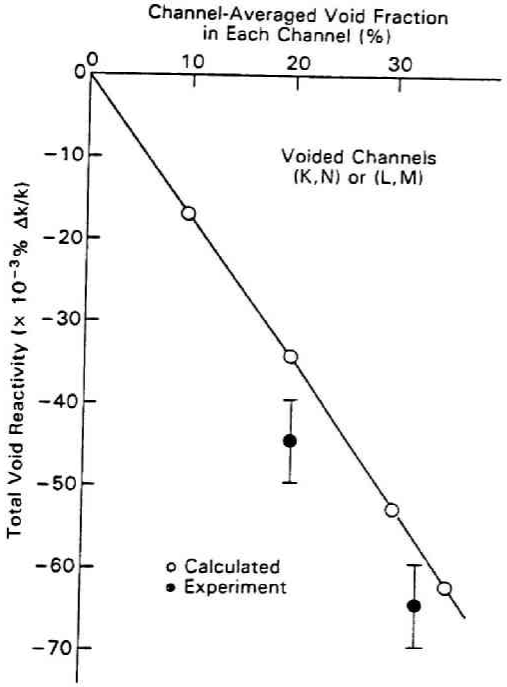

Fig. V-12

Void Reactivity versus Channel-Averaged Void Fraction for the MEU Core with Two Separate Voided Channels (The second run in the second series of experiments)

V-3-B. Discussion

As for the k_{eff} in the core without voids, the calculated results agreed with the experimental data to within 0.5 % in the C/E ratio, regardless of whether the core was loaded with HEU or MEU fuel and with or without boron. Note that the excess reactivity was measured under the condition that the needle-like nozzle was installed in the core. The reactivity effect of the needle-like nozzle was estimated as approximately -0.3 %Δk/k. Therefore, the agreement between the calculated and measured results is considered to be much better (within 0.2 % in C/E ratio).

For reference, another calculation was performed to obtain k_{eff} in the MEU core without boron using the group constants obtained by EPRI-CELL[67] which is used for the generation of group constants in Chapter IV, for the purpose of assessing the present method of group constants generation through a comparison. The calculated k_{eff} and the C/E ratio were 1.0158 and 1.0139, respectively. Whereas those were 1.0058 and 1.0039 in the present study as shown in Table V-3. Therefore, the better results were obtained with use of SRAC than those by the EPRI-CELL code. In the present study, a two-dimensional treatment was employed in the generation process of group constants using SRAC, whereas only one-dimensional treatment is available in EPRI-CELL. This indicates that a two-dimensional treatment is preferable to take into account the geometrical heterogeneity in the KUCA core for the generation of group constants. This result also provides good information to establish a self-consistent system for the neutronics calculations in the KUCA.

For the void reactivity of a single voided channel, the discrepancy between the experiment and calculation was less than 0.05×10^{-3} Δk/k. This discrepancy is the order of the experimental error for the excess

reactivity measurement in the KUCA cylindrical core, since this error was estimated to be approximately ± 0.05 × 10^{-3} Δk/k from the past experiences.

The spatial dependence was reproduced by the calculation fairly well except for the several cases. There are four possible causes for these exceptions:

(1) The neutron flux and adjoint flux in the voided flow channels were calculated by the diffusion code (2D-FEM-KUR). Generally speaking, a diffusion calculation is not adequate in the vicinity of the boundary such as that between the water reflector and fuel region or in the vicinity of a strong absorber, because anisotropic scattering cannot be neglected near the boundary and Fick's law is not suitable in a strong absorber. Therefore, the calculated neutron flux and adjoint flux may not be accurate in those regions.

(2) In generating the 4-group constants in the voided flow channel, the weighting spectrum in collapsing the energy groups was the standard spectrum (fission + 1/E + Maxwellian) installed in SRAC. This weighting spectrum did not take into account the spatial dependence of the neutron spectrum upon the location of voided flow channels in the core.

(3) The calculation employed the axial buckling obtained experimentally in the core without voids. Therefore, the change in axial buckling caused by void generation was not considered in the perturbation calculation for void reactivities. This may have contributed to the underestimation of the void reactivities.

(4) In an actual core, the neutron spectrum in the fuel region varies its feature, position by position. Therefore, the effective cross sections in an actual fuel region are space dependent. This effect is considered to be remarkable near the boundary of the fuel region,

since the regions containing light-water exist around the under-moderated fuel region. Whereas the group constants in the fuel region are obtained by averaging over the whole fuel region in the cell calculation, even if the neutron reflection effect caused by light-water existing in the vicinity of the fuel region is taken into consideration in the generation process of group constants. This may cause a difference between the calculated and measured results of the localized void reactivity such as for a few voided channels in the fuel region. This difference is considered to be fairly large near the boundaries between the fuel region and the light-water region including the central flux trap, control rod, and outer vessel regions (channels A, C, D, E, and G), where the neutron spectrum may be remarkably softened.

Greater attention should be paid to the calculation of void reactivity in the slightly over-moderated fuel region next to the thick light-water layer, and it is desirable to study further on the improvement of the computational method for the void reactivity in such a region. From the above, it is considered that the agreement between the calculated and measured results would be better, when the void is generated uniformly in the whole fuel region.

Since the apparent density of light-water moderator decreases with the increase in void fraction, the void reactivity is affected by the following three competing effects:

(1) Neutron absorption is diminished,

(2) Diffusion length becomes longer, which increases the neutron leakage from the core,

(3) Moderation of neutrons is degraded.

The contributions of these effects to the void reactivity were calculated by the 2D-FEM-KUR code in order to make a physical image clear, and they are tabulated in Tables V-4 and V-5. It was the degradation of the moderation effect that causes the dominant void reactivity, and accounts for the negative sign of the void reactivity coefficient. The decrease in neutron absorption had a positive contribution to the reactivity change. The effect of an increase in the diffusion length was positive in the horizontal direction except for two of the voided flow channels: either at the center of, or at the outermost edge of, the outer fuel element. On the other hand, this diffusion effect was negative in the vertical direction for all voided flow channels. The total reactivity change by this diffusion effect turned out to be negative except for the voided flow channels at the innermost flow channel of the inner fuel element. The diffusion effect mentioned above suggests that the reflection by light-water in the center of core might be considerable and much larger than the reflection by heavy-water surrounding the fuel regions.

In order to examine the further application of the computational method, void reactivities with two voided channels were calculated and compared with the experimental results as shown in Tables V-6 and V-7 and Figs. V-10 through V-12. The discrepancy between the calculated and measured void reactivities was less than 0.10×10^{-3} $\Delta k/k$, which was approximately twice as much as that for a single voided channel shown in Table V-6. It might be necessary to improve the method of calculation if the void reactivity in the core with several voided channels is to be calculated. The reason is that, with use of perturbation theory, the discrepancy between the calculated and measured void reactivities for several voided channels in the fuel region might grow larger than that for

a single voided channel.

The developed method of calculation employing perturbation theory was assessed to be adequate for the calculation of localized void reactivity, since the discrepancy between the measured and calculated void reactivities was approximately equal to the experimental error for a single voided channel in the fuel region. In addition, the perturbation calculation employed in this study might be applicable to calculate the void reactivity when voids are generated uniformly over the fuel region. In this case, more attention should be paid to the generation of the few-group constants in the voided region, because the voided region is so wide that the interference effect may well exist between voided fuel elements. On this purpose, the eigenvalue calculation employed in the criticality calculation might be also applicable, because the void reactivity would be large enough for an eigenvalue calculation. Moreover, the moderator temperature coefficient which is also related closely to the safety of water-moderated reactors could be calculated by the eigenvalue calculation employed in the present study.

It should be noted that the void reactivity in the unpoisoned MEU core with single voided channel was not calculated in this study. The reason was that the core configuration employed for the measurement in the unpoisoned MEU core with a single voided channel provided an additional difficulty for precise modelling in the calculation. Among the cores employed in the void reactivity measurements, only this core had aluminum tubes with small diameter at a specific location in the annular control rod region and one fuel plate inserted apart from the normal fuel region where fuel plates were arranged with 3.80 mm pitch as shown in Fig. III-24 in Section III-8-B. Since a poor modelling for a core configuration would lead to an inaccurate result of calculation for the void reactivity, such a core was

thought to be not adequate for the special purpose of examining the effect of reducing fuel enrichment on the void reactivity by the calculation in comparison with the experimental result.

On the other hand, for the unpoisoned MEU core, the void reactivity with two voided channels was measured in the preceding study employing a core which was very close in the configuration to the poisoned MEU and unpoisoned HEU cores with a single voided channel. Since the interference effect was found to be negligible in the experiments, the effect of reducing enrichment on the void reactivity could be examined indirectly through the calculations for the unpoisoned HEU core with a single voided channel and for the unpoisoned MEU core with two voided channels.

V-4. Conclusions

The results obtained through this study are summarized as follows:

(1) The calculated results for k_{eff} in the core without voids, agreed with the experimental data to within 0.5 % in the C/E ratio, regardless of whether the core was loaded with MEU or HEU fuel and with or without boron. Therefore, there is a good prospect of the application of the computational method to the core loaded with LEU fuel.

(2) With regard to the void reactivity in a single flow channel, the calculation approximately reproduced the dependence of the void reactivity upon the void-injected location except for the few cases. The discrepancy between the calculated and measured void reactivities was less than 0.05×10^{-3} $\Delta k/k$, regardless of whether the core was loaded with MEU or HEU fuel and with or without boron. Additionally,

the perturbation calculation showed that the degradation of the moderation effect dominated the void reactivity in the under-moderated fuel region.

(3) The discrepancy between the calculated and measured void reactivities for two voided channels was approximately twice as much as that for a single voided channel. If the void reactivities in the core with several voided channels where the interference effect might exist are to be calculated, it might be necessary to improve the method of calculation.

(4) SRAC is more advantageous than EPRI-CELL for the generation of group constants in the KUCA annular core. The reason is that SRAC has a capability of two-dimensional treatment which facilitates to take into account more accurately the heterogeneity in a core than EPRI-CELL which can treat only the one-dimensional problems.

VI. ANALYSES OF THE TEMPERATURE REACTIVITY EFFECT

I. Introduction

The temperature coefficients of reactivity are important parameters to estimate the inherent stabilities of reactor cores. If the reactor is designed to have a negative temperature coefficient, an increase in temperature due to the increase in reactor power causes a decrease in reactivity; the power will then tend to decrease. Thus, the reactor is inherently self-stabilizing. If the negative temperature coefficient is too large in magnitude, however, a reactivity change caused by the increase from the room temperature to an operating temperature, the so-called temperature defect, will be so large that it will be difficult to assure a sufficient excess reactivity under an operating condition and a sufficient anti-reactivity margin of the control systems for a safe cold shutdown. In order to minimize the temperature defect while maintaining a stability in operation, a precise understanding and accurate predictions of temperature effects are required. Moreover, when low temperature coolant is introduced into a core having a large negative temperature coefficient, an accident may occur due to an introduction of a large positive reactivity.

Quite many studies have been performed on this subject, since the temperature coefficient of reactivity is an important physical quantity.[73,113-116] Moreover, this quantity is usually measured in any reactor before a regular operation to assure the safety. However, there has been no data for a core loaded with MEU fuel. A purpose of the present study was to understand in certain depth the physical processes of temperature effects and to predict the temperature effects precisely, especially for a

light-water-moderated and heavy-water-reflected high flux reactor which uses either HEU or MEU fuel. The other purpose was to establish a self-consistent system for the neutronics calculations in the KUCA through the analysis of the temperature effect on reactivity.

According to the physical processes involved, temperature effects can be divided into following three categories:

(1) Doppler broadening effect.

(2) Thermal expansion effect.

(3) Thermal neutron spectral shift effect.

The above three categories were taken into consideration for the calculation of the temperature effect on reactivity. In the present study, the temperature effect on the axial buckling was investigated using one- and two-dimensional cylindrical geometries in the calculation. The dependencies on the three categories were also examined as well as the region-dependent temperature effects.

VI-2. Calculations

There are two general methods to calculate the temperature effect on reactivity; namely, the integral and perturbation theory methods. The integral method is as follows: Calculate the effective multiplication factors $k_{eff}(T_i)$ and $k_{eff}(T_j)$ of a reactor system at temperatures T_i and T_j. Then, obtain the temperature effect on reactivity $\rho(T_{ij})$ as,

$$\rho(T_{ij}) = \frac{k_{eff}(T_i) - k_{eff}(T_j)}{k_{eff}(T_i) \times k_{eff}(T_j)} \quad , \qquad \text{(VI-1)}$$

where,

$$T_{ij} = (T_i + T_j) / 2 \quad . \tag{VI-2}$$

The temperature coefficients is obtained as,

$$\alpha(T_{ij}) = \rho(T_i) / (T_i - T_j) \quad . \tag{VI-3}$$

Since a high accuracy in the k_{eff} calculations is required to obtain accurate results by the integral method, a detailed cell calculation model, and a multi-group and multi-dimensional core calculation model were used with the most advanced techniques for the reactor calculations. In order to calculate the temperature effect on reactivity in the complex core described in Section III-9-B, such a treatment mentioned above was considered to be unavoidable. However, it was difficult to know the contributions of the nuclear parameters to the temperature effects quantitatively by this method.

In order to investigate directly the quantitative contributions of the nuclear parameters to the temperature effect, one should perform the calculation based on perturbation theory. It is evident that perturbation theory is especially powerful to calculate a localized reactivity effect such as the void reactivity effect in a single flow channel between the fuel plates. Although perturbation theory is suitable for a detailed understanding on the mechanism of the temperature effect, it was considered to be difficult to apply for an analysis of the temperature effect on reactivity measured in the complex KUCA core. Moreover, it is considered to be difficult to calculate the temperature effect on reactivity by a simple perturbation theory, which assumes the unchangeableness in the neutron and adjoint flux distributions, since the temperature of the whole core changed uniformly in the measurement.

In view of the above, the temperature effects were calculated by the integral method with use of the SRAC code system.[71] The effective multiplication factors were calculated at the three temperatures (namely, 300 K (27°C), 325 K (52°C), 350 K (77°C)) for which the scattering kernels are prepared for the neutron cross section library in SRAC. The flow chart for the calculation is shown in Fig. VI-1.

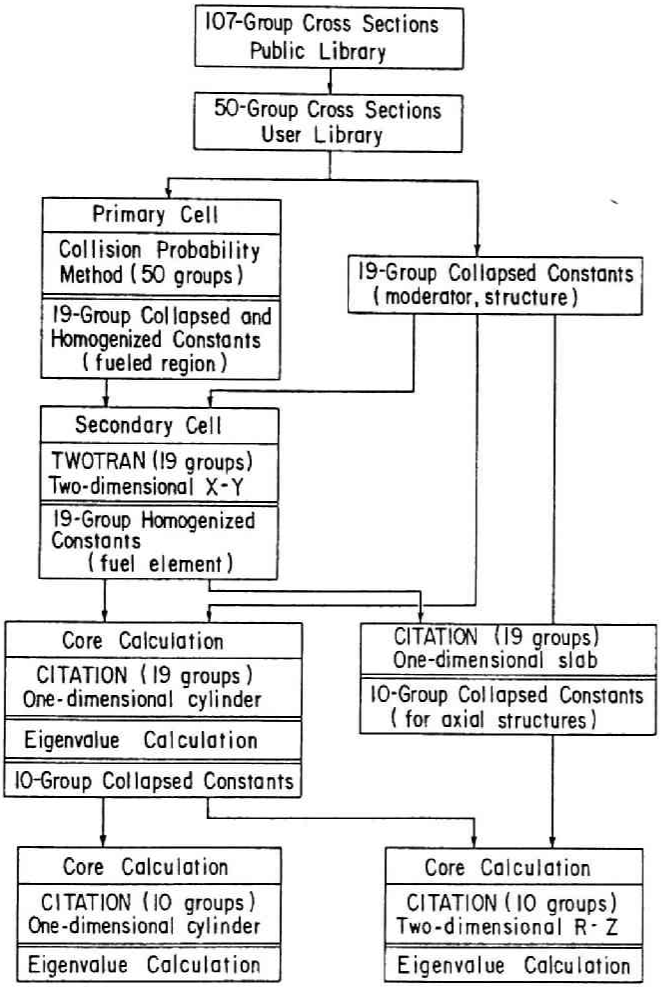

Fig. VI-1
Flow Chart for the Temperature Effect Calculations

Note that, in the present study, the 2D-FEM-KUR code[69] is not used, whereas this code is successfully used in Chapters IV and V. The reason is that the 2D-FEM-KUR code has no option for a two-dimensional cylindrical geometry [R-Z] which approximately facilitates a three-dimensional treatment. For a calculation of the temperature effect, it is considered that a

change in a neutron reflection efficiency of a water reflector should be taken into consideration not only in the horizontal direction but also in the vertical direction, since the fuel region of the KUCA annular core behaves as a under-moderated region as described in Chapters IV and V. On the other hand, SRAC has an R-Z option as well as a one-dimensional option for the core calculation. Therefore, SRAC is employed in the present study with sacrificing a precise representation in geometry for the azimuthal direction of the KUCA annular core, that is available by 2D-FEM-KUR, in a step of the core calculation. Instead, a special attention is paid to taken into account the geometrical heterogeneity effect in a generation process of the group constants.

VI-2-A. Library for the Generation of Group Constants

The fundamental library of group constants was produced mainly from the ENDF/B-IV nuclear data file[104] with 107 energy groups. The transport cross sections for the P_0 transport calculation were calculated by the B_1 approximation, and the diffusion coefficients were obtained assuming $D = 1/(3\Sigma_{tr})$. The resonance absorption for heavy nuclides was calculated by two method; a table look-up method for the neutron energy $E \geq 130.07$ eV, and a collision probability method using the ultrafine energy points of 4600 for $130.07\ \text{eV} \geq E \geq 0.68256$ eV (thermal cut off). Thus, the user library was constructed with a structure of 50 energy groups (23 fast groups and 27 thermal groups), as shown in Table VI-1.

In this procedure, the temperature effects according to the following three physical processes were taken into account:

(1) Doppler broadening effect.

(2) Thermal expansion effects (decrease in the number densities of

the light-water and heavy-water).

(3) Thermal neutron spectral shift effects (which are caused by a change of the scattering kernels in the thermal region).

Table VI-1 Energy Group Structures Used in the Calculation

Group No. Fine	Group No. Coarse	Fast Energy (eV)	Group No. Fine	Group No. Coarse	Thermal Energy (eV)
1	1	0.10000E+8*	24	11	0.68256E-0
2		0.47237E+7	25		0.41399E-0
3	2	0.22313E+7	26		0.34206E-0
4		0.10540E+7	27	12	0.29792E-0
5	3	0.49787E+6	28		0.25683E-0
6		0.23518E+6	29		0.21878E-0
7	4	0.11109E+6	30	13	0.18378E-0
8		0.52475E+5	31		0.15183E-0
9	5	0.24788E+5	32		0.13700E-0
10		0.11709E+5	33	14	0.12293E-0
11	6	0.55308E+4	34		0.10963E-0
12		0.26126E+4	35		0.97080E-1
13	7	0.12341E+4	36	15	0.85397E-1
14		0.58295E+3	37		0.74276E-1
15	8	0.27536E+3	38		0.64017E-1
16		0.13007E+3	39	16	0.54520E-1
17		0.61442E+2	40		0.45785E-1
18	9	0.29023E+2	41		0.37813E-1
19		0.13710E+2	42	17	0.30602E-1
20		0.64760E+1	43		0.24154E-1
21	10	0.30590E+1	44		0.18467E-1
22		0.18554E+1	45	18	0.13543E-1
23		0.11253E+1	46		0.93805E-2
		0.68256E-0	47		0.59804E-2
			48	19	0.33423E-2
			49	10	0.14663E-2
			50		0.35238E-3
					0.10000E-4

* : Read as 0.10000×10^{8}.

VI-2-B. Procedure of the Calculations

Step 1: Primary Cell Calculation

The primary cell calculation was performed to obtain the cell-averaged cross sections for the so-called fuel meat region, which is composed of fuel meat (U-Al alloy in HEU fuel and UAl_x-Al dispersion aluminide in MEU fuel), aluminum cladding and light-water moderator. Assuming a fixed source problem, this calculation was performed using the collision probability routine in SRAC. Although the actual fuel plate has a curved geometry, it was approximated by a slab geometry as shown in Fig. V-3. In this step, the 50 groups were collapsed to 19 groups (10 fast and 9 thermal groups as shown in Table VI-1).

Step 2: Secondary Cell Calculation

The secondary cell calculation was performed using the TWOTRAN code[111] in SRAC. Using TWOTRAN, a P_0 and S_4 calculation was performed in order to take into account the neutron flux distributions in the azimuthal direction.

In this step, the cell-averaged 19-group constants of the fuel element were generated using the 19-group constants for the fuel meat region (Region E in Fig. V-4) obtained in Step 1. Note here that, for region other than the fuel meat region, the 19-group constants were generated in advance of the calculation by collapsing the 50-group constants (user library) using the standard spectrum (fission + 1/E + Maxwellian) installed in SRAC.

For simplicity, a curved geometry of the fuel element was approximated by a rectangular one as shown in Fig. V-4. Here, special attention was paid to conserve the volumes of the fuel meat and boron loaded regions. As shown in Fig. V-4, in the actual curved geometry, the widths of fuel plates increase with the distance from the center of core, but the thickness of the side plate regions are almost constant. Therefore, the fuel elements were divided into several regions along the radial direction and plural secondary cell calculations were performed for one fuel element, as illustrations are shown in Figs. V-2 through V-7.

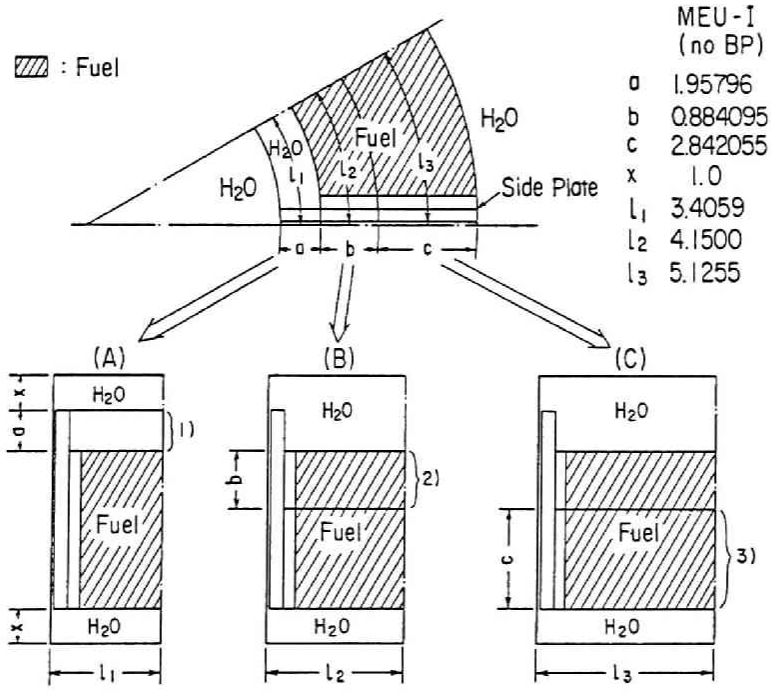

	MEU-I (no BP)	MEU-I (Outer BP)	HEU-I
a	1.95796	0.50528	1.07346
b	0.884095	2.336775	1.768045
c	2.842055	2.842055	2.841505
x	1.0	1.0	1.0
l_1	3.4059	3.0256	3.1828
l_2	4.1500	3.7697	3.9267
l_3	5.1255	5.1255	5.1334
			(cm)

1) Al Side Plate+H 0 2) Inner Fuel Region I 3) Inner Fuel Region II

Fig. VI-2 Secondary Cell Model for a Partially Loaded Inner Fuel Element without Boron

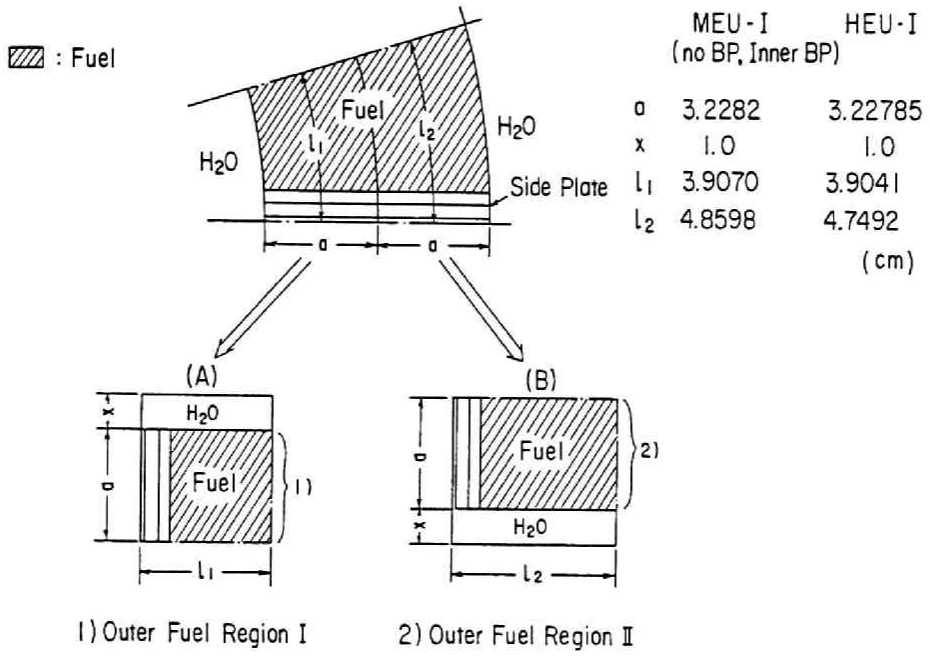

Fig. VI-3 Secondary Cell Model for a Fully Loaded Outer Fuel Element without Boron

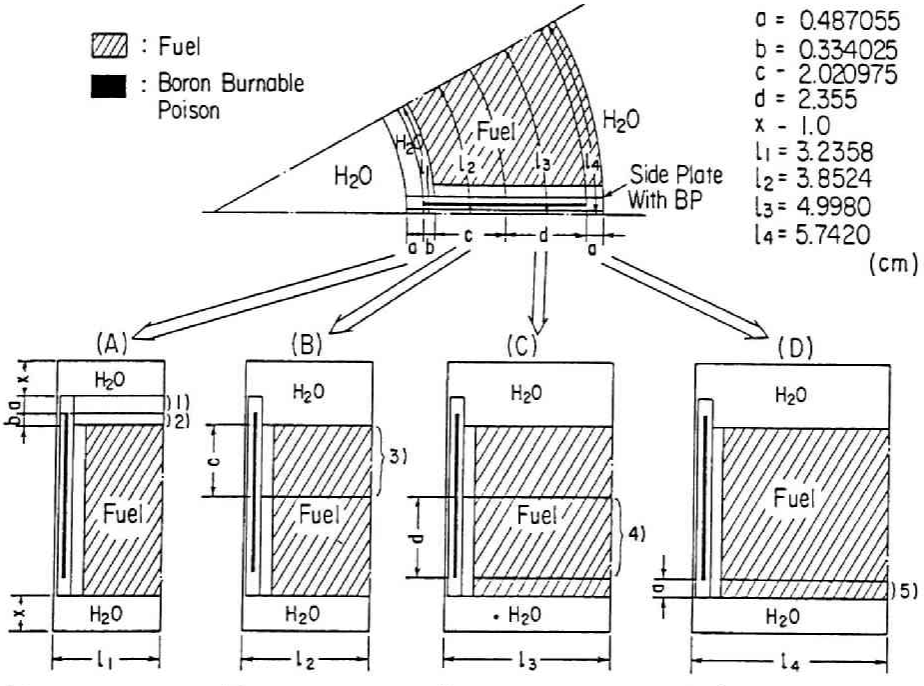

Fig. VI-4 Secondary Cell Model for a Partially Loaded Inner Fuel Element with Boron

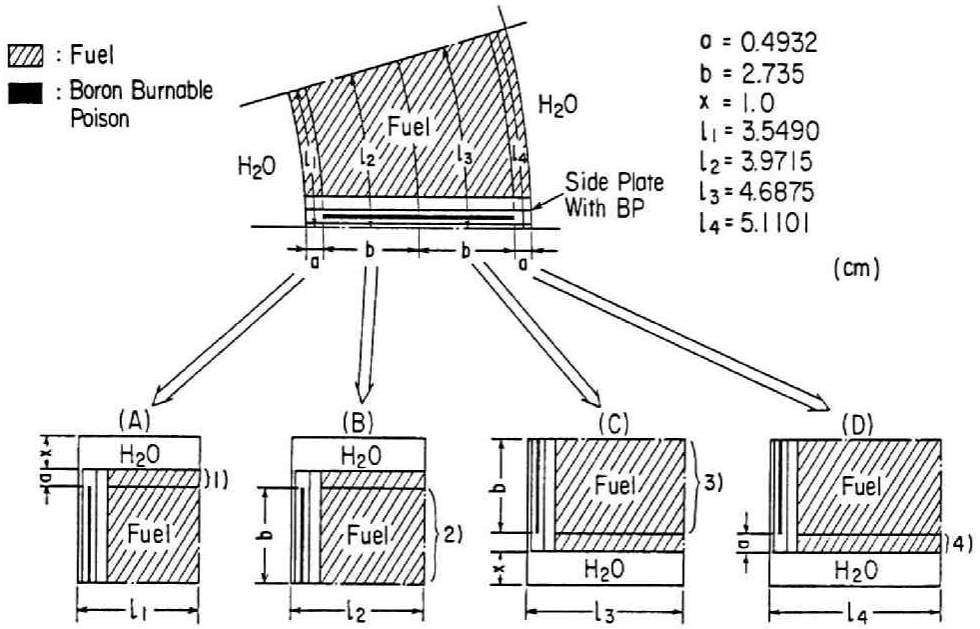

1) Outer Fuel Region I 2) Outer Fuel Region II 3) Outer Fuel Region III 4) Outer Fuel Region IV

Fig. VI-5 Secondary Cell Model for a Fully Loaded Outer Fuel Element with Boron

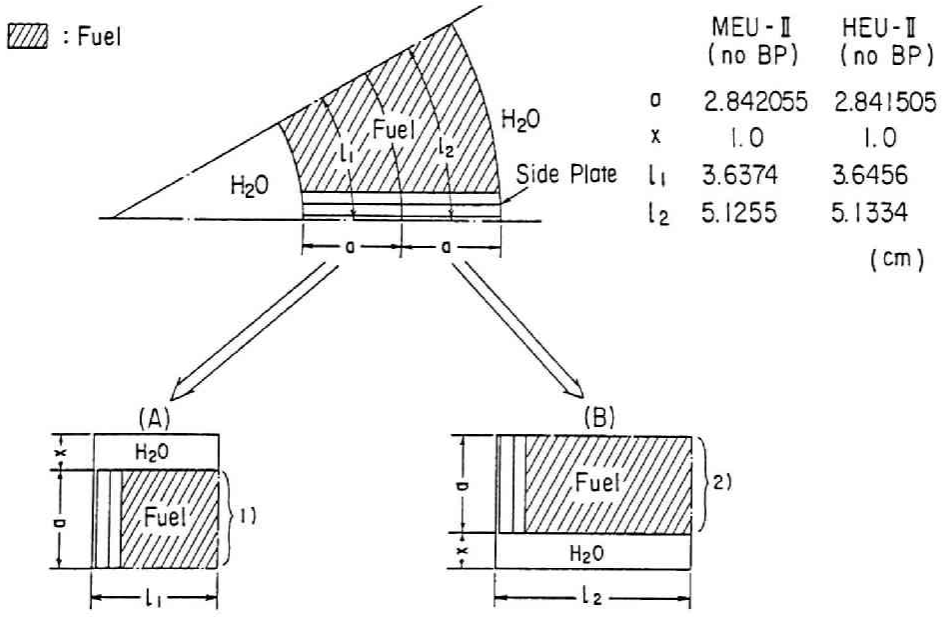

	MEU-II (no BP)	HEU-II (no BP)
a	2.842055	2.841505
x	1.0	1.0
l_1	3.6374	3.6456
l_2	5.1255	5.1334

(cm)

1) Inner Fuel Region I 2) Inner Fuel Region II

Fig. VI-6 Secondary Cell Model for a Fully Loaded Inner Fuel Element without Boron

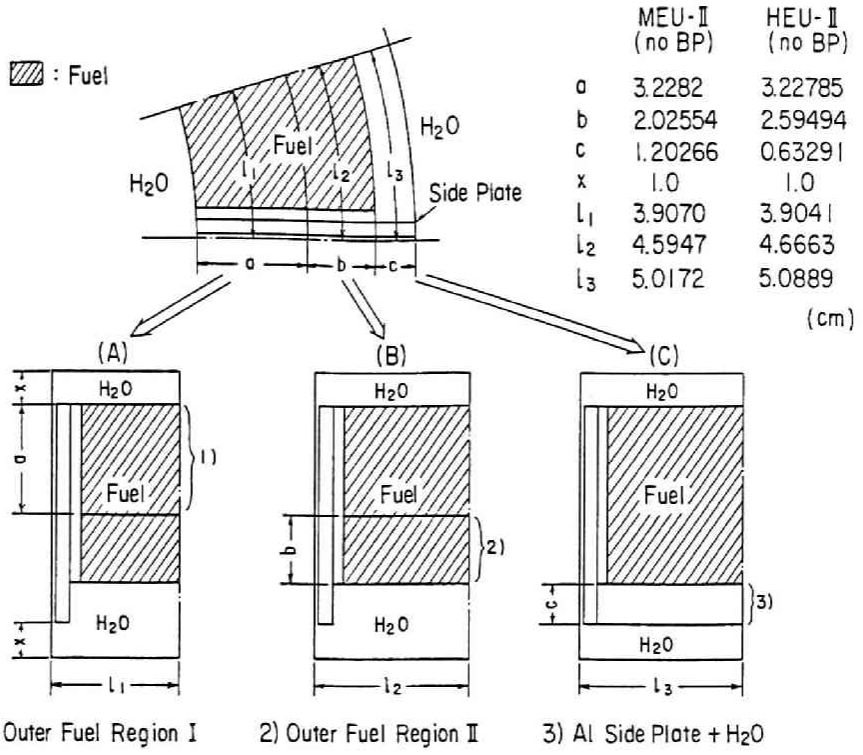

	MEU-II (no BP)	HEU-II (no BP)
a	3.2282	3.22785
b	2.02554	2.59494
c	1.20266	0.63291
x	1.0	1.0
l_1	3.9070	3.9041
l_2	4.5947	4.6663
l_3	5.0172	5.0889

(cm)

Fig. VI-7 Secondary Cell Model for a Partially Loaded Outer Fuel Element without Boron

Step 3: Core Calculation

Using the 19-group constants obtained by the above process, the core calculation was performed using the CITATION code[112] in SRAC. A one-dimensional [1-D] cylindrical geometry was employed for this eigenvalue calculation as shown in Fig. VI-8 and 10-group constants (5 fast group and 5 thermal group) for a two-dimensional [2-D] R-Z calculation were also generated.

In the vertical direction, the axial buckling obtained experimentally was used, which is tabulated in Table VI-2. Note here that, since the axial thermal neutron flux in the inner fuel region of the MEU core is not measured, the vertical buckling for the outer fuel region of the MEU core

is used for the inner fuel region.

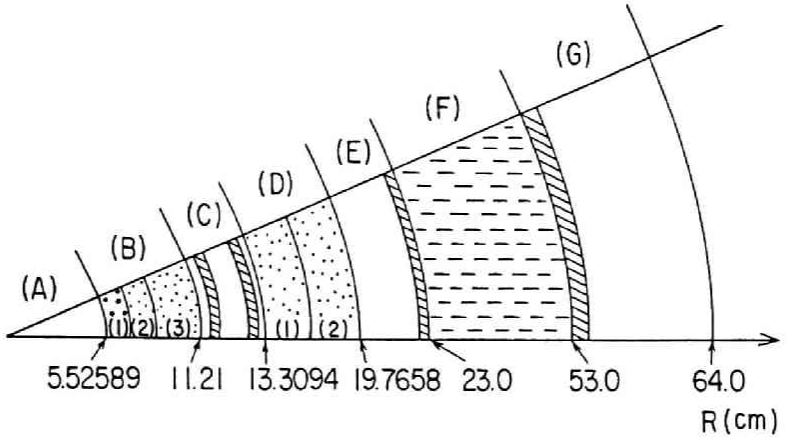

(A) Light-Water Region at the Center of Core
(B)-(1) Al Side Plate+H_2O Region
(B)-(2) Inner Fuel Region I
(B)-(3) Inner Fuel Region II
(C) Control Rod Region
(D)-(1) Outer Fuel Region I
(D)-(2) Outer Fuel Region II
(E) Outer Vessel Region Between the Outer Fuel Region and the Heavy-Water Region
(F) Heavy-Water Reflector Region
(G) Light-Water Reflector Region Outside the Heavy-Water Tank

▨ : Al ▭ : H_2O

Fig. VI-8 One-Dimensional Model for the Type-I MEU Core without Boron

Table VI-2 Vertical Buckling and Reflector Saving

Region*	MEU Core Buckling, B^2 ($10^{-3}cm^{-2}$)	MEU Core Reflector Saving (cm)	HEU Core Buckling, B^2 ($10^{-3}cm^{-2}$)	HEU Core Reflector Saving (cm)
(A)	1.6966	8.14	1.6867	8.25
(B)	1.7289	7.78	1.7214	7.86
(C),(D),(E)			1.6794	8.33
(F),(G)	1.5595	9.78	1.5577	9.80

* : Refer to Fig. VI-8.

Using the group constants obtained by this one-dimensional core calculation, two-dimensional R-Z core calculations were performed by the CITATION code using a calculation model shown in Fig. VI-9. To estimate the difference between the 1-D and 2-D calculation models for temperature effects, 1-D calculations of the same energy structure were also performed.

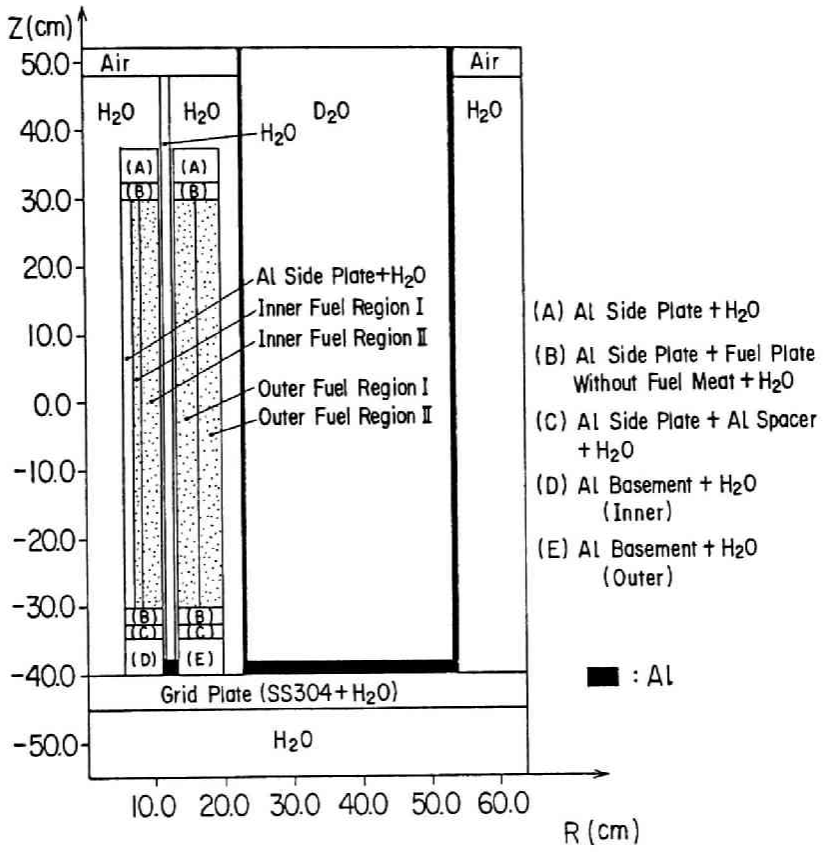

Fig. VI-9 Two-Dimensional Model for the Type-I MEU and HEU Cores

VI-3. Results and Discussion

VI-3-A. Comparison between the Calculated and Measured Results

Table VI-3 Calculated and Measured k_{eff} Values at 300 K

Designation of Core	ρ_{ex} at 300 K*1 (%Δk/k)	Effective Multiplication Factor Experiment*2	Calculation			C/E
MEU-I (no BP)	0.101	1.0010	19g.*3	1-D*5	1.0125	1.0115
			10g.*4	1-D*5	1.0120	1.0110
				2-D*6	1.0173	1.0163
MEU-II (no BP)	0.146	1.0015	19g.	1-D	1.0203	1.0188
			10g.	1-D	1.0199	1.0184
				2-D	1.0236	1.0221
MEU-I (Outer BP)	0.031	1.0003	19g.	1-D	1.0069	1.0066
			10g.	1-D	1.0065	1.0062
				2-D	1.0117	1.0114
MEU-I (Inner BP)	0.067	1.0007	19g.	1-D	1.0088	1.0081
			10g.	1-D	1.0082	1.0075
				2-D	1.0141	1.0134
HEU-I (no BP)	0.014	1.0001	19g.	1-D	1.0212	1.0211
			10g.	1-D	1.0206	1.0205
				2-D	1.0243	1.0242
HEU-II	0.047	1.0005	19g.	1-D	1.0260	1.0255
			10g.	1-D	1.0254	1.0249
				2-D	1.0283	1.0278

*1,*2 : Interpolated value at 300 K from the experimental data using the method of least-squares.
*3 : Core calculation was performed with use of the 19-group constants.
*4 : Core calculation was performed with use of the 10-group constants.
*5 : Core calculation was performed with use of the one-dimensional model.
*6 : Core calculation was performed with use of the two-dimensional model.

Table VI-3 shows the calculated effective multiplication factors at 300 K in comparison with experimental values. The experimental values at 300 K are obtained from the interpolation of the measured data using the quadratic curves obtained by the method of least squares. This table shows the dependencies of k_{eff} values on the energy group structure when one-dimensional models are used with 10- and 19-group constants and the differ-

ences between k_{eff} values calculated by the one- and two-dimensional models with 10-group constants. The calculated values are approximately 1 ∿ 3% larger than experimental values. This may be caused by a poor representation of the annular core for the azimuthal direction in a step of the core calculation. Note that the excess reactivity was measured under the condition that a heater, a stirrer, and several thermometers were installed in the core, whereas the calculation did not take into account this effect. The total reactivity effect of a heater, a stirrer, and several thermometers was estimated to be around -0.2 ∿ -0.3 %Δk/k by the experiment. The agreement of the calculated and measured k_{eff} values is considered to be better than that shown in Table VI-3.

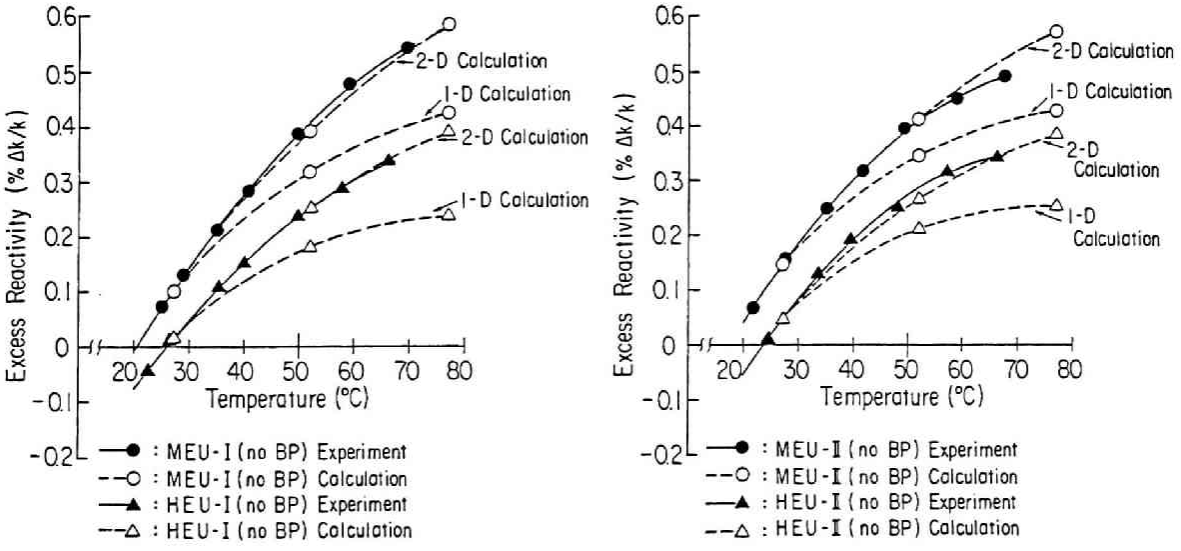

Type-I (a) Type-II (b)

Fig. VI-10 Temperature Effects on the Excess Reactivity in the MEU and HEU Cores without Boron
(The calculated values are normalized to the experimental quadratic curves at 300 K)

Although small effects are observed in Table VI-3 depending on the energy group structure, the values calculated by two-dimensional models are greater than those by one-dimensional models. This indicates that the temperature effect on the axial buckling is not negligible.

Figures VI-10 through VI-13 show the temperature effects on the excess reactivities in the individual cores. Figure VI-10(a) corresponds to the Type-I MEU and HEU cores without boron, Fig. VI-10(b) to the Type-II MEU and HEU cores without boron. Figures VI-11(a) and VI-11(b) corresponds to the Type-I MEU cores loaded with all inner and outer side-plates containing boron, respectively. In these figures, the curves for the experimental data are quadratic ones determined by the method of least squares. Note that the calculated values are normalized to the experimental ones interpolated at 300 K.

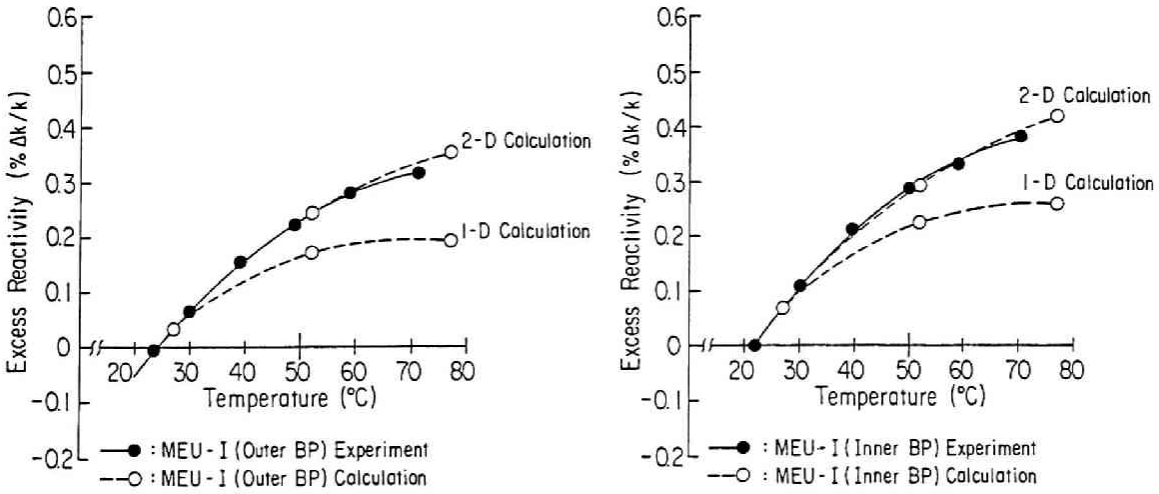

Outer Boron (a)

Inner Boron (b)

Fig. VI-11 Temperature Effects on the Excess Reactivity in the Type-I MEU Core with Boron
(The calculated values are normalized to the experimental quadratic curves at 300 K)

The tendency in the temperature effects on reactivity calculated by two-dimensional models excellently agree with the experimental data, whereas calculated ones by one-dimensional models underestimate the temperature effects. This can be attributed to the neglect of the positive temperature effects of the light-water reflectors above and below the core in the one-dimensional model. The positive temperature effect due to the axial reflectors is considered to be fairly large, since the KUCA annular core behaves as an under-moderated core as described in Chapters IV and V.

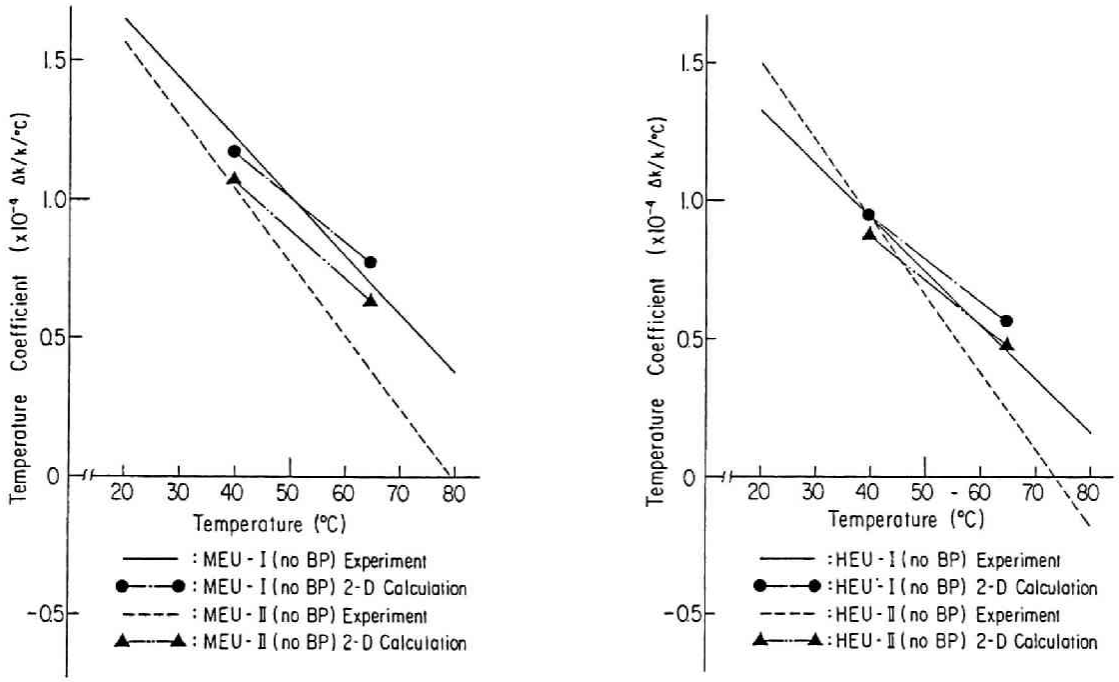

MEU (a) HEU (b)

Fig. VI-12 Temperature Coefficients in the Type-I and Type-II MEU and HEU Cores without Boron

Figures VI-12 and VI-13 show the temperature coefficients of the individual cores. Figure VI-12(a) corresponds to the Type-I and Type-II MEU cores without boron, Fig. VI-12(b) to the Type-I and Type-II HEU cores without boron, and Fig. VI-13 to the Type-I MEU core loaded with all inner or outer side-plates containing boron. In these figures, the lines that

represent the experimental data are obtained by differentiating the quadratic equations as described in Section III-9-B.

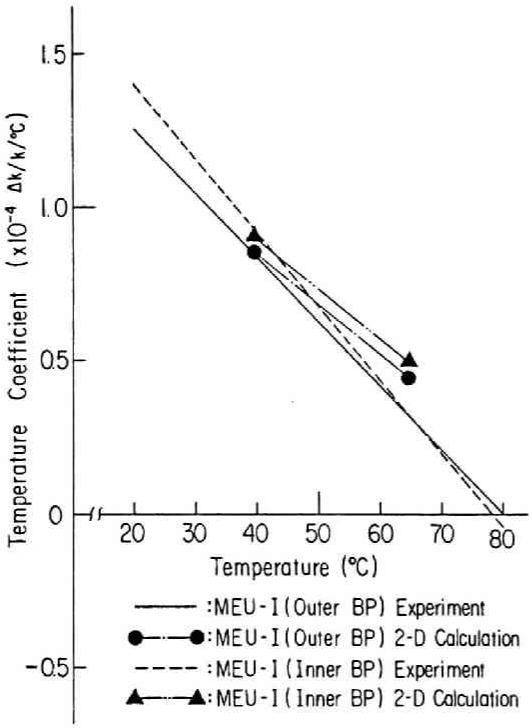

Fig. VI-13
Temperature Coefficients in the Type-I MEU Cores with Inner and Outer Boron

These figures show that the calculated results approximately reproduce the measured temperature coefficients. However, there exist some discrepancies between the gradients of the calculated and measured temperature coefficients. The agreement of the calculated and measured gradients in the Type-I core is better than that in the Type-II core. This tendency was also observed in the analyses of the boron reactivity effects described in Section IV-3. The diameter of the central light-water region in the Type-I core is larger than that in the Type-II core, whereas the thickness of the light-water gap between the outer fueled region and the heavy-water reflector in the Type-I core is thinner than that in the Type-II core. Therefore, the neutron importance of the inner fuel region is higher in the Type-II core than the Type-I core. Moreover, the inner fuel region has a more curved geometry than that of the outer fuel region. However, in the

generation process of the group constants, both fuel regions are assumed to be slabs in the primary cell calculation or rectangles in the secondary cell calculation, although plural cell calculations were performed along the radial direction in the secondary cell calculation. This may affects the results of calculations, since even small differences in group constants may cause a large difference in reactivity at a region having a high neutron importance.

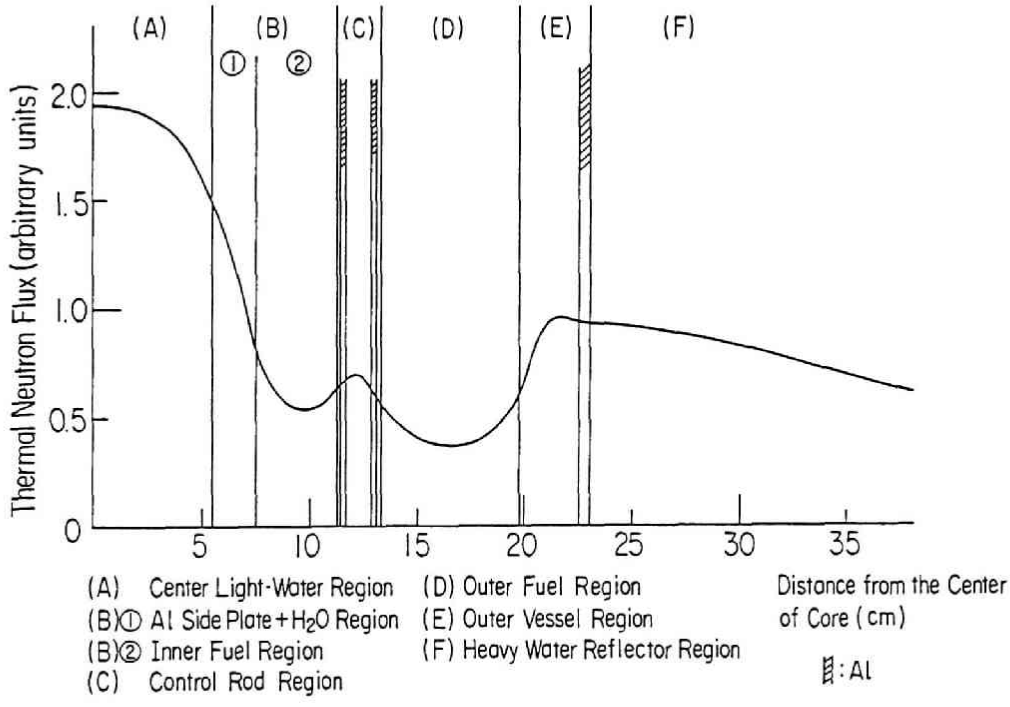

Fig. VI-14 Calculated Horizontal Distribution of Thermal Neutrons in the Type-I MEU Core without Boron

Figure VI-14 shows a calculated flux distribution of thermal neutrons in the horizontal direction for the Type-I MEU core without boron. This flux distribution reproduces well the tendency observed in the neutron flux measurements described in Section III-6. In the Type-II core, the neutron flux peak is much sharper at the central flux trap region than that in the Type-I Core. This figure indicates that the temperature effects in the

light-water regions, where the neutron flux peaks are observed, would be fairly large, since a flux leveling effect would occur due to the decrease in absorption cross section of light-water with the increase in temperature. The temperature effect in the central flux trap region is especially important, since the level of flux peak is the highest.

VI-3-B. Examinations on the Physical Processes of the Temperature Effect

Since good agreements have been obtained in general, the method employed in the present study could be regarded as reasonable. Therefore, several examinations were performed using the assessed method of calculation for the purpose of further understanding on the physical processes of the temperature effect. In these examinations, the temperature effects of the light-water reflectors above and below the core are not considered, since all calculations are performed by one-dimensional models for the simplicity. Consequently, in order to compare these calculated values with the experimental data, this effect (namely, the difference between one-dimensional calculations and two-dimensional calculations) should be compensated.

Figure VI-15 shows the results of calculations considering three physical processes of temperature effects individually; namely, (1) the Doppler effect, (2) the thermal expansion effect, and (3) the thermal neutron spectral shift effect. Figures VI-15(a) and VI-15(b) correspond to the Type-I MEU and HEU cores without boron, respectively. From these figures, the Doppler effect is slightly negative in the MEU core and almost zero in the HEU core; the thermal expansion effect is negative in the either MEU or HEU core; the thermal neutron spectral shift effect is positive for the both cores; and overall, the temperature effects are

positive.

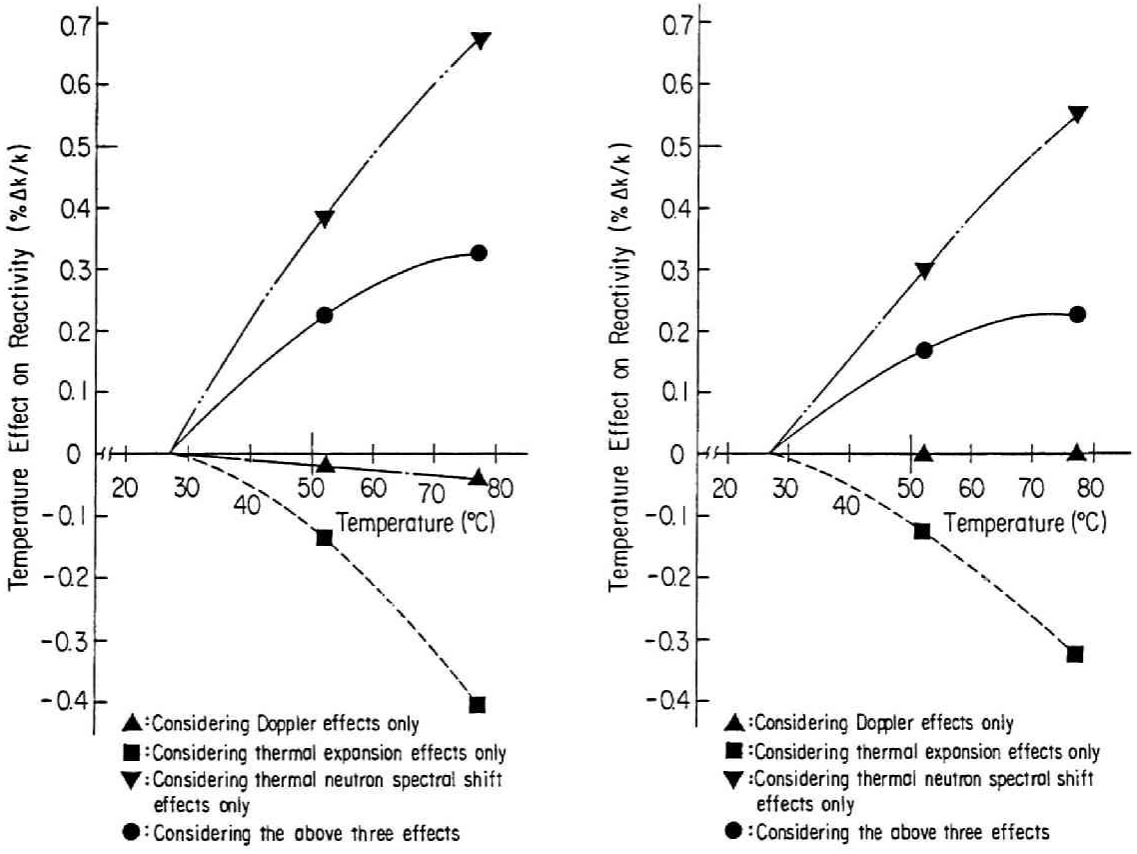

Fig. VI-15 Temperature Effects of the Three Physical Processes in the Type-I MEU and HEU Cores without Boron

The main contribution of the thermal expansion effect for a negative reactivity can be regarded as the increase in fast neutron leakage due to the decrease in number density of the light-water moderator in the core region. Although the thermal neutron leakage also increases with the decrease in number density of light-water, the thermal neutron nonleakage probability depends mainly upon the neutron temperature, rather than upon the number density of the light-water. A positive temperature effect caused by the thermal neutron spectral shift can be attributed mainly to the positive temperature effect of the light-water reflector due to a flux

leveling effect. Since this positive effect outweighs the negative one caused by the thermal neutron leakage, the thermal neutron spectral shift effect gives a positive temperature effect.

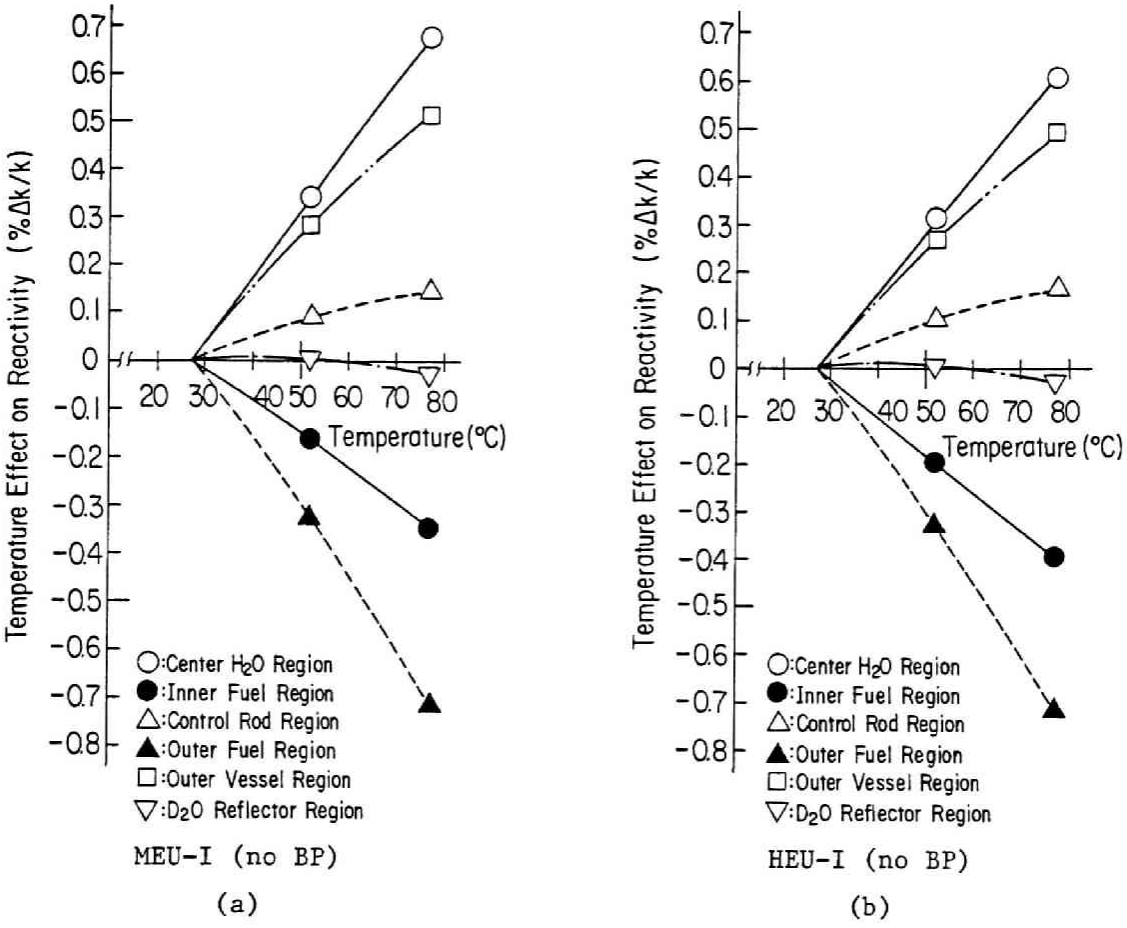

Fig. VI-16 Region Dependent Temperature Effect on Reactivity in the Type-I MEU and HEU Cores without Boron

Figures VI-16 through VI-18 show the region-dependent temperature effect on reactivity in each core. In all the cores, the temperature effects of the fuel regions are negative, those of the light-water regions are positive, and those of the heavy-water reflector regions are almost zero. Though a negative void coefficient of the control rod region is experimentally proven as described in Section III-8-A, the calculated temperature coefficient of this region is positive. This phenomenon can be

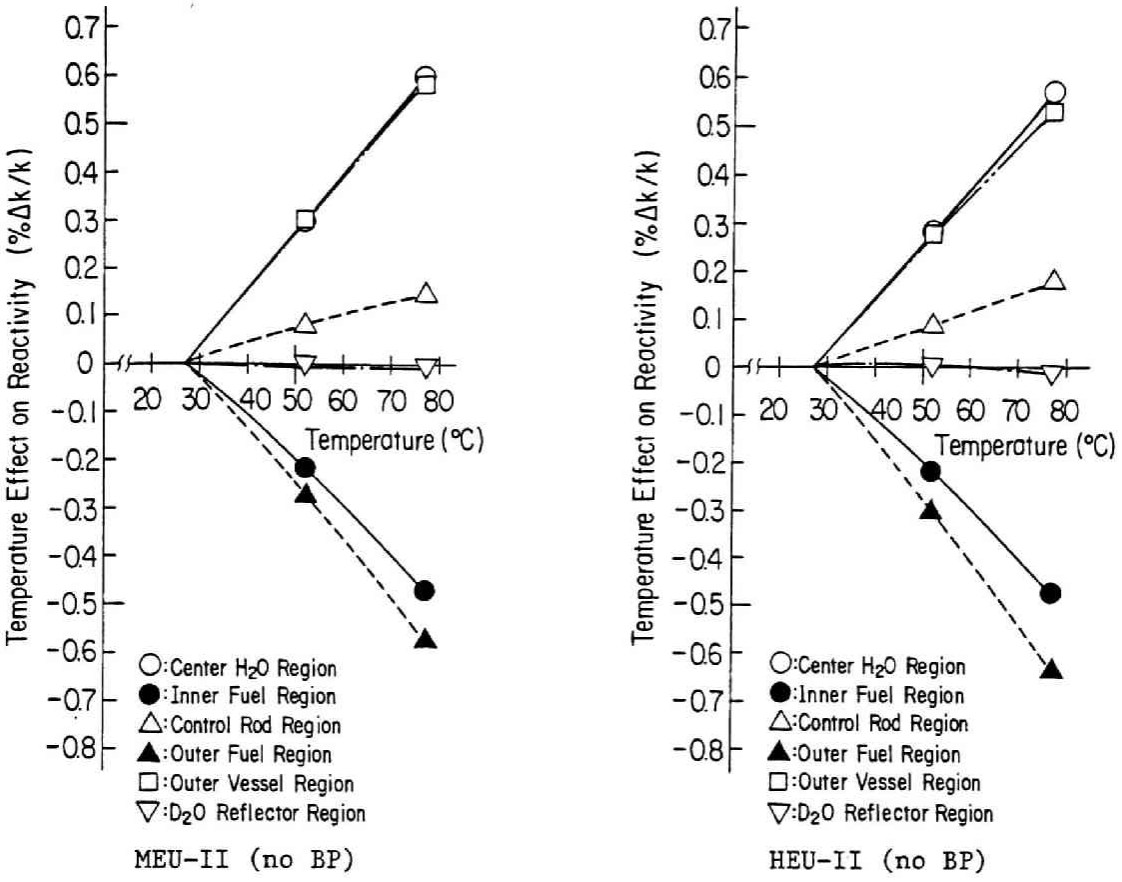

Fig. VI-17 Region Dependent Temperature Effect on Reactivity in the Type-II MEU and HEU Cores without Boron

referred to the decrease in the absorption cross section of light-water with increasing thermal neutron temperature. In the Type-I cores without boron, the positive temperature effect of the central light-water region is the greatest among all regions, whereas in the Type-II cores without boron, the temperature effect of the central light-water region is approximately equivalent to that of the outer vessel region. This is simply attributed to the sizes of the central light-water region and the light-water gap region between the outer fueled region and the heavy-water tank. In the cores with boron, the magnitudes of the temperature effects in the fuel region containing boron and in the light-water regions adjacent to the fuel

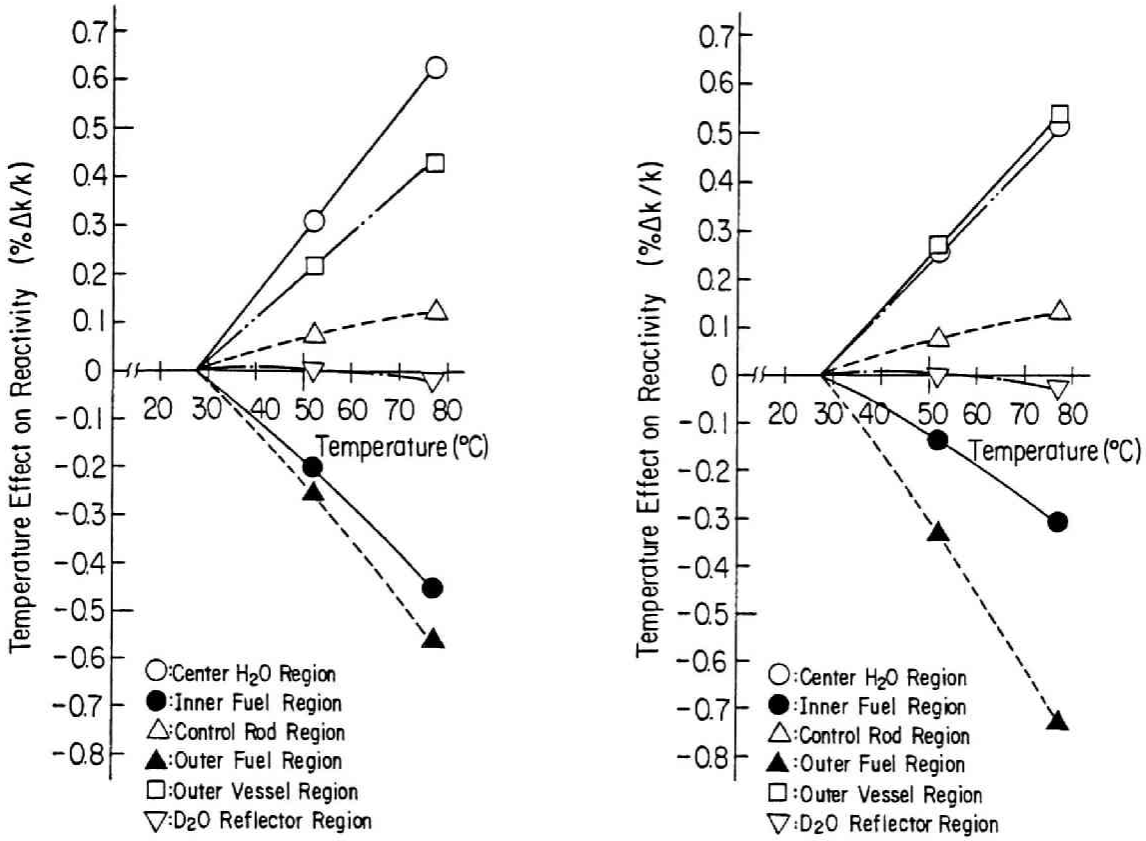

MEU-I (Outer BP)

(a)

MEU-I (Inner BP)

(b)

Fig. VI-18 Region Dependent Temperature Effect on Reactivity in the Type-I MEU Cores with Outer and Inner Boron

regions containing boron is small. This is because the existence of boron reduces the importance of the areas in the vicinity of boron. Further investigation would be necessary to understand the difference in the temperature effect between the core loaded with MEU and HEU fuels or between the cores with and without boron, since the cores employed in the measurements were different with each other in the core configuration.

Note that, in the actual design of a light-water-moderated and heavy-water-reflected high flux reactor, the thickness of the light-water layer between the fueled region and the heavy-water reflector would be reduced for the purpose of separating completely the light-water moderator from the

heavy-water reflector.[63] Furthermore, in the actual design of a high flux reactor, the size of the central light-water region would be reduced by the installation of an irradiation facility or by the introduction of a central void tube as a second instrument for the reactor shut down.[63] These devices in the actual design would assure the negative temperature effect on reactivity.

VI-4. Conclusions

The results obtained through this study are summarized as follows:

(1) The measured temperature coefficients are approximately simulated by the calculations for the Type-I MEU cores with and without boron, the Type-II MEU core without boron, and the Type-I and Type-II HEU cores without boron. The agreement is better for the Type-I cores which have larger central light-water regions than the Type-II cores.

(2) The results of two-dimensional calculations agreed with the experimental data better than those of one-dimensional calculations. This indicates that the temperature effect on the axial buckling may not negligible.

(3) The Doppler effect causes a slightly negative reactivity effect in the MEU cores with the increase in temperature, whereas it is close to zero in the HEU cores. The thermal expansion effect causes a negative effect in the either MEU or HEU cores, whereas the thermal neutron spectral shift effect causes a positive effect in the both MEU and HEU cores with the increase in temperature. The total effect of the above three processes is positive.

(4) The temperature effect on reactivity in the fuel region is negative and, in contrast, that in the light-water region where there is a thermal neutron flux peak is positive. They compete each other and totally give a positive effect.

VII. Concluding Remarks

Through the present study on the nuclear characteristics of a light-water-moderated and heavy-water-reflected core loaded with MEU fuel using the KUCA, several interesting characteristics of an MEU core are revealed by the comparison with an HEU core. Note here again that MEU and HEU fuels employed in this study consist of UAL_x-Al dispersion aluminide and U-Al alloy, respectively. MEU and HEU fuels are of 45 wt% and 93 wt% ^{235}U enrichments, and contain 42 wt% and 22 wt% total U, respectively, and the KUCA cores employed in this study is light-water-moderated and heavy-water reflected annular ones with the central flux trap of light-water, which has been proposed for a high flux reactor. The KUCA cores have rather thick light-water layer between the outer fueled region and the heavy-water reflector, whereas this layer would be reduced its thickness in an actual high flux reactor for the purpose of separating the light-water moderator from the heavy-water reflector.

In general, the nuclear characteristics of the core does not change so much with the conversion from HEU to MEU fuels. Therefore, it is concluded that MEU fuel is considered to be feasible for a high flux reactor in place of HEU fuel without any significant reduction in reactor performance.

Through the experimental study, although a direct comparison between the HEU and MEU cores is not available due to the limitations in the experimental conditions, the nuclear characteristics of a light-water-moderated and heavy-water-reflected annular core with a central flux trap are mostly clarified. The main features of the MEU and HEU cores obtained in the experimental study can be summarized as follows:

(1) The minimum critical mass of ^{235}U increases approximately 18 % in the MEU core compared with the HEU core due to the increase in ^{238}U loading. MEU fuel has a 2 ∿ 3 % larger reactivity worth per fuel plate than HEU fuel, since MEU fuel contains slightly excessive ^{235}U compared with HEU fuel. Therefore, it may be possible to reduce slightly the U content in MEU fuel in order to attain the same reactivity effect as HEU fuel.

(2) The level of the thermal neutron flux at a specified reactor power in the fueled region decreases approximately 10 % in the MEU core compared with the HEU core, since the ^{235}U mass loaded to the core is larger in the MEU core than in the HEU core. However, the thermal neutron flux in a reflector region decreases a few percent in the MEU core, because the neutron spectrum in the MEU core is harder than that of the HEU core. This indicates that, at the vicinity of a reflector, the peak of power density in the MEU core would be slightly higher (a few percent) than that in the HEU core.

At a central flux trap of light-water, a highest flux peak of thermal neutrons is observed in both the MEU and HEU cores, and the height of this peak is 2 ∿ 3 times higher than that at a heavy-water reflector. The thermal neutron flux peaks are also observed at the space for the control rods, at the side-plate region, at the light-water gap between the heavy-water reflector and the outer fueled region, and at the upper and lower sites of the fuel region. With the introduction of a large central void, a level of thermal neutron flux in the central flux trap becomes lower and that in the heavy-water reflector grows larger. In the core with a large central void, the highest peak of thermal neutron flux can be observed in the light-

water gap between the heavy-water reflector and the outer fueled region. The thermal neutron flux in the inner fuel region is higher than that in the outer fuel region.

(3) The control rod worth in the MEU core is approximately 10 % lower than that of the HEU core, when a thermal neutron absorber is used as a material for the control rods. The reason is that the neutron spectrum in the MEU core is harder than that in the HEU core.

(4) The total reactivity effect of boron loaded in the side-plates as burnable poison is approximately 8 %Δk/k in the MEU core and this is sufficient for suppressing the excess reactivity in an initial loading core of a high flux reactor. The reactivity effects of the boron loaded side-plates are larger in the inner fuel region than in the outer fuel region, contrary to the fact that the mass of boron contained in an inner side-plate is slightly less than that of an outer side-plate. This is consistent with the thermal neutron flux distribution. The boron reactivity effect in the HEU core would be slightly higher (around 10 %) than that of the MEU core, since the control rod worth is higher in the HEU core than in the MEU core.

(5) The void reactivity effect in the fueled region of the MEU core is slightly more negative than that of the HEU core. The void reactivity effects are positive in the central flux trap of light-water and in the light-water gap between the heavy-water reflector and the outer fueled region, where large flux peaks of thermal neutrons are observed. The other regions have negative void reactivity effects.
The void reactivity is affected by the following three competing effects; namely, the neutron (A) absorption, (B) diffusion, and (C)

moderation effects. In the fueled region, the neutron moderation effect dominates the void reactivity and causes a negative effect. On the contrary, in a thick light-water region near the fuel region, the neutron absorption effect dominates the void reactivity and causes a positive effect. The neutron diffusion effect provides a negative reactivity in the middle of the fuel region and increases its value to positive in the light-water region next to the fuel region.

(6) The temperature effects on reactivity in the MEU and HEU cores are approximately equivalent with each other. The temperature reactivity effects are positive in the KUCA cores regardless of MEU or HEU and of with or without boron. The temperature effect on reactivity is positive in all light-water regions, whereas the void reactivity effects is negative in the space for the control rods, and that is negative in a fueled region. In the KUCA core, the large positive temperature effects in the central flux trap of light-water and in the light-water gap between the heavy-water reflector and the outer fueled region overweigh the negative effects in the fuel regions.

The temperature effects are determined by the following three competing effects; namely, the (A) Doppler, (B) thermal expansion, and (C) neutron spectral shift effects. The Doppler effect in the MEU core causes a slightly negative reactivity effect, while that is close to zero in the HEU core. However, the Doppler effect is fairly small among the above three effects. The thermal expansion causes a negative effect that is analogous to the void reactivity effect, while the thermal neutron spectral shift causes a positive effect. The thermal neutron spectral shift effect in a light-water region, from which neutrons are reflected into fuel region, is especially important,

since this effect mainly causes the decrease in absorption cross sections of light-water.

(7) The kinetic parameters β/ℓ in the MEU and HEU cores are approximately equivalent with each other. The kinetic parameter is mostly determined by a core configuration. In the KUCA core, a value of β/ℓ is positioned at the middle of that in a light-water moderated and reflected core and a heavy-water moderated and reflected core.

One should be careful to design a light-water-moderated and heavy-water-reflected annular high flux reactor with a central flux trap, since a size of central flux trap is essential for the temperature effect on reactivity and a central light-water region also has a large positive void reactivity effect. In order to investigate further on the effects of reducing fuel enrichment precisely and on the nuclear characteristics of a light-water-moderated and heavy-water-reflected core itself, the analytical study should be necessary, since there are several limitations in the experimental conditions. For this purpose, an assessed self-consistent system for the neutronics calculations, including the nuclear data file, processing codes for the generation of group constants, and core calculation codes based on diffusion or transport theory, should be necessary.

In the analytical study, the assessment of the computer codes are carried out through the comparison with the experimental data in order to establish a self-consistent system for the neutronics calculations in the KUCA. The results obtained through this assessment can be summarized as follows:

(1) The assessed computer codes in this study are EPRI-CELL, DIF3D, 2D-FEM-KUR, and SRAC. With use of all codes employed in this study,

the calculated results of effective multiplication factors agree with the experimental data within 2 ∿ 3 %. Further study would be necessary to obtain much accurate results, however, SRAC and 2D-FEM-KUR are considered to be the main codes in the self-consistent system for the neutronics calculations in the KUCA.

(2) The calculated results of the boron, void, and temperature effects agree mostly with the experimental data. The finite-element method is successful for the accurate modeling of the complex core configuration and powerful for the analysis of the localized reactivity effects. The conventional finite-difference method can be applicable to a complex core with a device in the generation of the group constants.

(3) A special attention should be paid in the generation process of the group constants to take into account the geometrical heterogeneity of a core. One should be careful, when the artificial extra region is attached in the cell calculation. Further study would be necessary to generate the proper group constants especially in the inner fuel region, where the neutron importance is highest and a strongly curved geometry is used.

(4) For the accurate calculation of the void and temperature effects on reactivity, a change in vertical buckling should be taken into consideration. Therefore, the three-dimensional calculation would be necessary to obtain more accurate result.

(5) With use of the computer codes assessed in the present study, further examination on the characteristics of the MEU and HEU cores would become possible with a certified accuracy. This is essentially important, since the experimental conditions are limited in an actual

reactor system. In contrast, the calculations would allow any condition in an ideal reactor system. Therefore, one can perform the further investigations on the use of MEU fuel and the differences between the MEU and HEU cores would be revealed in detail. In addition, one can perform the study on the design of a high flux reactor similar to the KUCA core employed in this study.

Through the present study, the self-consistent system for the neutronics calculations in the KUCA has been basically established with use of the ENDF/B-IV data file, the SRAC code system and the 2D-FEM-KUR code as main parts.[117] This self-consistent system is anticipated to be applied widely to the analyses of the critical experiments performed in the KUCA, and to be refined through the further assessments comparing the calculated results with the various experimental data.

VIII. ACKNOWLEDGEMENT

The author would like to express his sincere thanks to Professor Hiroshi Nishihara of Kyoto University for his kind guidance of this study, and for his helpful advise and valuable suggestions on this subject.

The author also wish to express his thanks to Professors Toshikazu Shibata, Itsuro Kimura, and Keiji Kanda of KURRI for their continuous encouragement and valuable discussions through the course of this study.

The author is deeply indebted to all staffs of the KUCA including Messrs. Masatoshi Hayashi and Keiji Kobayashi for their generous supports and assistance in the experiments. The author is grateful to Messrs. Yoshihiro Nakagome and Toshimitsu Sagane who made efforts to fabricate MEU and HEU fuels for the KUCA experiments. The author must express his thanks to Dr. Kaichiro Mishima, Messrs. Hiroshi Fukui and Yasuhide Senda for their cooperations in the experiment and analysis of the void reactivity effect, and to Mr. Masa-aki Mori for his cooperation in the experiment and analysis of the temperature reactivity effect.

The author is grateful to Professor Yuichi Ogawa's group of Hokkaido University, Professor Otohiko Aizawa's group of Musashi Institute of Technology, Professors Shozo Nakadoi and Shigeyasu Sakamoto's group of Tokai University, Professor Kojiro Nishina's group of Nagoya University, Professor Kenji Sumita's group of Osaka University, Professor Ryota Miki's group of Kinki University, and Professor Kazuhiko Kudo's group of Kyushu University for their cooperations in the part of experiments and fruitful discussions. The author is also grateful to the members of the KUCA Technical Committee chaired by Professor Hiroshi Nishihara of Kyoto University, including Professor Naohiro Hirakawa of Tohoku University, Professor Masaharu Nakazawa of Tokyo University, Professor Keisuke

Kobayashi of Kyoto University, Professor Akito Takahashi of Osaka University, and Dr. Shojiro Matsuura, Dr. Iwao Kobayashi, and Dr. Masaharu Nakano of JAERI, for invaluable discussions.

The author appreciate the generous instruction and helpful suggestions for the use of SRAC by Dr. Keichiro Tsuchihashi of JAERI. The author is also grateful to Dr. Yoshitaka Naito of JAERI and Mr. Shin-ichiro Tsuruta of the Japan Information Service who mainly developed 2D-FEM-KUR. The author must express his thanks to all members of RERTR/ANL including Dr. W. L. Woodruff, Dr. M. M. Bretscher, Dr. J. E. Matos, and Dr. A. Travelli for their generous help and valuable suggestions on the use of the ANL code system.

The calculations were mainly performed at the Data Processing Center of Kyoto University and partly at the computer centers of ANL and JAERI.

A part of this study was performed as the ANL-KURRI joint study.

This study was financially supported by the Ministry of Education, Science and Culture.

References

1. Directory of Nuclear Reactors, Vol. X, IAEA, Vienna (1976).

2. Directory of Nuclear Reactors, Vol. III, IAEA, Vienna (1960).

3. Directory of Nuclear Reactors, Vol. V, IAEA, Vienna (1964).

4. Research Reactor Core Conversion from the Use of Highly Enriched Uranium to the Use of Low Enriched Uranium Fuels, Guidebook, IAEA-TECDOC-233 (1980).

5. A. Travelli, D. Stahl, and T. Shibata, "The US RERTR Program, Its Fuel Development Activities, and Application in the KUHFR", ANS Trans, Vol. 36, p. 92 (1981).

6. Research Reactor Core Conversion from the Use of Highly Enriched Uranium to the Use of Low Enriched Uranium Fuels, Guidebook Addendum: Heavy Water Moderated Reactors, IAEA-TECDOC-324 (1985).

7. John R. Lamarsh, Introduction to Nuclear Reactor Theory, Addison-Wesley Publishing Company Inc., Reading, Massachusetts (1966).

8. Technical Foundations of TRIGA, GA-471, General Atomic (1958).

9. K. Kanda, T. Shibata, I. Miyanaga, H. Sakurai, and M. Kanbara, "Status of Reduced Enrichment Program for Research Reactor Fuel in Japan", Proc. 1984 International Meeting on Reduced Enrichment for Research and Test Reactors, ANL/RERTR/TM-6 CONF-8410173, p. 11 (1985).

10. Y. Kaneko, F. Akino, K. Kitadate, and R. Kurokawa, Critical Experiments on Enriched Uranium Graphite Moderated Cores, JAERI 1257 (1978) in Japanese.

11. JRR-2 Critical Experiments Group, Critical Experiments and Characteristic Measurement for JRR-2, JAERI 1025 (1962) in Japanese.

12. K. Kanda and S. Matsuura, "Reducing the Enrichment of Fuels for Research Reactors", J. At. Energy Soc. Japan, Vol. 22, No. 11, p. 763 (1980) in Japanese.

13. S. Matsuura, et al., "Summary of INFCE and Future Prospect", J. At. Energy Soc. Japan, Vol. 22, No. 7, p. 435 (1980) in Japanese.

14. Report of INFCE Working Group 8, IAEA (1980).

15. Seminar on Research Reactor Operation and Use, IAEA-SR-77 (1981).

16. Proc. International Meeting on Development, Fabrication and Application of Reduced Enrichment Fuels for Research and Test Reactors, ANL/RERTR/TM-3 CONF-801144 (1983).

17. Proc. International Meeting on Research and Test Reactor Core Conversion from HEU to LEU Fuels, ANL/RERTR/TM-4 CONF-821155 (1983).

18. K. Tsuchihashi, ed., Proc. International Meeting on Reduced Enrichment for Research and Test Reactors, JAERI-M 84-073 (1984).

19. Proc. 1984 International Meeting on Reduced Enrichment for Research and Test Reactors, ANL/RERTR/TM-6 CONF-8410173.

20. D. C. Losey, F. B. Brown, W. R. Martin, and J. C. Lee, "Core Physics Analysis in Support of the FNR HEU-LEU Demonstration Experiment", Proc. International Meeting on Development, Fabrication and Application of Reduced Enrichment Fuels for Research and Test Reactors, ANL/RERTR/TM-3 CONF-801144, p. 450 (1983).

21. D. K. Wehe and J. S. King, "The RERTR Demonstration Experiments Program at the Ford Nuclear Reactor", ibid., p. 499 (1983).

22. D. K. Wehe and J. S. King, "FNR Demonstration Experiments - Part 1: Beam Port Leakage Currents and Spectra", Proc. International Meeting on Research and Test Reactor Core Conversion from HEU to LEU Fuels, ANL/RERTR/TM-4 CONF-821155, p. 355 (1983).

23. D. K. Wehe and J. S. King, "FNR Demonstration Experiments - Part 2: Subcadmium Neutron Flux Measurements", ibid., p. 348 (1983).

24. J. A. Rathkopf, C. R. Drumm, W. R. Martin, and J. C. Lee, "Analysis of the Ford Nuclear Reactor LEU Core", ibid., p. 377 (1983).

25. M. M. Bretscher and J. L. Snelgrove, "Comparison of Calculated Quantities with Measured Quantities for the LEU-Fueled Ford Nuclear Reactor", ibid., p. 397 (1983).

26. D. K. Wehe, C. R. Drumm, J. S. King, W. R. Martin, and J. C. Lee, "Operating Experience, Measurements, and Analysis of the LEU Whole Core Demonstration at the FNR", Proc. International Meeting on Reduced Enrichment for Research and Test Reactors, (K. Tsuchihashi, ed.), JAERI-M 84-073, p. 246 (1984).

27. K. Arigane and K. Tsuchihashi, "Analysis of Critical Experiments of FNR LEU Core", ibid., p. 350 (1984).

28. R. Oyamada, Y. Nagaoka, and T. Niibo, "An Analytical Study of Reactivity Transients Response to JMTRC HEU and MEU Fuel Cores", Seminar on Research Reactor Operation and Use, IAEA-SR-77/35 (1981).

29. Y. Nagaoka, K. Takeda, S. Shimakawa, S. Koike, and R. Oyamada, "Critical Experiments of JMTRC MEU Cores", Proc. International Meeting on Reduced Enrichment for Research and Test Reactors, (K. Tsuchihashi, ed.), JAERI-M 84-073, p. 360 (1984).

30. M. Hayashi, "Generation of Thermal Neutron Flux Peak", Present Status and Future Subjects of Research on Reactor Neutrons, Technical Committee on the Use of Reactor Neutrons, At. Energy Soc. Japan (1976) in Japanese.

31. T. Shibata, "Construction of a High Flux Research Reactor and Conversion of Kyoto University Reactor KUR to a TRIGA Type Reactor", Research Reactor Renewal and Upgrading Program, IAEA-214, p. 183 (1978).

32. Application of Reactor Installation License for the Construction of High Flux Reactor, Kyoto Univ. (1976) submitted to the Japanese Government.

33. The ORPHEE Reactor, Pamphlet, Laboratorie Léon Brillouin, CEA-CNRS, France.

34. "ORPHEE: A New Test Reactor", Rev. Gen. Nucl. (France), Vol. 5, p. 411 (1978).

35. D. Cribier and P. Breant, "A New Aid to Primary and Applied Research : The ORPHEE Reactor in Saclay", Rev. Gen. Nucl. (France), Vol. 6, p. 548 (1981).

36. H. Ichikawa, H. Ikawa, H. Ando, M. Takayanagi, H. Tsuruta, and Y. Miyasaka, "Neutronic and Thermo-Hydraulic Design of JRR-3(M) Reactor", Proc. International Meeting on Reduced Enrichment for Research and Test Reactors, (K. Tsuchihashi, ed.), JAERI-M 84-073, p. 331 (1984).

37. H. Tsuruta, H. Ichikawa, and J. Iwasaki, Neutronic Design of Upgraded JRR-3 Research Reactor, JAERI-M 84-099 (1984) in Japanese.

38. J. Iwasaki, H. Ichikawa, and H. Tsuruta, Neutronic Calculation of Upgraded JRR-3 Research Reactor (Few-group Constants), JAERI-M 84-159 (1984) in Japanese.

39. H. Tsuruta, H. Ichikawa, and J. Iwasaki, "Neutonics Design of Upgraded JRR-3 Research Reactor", Proc. 1984 International Meeting on Reduced Enrichment for Research and Test Reactors, ANL/RERTR/TM-6 CONF-8410173, p. 275 (1985).

40. Y. Sudo, H. Ando, H. Ikawa, and N. Ohnishi, "Core Thermohydraulic Design with LEU Fuels for Upgraded Research Reactor, JRR-3", ibid., p. 289 (1985).

41. K. Böning, W. Gläser, J. Meier, G. Rau, A. Röhrmoser, and L. Zhang, "Design of a Novel Compact Core with Reduced Enrichment for Upgrading the research Reactor Munich FRM", Proc. International Meeting on Reduced Enrichment for Research and Test Reactors, (K. Tsuchihashi, ed.), JAERI-M 84-073, p. 321 (1984).

42. K. Böning, W. Gläser, J. Meier, G. Rau, A. Röhrmoser, and L. Zhang, "Status of the Compact Core Design for the Munich Research Reactor", Proc. 1984 International Meeting on Reduced Enrichment for Research and Test Reactors, ANL/RERTR/TM-6 CONF-8410173, p. 456 (1985).

43. W. L. Woodruff, M. Hayashi, S. Shiroya, and K. Kanda, "RERTR/ANL-KURRI Results and Comparison on Reduced Enrichment for the KUHFR", Symposium on Use of Medium Enriched Uranium for Research Reactor, (K. Kanda and Y. Nakagome, ed.), KURRI-TR-192, p. 12 (1979).

44. T. Shibata and K. Kanda, "ANL-KURRI Joint Study on the Use of Reduced Enrichment Fuel in KUHFR —— Phase A Report ——", (February 15, 1979) submitted to the US and Japanese Governments.

45. T. Shibata and A. Travelli, "ANL-KURRI Joint Study on the Use of Reduced Enrichment Fuel in KUHFR —— Status Report on Phase B ——", (December 12, 1980) submitted to the US and Japanese Governments.

46. K. Kanda, "Use of Medium Enrichment Fuels for Research Reactors", Nucl. Eng., Vol. 26, No. 10, p. 59 (1980) in Japanese.

47. K. Kanda, "KUCA Critical Experiment Program Using HEU and MEU fuels", Proc., International Meeting on Development, Fabrication, and Application of REDUCED ENRICHMENT FUELS for Research and Test Reactors, ANL/RERTR/TM-3 CONF-801144, p. 567 (1983).

48. K. Kanda, S. Shiroya, M. Hayashi, Y. Nakagome, and T. Shibata, "KUCA Critical Experiments Using MEU Fuel", Seminar on Research Reactor Operation and Use, IAEA-SR-77/30 (1981).

49. T. Shibata and K. Kanda, "Critical Experiments Using Medium Enriched Uranium", J. At. Energy Soc. Japan, Vol. 24, No. 5, p. 363 (1982) in Japanese.

50. K. Kanda, S. Shiroya, M. Hayashi, K. Kobayashi, Y. Nakagome, and T. Shibata, "KUCA Critical Experiments Using Medium Enriched Uranium Fuel", Annu. Rep. Res. Reactor Inst. Kyoto Univ., Vol. 15, p. 1 (1982).

51. S. Shiroya, H. Fukui, Y. Senda, M. Hayashi, and K. Kobayashi, "Measurements of Neutron Flux Distributions in a Medium Enriched Uranium Core", ibid., p. 141 (1982).

52. H. Fukui, Study on the Void Reactivity Coefficient in the KUCA, Master Thesis, Dept. Nucl. Eng., Facl. Eng., Kyoto Univ. (1983) in Japanese.

53. T. Shibata and A. Travelli, "ANL-KURRI Joint Study on the Use of Reduced Enrichment Fuel in KUHFR —— Joint Report on Phase B ——", (March 31, 1983) submitted to the US and Japanese Governments.

54. K. Kanda, M. Hayashi, S. Shiroya, K. Kobayashi, H. Fukui, K. Mishima, and T. Shibata, "KUCA Critical Experiments Using MEU Fuel (II)", Proc. International Meeting on Research and Test Core Conversions from HEU to LEU Fuels, ANL/RERTR/TM-4 CONF-821155, p. 426 (1983).

55. H. Fukui, K. Mishima, S. Shiroya, M. Hayashi, K. Kanda, and H. Nishihara, "Experimental Study on the Void Reactivity Coefficient in the KUCA", Annu. Rep. Res. Reactor Inst. Kyoto Univ., Vol. 16, p. 1 (1983).

56. Y. Senda, Measurements and Analysis of the Void Effect on Reactivity in the KUCA, Master Thesis, Dept. Nucl. Eng., Facl. Eng., Kyoto Univ. (1984).

57. K. Kanda, K. Mishima, S. Shiroya, M. Hayashi, H. Fukui, and H. Nishihara, "Experimental Study on the Void Reactivity Coefficient in the KUCA", Proc., International Meeting on Reduced Enrichment for Research and Test Reactors, (K. Tsuchihashi, ed.), JAERI-M 84-073, p. 388 (1984).

58. H. Fukui, K. Mishima, S. Shiroya, M. Hayashi, K. Kanda and Y. Senda, "Effect of Reducing Fuel Enrichment on the Void Reactivity — Part I: Experimental Study", Nucl. Technol., Vol. 70, No. 3, p. 301 (1985).

59. M. Hayashi and S. Shiroya, "Few-Group Constants for the HEU and MEU Cores in the KUCA", Annu. Rep. Res. Reactor Inst. Kyoto Univ., Vol. 14, p. 153 (1981).

60. S. Shiroya, M. Hayashi, K. Kanda, T. Shibata, W. L. Woodruff, and J. E. Matos, "Analysis of the KUCA MEU Experiments Using the ANL Code System", Proc., International Meeting on Research and Test Reactor Core Conversions from HEU to LEU Fuels, ANL/RERTR/TM-4 CONF-821155, p. 426 (1983).

61. T. Mori and K. Tsuchihashi, "An Analysis of KUCA MEU Cores by the JAERI SRAC Code System", ibid., p. 462 (1983).

62. S. Shiroya, M. Hayashi, K. Kanda, and T. Shibata, W. L. Woodruff, and J. E. Matos, "Analysis of the KUCA MEU Experiments Using the ANL Code System", Annu. Rep. Res. Reactor Inst. Kyoto Univ., Vol. 16, p. 17 (1983).

63. S. Shiroya, M. Hayashi, K. Kanda, and T. Shibata, "Analysis on the KUCA MEU Experiments (II) —— Boron Burnable-Poison Effect", Proc., International Meeting on Reduced Enrichment for Research and Test Reactors, (K. Tsuchihashi, ed.), JAERI-M 84-073, p. 369 (1984).

64. Y. Senda, S. Shiroya, M. Hayashi, K. Kanda, and T. Shibata, "Analysis on the Void Reactivity Measurements in the KUCA", ibid., p. 399 (1984).

65. S. Shiroya, M. Hayashi, K. Kanda, and T. Shibata, "Analysis of Critical Experiments Using Medium-Enriched-Uranium Fuel in Kyoto University Critical Assembly (KUCA), Criticality and Burnable-Poison Effect", J. Nucl. Sci. Technol., Vol. 22, No. 7, p. 507 (1985).

66. Y. Senda, S. Shiroya, M. Hayashi, and K. Kanda, "Effect of Reducing Fuel Enrichment on the Void Reactivity —— Part II: Analytical Study", Nucl. Technol., Vol. 70, No. 3, p. 318 (1985).

67. B. A. Zolotar, et al., "EPRI-CELL Code Description", Advanced Recycle Methodology Program System Documentation, Part II, Chapter 5, EPRI Rep. (Oct. 1975).

68. D. R. Ferguson and K. L. Derstine, "Optimized Iteration Strategies and Data Management Consideration for Fast-Reactor Finite-Difference Diffusion Theory Codes", Nucl. Sci. Eng., Vol. 64, p. 593 (1977).

69. M. Hayashi, S. Shiroya, Y. Naito, and S. Tsuruta, User's Manual for 2D-FEM-KUR: A Two-Dimensional Diffusion Code by Finite Element Method, KURRI-TR, to be published.

70. Y. Naito, S. Tsuruta, and M. Hayashi, "A New Mixed Method with Finite Difference and Finite Element Method for Neutron Diffusion Calculation", J. Nucl. Sci. Technol., Vol. 18, No. 8, p. 571 (1981).

71. K. Tsuchihashi, H. Takano, K. Horikami, Y. Ishiguro, K. Kaneko, and T. Hara, SRAC: JAERI Thermal Reactor Standard Code System for Reactor Design and Analysis, JAERI-1285 (1983).

72. K. Tsuchihashi, Collision Probability in Two-Dimensional Lattice by Ray-Trace Method and Its Application to Cell Calculations, JAERI-M 85-034 (1985).

73. J. A. Larrimore, Temperature Coefficients of Reactivity in Homogenized Thermal Nuclear Reactors, Doctor Thesis, Dept. Nucl. Eng., MIT (1962).

74. W. R. Cadwell, PDQ-7 Reference Manual, WAPD-TM-678 (1967).

75. T. Tsutsui and T. Ise, Generation of Multi-Group Constants Using the GGC-4 Code and Its Examinations, JAERI-M-5991 (1975) in Japanese.

76. B. J. Toppel and I. Baksys, The Argonne-Revised THERMOS Code, ANL-7023 (1965).

77. H. Tsuruta and K. Kobayashi, The preparation of Input Data for KR302DPT —— A two-dimensional diffusion and perturbation code ——, JAERI-memo 4775 (1972).

78. T. Shibata, K. Kanda and M. Yamamoto, "Kyoto University Critical Assembly", Nucl. Eng., Vol. 19, No. 4, p. 40 (1973) in Japanese.

79. T. Shibata, "Kyoto University Critical Assembly", J. At. Energy Soc. Japan, Vol. 17, No. 6, p. 296 (1975) in Japanese.

80. H. Tsujimoto, H. Nakamura, T. Kobayashi, and T. Shibata, Safety and Interlock System of the Kyoto University Critical Assembly, KURRI-TR-150 (1977) in Japanese.

81. H. Nakamura, H. Tsujimoto, and T. Shibata, Control Desk and Graphic Panel of the Kyoto University Critical Assembly, KURRI-TR-173 (1978) in Japanese.

82. T. Sagane and T. Shibata, Light-Water Moderated Core of the Kyoto University Critical Assembly, KURRI-TR-178 (1978) in Japanese.

83. S. Ishihara, M. Hayashi, K. Kanda and T. Shibata, Nuclear and Process Instrumentations of the Kyoto University Critical Assembly, KURRI-TR-183 (1979) in Japanese.

84. K. Kanda, K. Kobayashi, M. Hayashi, and T. Shibata, "Reactor Physics Experiments Using Kyoto University Critical Assembly", J. At. Energy Soc. Japan, Vol. 21, No. 7, p. 557 (1979) in Japanese.

85. Text of Graduate Course Experiments Using the Kyoto University Critical Assembly, (K. Kanda, ed.), Res. Reactor Inst., Kyoto Univ. (1984).

86. G. R. Keepin, Physics of Nuclear Kinetics, Addison-Wesley Publishing Company Inc., Reading, Massachusetts (1965).

87. K. Fushimi, ed., Nuclear Reactor, Series of Experimental Physics, Vol. 29, Kyoritsu-Shuppan Co., Tokyo (1972) in Japanese.

88. K. H. Beckurts and K. Wirtz, Neutron Physics, Springer-Verlag (1964).

89. M. M. R. Williams, Random Process in Nuclear Reactors, Pergamon Press (1974).

90. R. E. Uhrig, Random Noise Techniques in Nuclear Reactor System, Ronald Press (1970).

91. J. A. Thie, Reactor Noise, Rowman and Littlefield (1963).

92. R. P. Feynman, F. de. Hoffmann, and R. Serber, J. Nucl. Energy, Vol. 3, p. 64 (1956).

93. Y. Gotoh, "Measurement of Neutron Life in a D_2O System by Neutron Fluctuation", J. Nucl. Sci. Technol., Vol. 1, No. 6, p.193 (1964).

94. A. Furuhashi and S. Izumi, "A Proposal on Data Treatment in the Feynman-α Experiments", J. Nucl. Sci. Technol., Vol. 4, No. 2, p. 99 (1967).

95. K. Terakawa, Measurements of the Reactivities and Kinetic Parameters Using the Feynman-α Technique, Master Thesis, Dept. Nucl. Eng., Facl. Eng., Kyoto Univ. (1977).

96. B. E. Simmons and J. S. King, Nucl. Sci. Eng., Vol. 3, p. 595 (1958).

97. J. L. Shapiro, "The Void Coefficient in an Enriched, Water Reactor", Nucl. Sci. Eng., Vol. 12, p. 449 (1962).

98. Y. Fujii-e, M. Mori, T. Matsui, and K. Miyazaki, "Measurement of Void Reactivity Coefficient", Bull. At. Energy Soc. Japan, Vol. 10, No. 2, p. 58 (1968) in Japanese.

99. S. Banerjee and R. T. Lahey, Jr., "Advances in Two-phase Flow Instrumentation", Advances in Nuclear Science and Technology, (J. Lewis and M. Becker, ed.), Vol. 13, p. 227, Plenum Press, New York, (1980).

100. K. Sekoguchi et al., "Study on the Void Measurement in Gas-Liquid Two-phase Flow", Proc. Japan Soc. Mech. Eng., No. 814-6, p. 59 (1981), in Japanese.

101. M. R. Özugü, J. C. Chen, and A. H. Stenning, "Local Liquid Film Thickness around Taylor Bubbles," J. Heat Transfer, Vol. 95, No. 8, p. 425 (1973).

102. G. D. Joanu and J. S. Dudek, GA-1850 (1961).

103. H. C. Honeck, BNL-5826 (1961).

104. ENDF/B Summary Documentation, BNL-NCS-17541 (ENDF-201), 2nd Edition, compiled by D. Garber, available from the National Nuclear Data Center, BNL, Upton, New York (1975).

105. H. Henryson II, B. J. Toppel, and C. G. Stenberg, ANL-8144 (1976).

106. N. M. Greene, et al., ORNL/TM-3706 (1976).

107. K. Tsuchihashi, F. Akino, Y. Nagaoka, and Y. Ishiguro, Benchmark Calculations by the Thermal Reactor Standard Nuclear Design Code system SRAC, JAERI-M 9781 (1981) in Japanese.

108. I. Senuma, Y. Miyoshi, T. Suzaki, and I. Kobayashi, Benchmark Calculations of the Solution-Fuel Criticality Experiments by SRAC Code System, JAERI-M 84-110 (1984) in Japanese.

109. M. Mori and K. Tsuchihashi, Study of Calculation Methods for the Analysis of the IAEA Research Reactor Benchmark Using the SRAC Code System, JAERI-M 84-230 (1984) in Japanese.

110. K. Arigane, T. Otsuka, H. Shitomi, S. Watanabe, and M. Morozumi, Nuclear Characteristic Measurements and Calculations by the SRAC Code System for LEU Fuel Element, JAERI-M 85-047 (1984) in Japanese.

111. K. D. Lathrop and F. W. Brinkly, Theory and Use of the General Geometry TWOTRAN Program, LA-4432, Los Alamos National Laboratory (1970).

112. T. B. Fowler, et al., Nuclear Reactor Core Analysis Code: CITATION, ORNL-TM-2496, Oak Ridge National Laboratory (1969).

113. T. Otsuka, N. Fukumura, and Y. Hachiya, "Measurements of Moderator Temperature Coefficients of Reactivity for Pressure-Tube-Type Reactors", Nucl. Sci. Eng., Vol. 74, No. 2, p. 95 (1980).

114. N. A. Hanan and S. K. Bhattacharyya, "The Calculation of the Temperature Feedback Reactivity Coefficient of the Upgraded TREAT Reactor", Trans. Am. Nucl. Soc., Vol. 41, p. 616 (1982).

115. S. Wakamatsu, K. Hashimoto, and K. Nishina, "Calculation of Temperature Coefficients for the Light-Water-Moderated Core of Kyoto University Critical Assembly", J. At. Energy Soc. Japan, Vol. 24, No. 12, p. 963 (1982) in Japanese.

116. R. S. Podar and M. S. Trasi, "Temperature Coefficients for Global Stability in a Reactor with Two-Temperature Feedback", Z. Angew. Math. and Phys., Vol. 34, No. 2, p. 164 (1983).

117. Division of Critical Facility, Nuclear Data and Codes Available in the KUCA, KURRI-TR-262 (1985) mostly in Japanese.